CHARACTERIZATION OF A VERTICAL TWO AXIS LATHE

A Thesis
Presented to
The Academic Faculty

By

Michael Edward Leclerc

In Partial Fulfillment
Of the Requirements for the Degree
Master of Science in Mechanical Engineering

Georgia Institute of Technology

May, 2005

CHARACTERIZATION OF A VERTICAL TWO AXIS LATHE

Approved by:

Dr. Thomas Kurfess, Chair
School of Mechanical Engineering
Georgia Institute of Technology

Dr. Steven Liang
School of Mechanical Engineering
Georgia Institute of Technology

Dr. Shreyes Melkote
School of Mechanical Engineering
Georgia Institute of Technology

Date Approved: March 15, 2005

Dad, Mom, Laura, Uncle Paul and Daniel, all I have done, all that I am is attributed to your participation in my life. This was for you

ACKNOWLEDGEMENTS

First and foremost, I would like to take this opportunity to thank my advisor Dr. Kurfess for giving me this opportunity and his indispensable assistance and words of wisdom. This work was made so much easier by the supporting research group under his advisement. More specifically, Meghan Schilling, Austin Chen, and Laine Mears, thank you very much for your knowledge and counseling. Austin's direction and answered questions were much appreciated. Steven Sheffield's machine tool guidance was a major contribution to the completion of this work.

This research would not have been possible without the generous financial support of Y12. I would also like to show appreciation to KGK International for kindly loaning their two axis vertical lathe.

TABLE OF CONTENTS

		Page
ACKNOWLEDGEMENTS		iv
LIST OF TABLES		viii
LIST OF FIGURES		ix
SUMMARY		xiii
CHAPTER		
1	INTRODUCTION	1
	Problem Statement	1
	Objective of Thesis	2
2	BACKGROUND	3
	Overview	3
	Measuring Instruments	3
	Reversal Technique	10
	Thermal Errors	11
	Tool Wear	14
	Fixturing	15
	Tool Setting Station	16
	Cutting Forces and Vibrations	18
	Homogeneous Transformation Matrix (HTM)	19
	Tool Path Correction	20

3 EQUIPMENT 24
Okuma Howa Vertical Lathe 24
Laser Interferometer 25
Renishaw QC10 Ball Bar 27
Coordinate Measurement Machine 28
4 METROLOGY PROCEDURES 30
Interferometer 30
Basic Guidelines 30
Interferometer Software and Sensor Setup 31
Mounting and Aligning Optics 32
Displacement Measurements 35
Angular Measurements 38
Ball Bar 39
5 THERMAL ANALYSIS 42
6 BALL BAR RESULTS 51
Experimental Results-Ball Bar 51
Ball Bar Compensation Case Study 52
7 INTERFEROMETER RESULTS 64
Linear Results 64
Straightness Results 71
Angular Results 76
Discussion of Interferometer Data 81
8 ERROR COMPENSATION 82

Homogenous Transformation Matrix 82

Implementation of the HTM 88

9 VERIFICATION 97

Coordinate Measurement Machine (CMM) Results of Test Parts 97

Discussion of Sources of Error 116

10 CONCLUSIONS AND RECOMMENDATIONS 118

Conclusions 118

Recommendations 121

APPENDICES

A PART PROGRAMS 123

REFERENCES 125

LIST OF TABLES

Table 1- Specifications of the Okuma Howa Lathe (Okuma Website) 25

Table 2- Laser Interferometer Specifications (HP)..... 27

Table 3- Specifications of the Brown & Sharpe Microval PFx CMM 29

Table 4- Coordinates of results of curve fit modes..... 59

Table 5- Results of different compensation modes..... 60

Table 6 Machine error results from interferometer test..... 91

Table 7- Results of Circle Fit..... 93

Table 8- Coordinates of actual and compensated tool path for facing and turning 95

Table 9- Root of sum of squares of the errors for each case..... 108

Table 10- Results of Facing 112

LIST OF FIGURES

Figure 1-Six Degrees of Freedom (HP Manual) 4

Figure 2- A typical laser and photo detector setup (Slocum 1992) 5

Figure 3- Laser interferometer Setup for linear displacements (Kurfess) 6

Figure 4- Example of ASME B5.57M output for analysis 8

Figure 5- Schematic of Ball Bar (Pahk 1997) 9

Figure 6- Spindle Error Measurement System (Choi 2003) 13

Figure 7- Cutting of cylindrical workpiece with 3 jaw chuck and out of roundness due to the chuck 15

Figure 8- The effect of tool offset on convex spherical surfaces (Zhou 2001) 16

Figure 9- Cutting Geometry with tool offset error (Zhou 2001) 17

Figure 10-Variation of form accuracy, z, with tool offset (Zhou 2001) 18

Figure 11- Software compensation schematic (Anjanappa 1998) 22

Figure 12- Okuma Howa V40R 24

Figure 13- Laser Interferometer on tripod 26

Figure 14- Coordinate Measurement Machine (CMM) 28

Figure 15-Example of proper sensor placement (HP) 32

Figure 16- Interferometer assembly (HP manual) 33

Figure 17- Front view of the laser head (HP manual) 34

Figure 18-Required hardware for linear measurements (HP manual) 35

Figure 19-Required hardware for straightness measurements (HP manual) 36

Figure 20- Optical configuration for displacement measurements (Donmez 1985) 37

Figure 21- Schematic of beam path in straightness measurements (Kurfess) 38

Figure 22- Straightness measurement (Kurfess)..... 38

Figure 23-Optical configuration for angular measurements (Kurfess)..... 39

Figure 24-Ball Bar system setup..... 40

Figure 25- Schematic of system for heating 43

Figure 26-Schematic of system for cooling..... 43

Figure 27- Thermocouple placed on the spindle housing..... 45

Figure 28- Warm up and cool down data of the spindle for 1000 rpm..... 47

Figure 29- Location of thermocouple for the z-axis 48

Figure 30-Warm up and Cool down behavior for the z-axis (f=2.54 m/min)..... 49

Figure 31- Ball Bar Errors for cold state 5μm/div..... 51

Figure 32- Ball Bar errors for hot state (5 μm/div)..... 52

Figure 33 Schematic of tool paths 53

Figure 34- MetroloGT circle fit for 0^{o} to 90^{o} 54

Figure 35- Results of Case Study for the first quadrant .05mm/div (CW direction)..... 55

Figure 36- Repeatability of ball bar tests..... 56

Figure 37- Results for circle fit (.1mm/div)..... 57

Figure 38- Results for two semi-circular fit (.1mm/div)..... 58

Figure 39-Results for 90 degree arc fit (.1mm/div) 59

Figure 40 Results of compensated quadrant 1 for robustness CW (.05mm/div)..... 61

Figure 41-Results of semi-circular fit for robustness 62

Figure 42- Demonstration of Ratio from Ball Bar test program to test part..... 63

Figure 43- Optical setup used for Z-axis linear measurements 65

Figure 44- Initial Position location of laser interferometer measurements..... 66

Figure 45- Results of linear Z-axis measurements for 177.8 mm (7 inch) travel..... 67

Figure 46- Results for linear Z-axis 50.8mm (2 inch) travel..... 68

Figure 47- Results for linear X-axis 114.6mm (4.5 inch) travel..... 69

Figure 48- Results for linear X-axis 50.8mm (2 inch) travel..... 69

Figure 49- Illustration of ball screw pitch affect on linear motion (Slocum, 1992)..... 70

Figure 50- Optical Setup for X-straightness in the vertical direction..... 71

Figure 51- Optical Configuration for vertical X-axis straightness..... 72

Figure 52- Vertical X straightness Results for 76.2 mm (3 inch) travel..... 73

Figure 53-Vertical X straightness results for 25.4 mm (1 inch) travel..... 74

Figure 54- Optical configuration for horizontal straightness along the Z-axis..... 75

Figure 55- Results of horizontal straightness along the Z- axis 50.4 mm (2 inches)..... 76

Figure 56- Optical configuration for pitch along the X-axis..... 77

Figure 57- Results of pitch along the X axis for 50.4 mm (2 inch) range..... 78

Figure 58- Results of pitch along the X axis for 152.4mm (6 inch) range..... 79

Figure 59- Yaw along the Z-axis for 50.4 mm (2 inches)..... 80

Figure 60- Yaw along the Z-axis for 177.8mm (7 inches)..... 80

Figure 61- Coordinate frame nomenclature for machine tool (Courtesy of Donmez)..... 83

Figure 62- Roll, Pitch and Yaw associated with the x axis (Courtesy of Donmez)..... 84

Figure 63- Schematic of straightness motion along each axis (Kurfess)..... 85

Figure 64- Nominal tool path of test part..... 89

Figure 65- Mesh overlay of circular profile..... 90

Figure 66- Actual and Corrected tool path for circular profile of 25.4 mm (1 inch) radius 92

Figure 67- Comparison of Ball Bar compensation path and HTM compensation path (0.05mm/div) 93

Figure 68- Actual and Corrected tool path of 25.4 mm (1 inch) face 95

Figure 69-Actual and Corrected tool path for 25.4 mm (1 inch) turn 96

Figure 70- Schematic of surface roughness (not to scale) 98

Figure 71- Ideal geometry of test part, radius is 31.75 mm (1.25inches) 100

Figure 72- Angle Convention for CMM plots 101

Figure 73- CMM results for test parts (0.01 in increments) 102

Figure 74- Test using precision sphere to verify accuracy of CMM 103

Figure 75- Comparison of errors found from ball bar test to CMM results for uncompensated part 104

Figure 76- Illustration of x-offset 106

Figure 77- Comparison of errors found from ball bar test to CMM results for ball bar compensated part 107

Figure 78- Comparison of errors found from ball bar test to CMM results for HTM compensated part 108

Figure 79- Test Part for facing and turning operation 110

Figure 80- CMM results for uncompensated facing 111

Figure 81- Comparison of CMM results for uncompensated test part and HTM prediction 112

Figure 82- CMM results of uncompensated and HTM compensated turned parts 114

Figure 83- Comparison of HTM predicted tool path to CMM results of uncompensated test part 115

Figure 84- Schematic of turning 116

SUMMARY

The primary barrier to the production of better machined parts is machine tool error. Present day applications are requiring closer machine part tolerances. The errors in dimensional part accuracy derive from the machine, in this case, a vertical two axis CNC lathe. A two axis vertical lathe can be utilized to produce a variety of parts ranging from cylindrical features to spherical features. A vertical lathe requires a spindle to rotate the work at speeds reaching 3000rpm, while simultaneously requiring the machine tool to be positioned in such a manner to remove material and produce an accurate part. For this to be possible, the machine tool must be precisely controlled in order to produce the correct contours on the part. There are many sources of errors to be considered in the two axis vertical lathe. Each axis of importance contains six degrees of freedom. The machine has linear displacement, angular, spindle thermal drift, straightness, parallelism, orthogonal, machine tool offset and roundness error. These error components must be measured in order to determine the resultant error.

The characterization of the machine addresses thermal behavior and geometric errors. This thesis presents the approach of determining the machine tool errors and using these errors to transform the actual tool path closer to the nominal tool path via compensation schemes. One of these schemes uses a laser interferometer in conjunction with a homogenous transformation matrix to construct the compensated path for a circular arc, facing and turning. The other scheme uses a ball bar system to directly construct the compensated tool path for a circular arc. Test parts were created to verify the improvement of the part accuracy using the compensated tool paths.

CHAPTER I

INTRODUCTION

Problem Statement

The primary barrier to the production of better machined parts is machine tool error. Present day applications are requiring closer machine part tolerances. The errors in dimensional part accuracy derive from the machine, in this case, a vertical two axis CNC lathe. A two axis vertical lathe can be utilized to produce a variety of parts ranging from cylindrical features to spherical features. A vertical lathe requires a spindle to rotate the work at speeds reaching 3000rpm, while simultaneously requiring the machine tool to be positioned in such a manner to remove material and produce an accurate part. The machine tool must be precisely controlled in order to produce the correct contours on the part. Of course the dynamics of the machine change the machine geometry. This change in machine geometry alters the tool path and creates an undesirable part. There are many sources of errors to be considered in the two axis vertical lathe. This discussion will be limited to the errors of importance. Each axis of importance contains six degrees of freedom. The machine will have linear displacement, angular, spindle thermal drift, straightness, parallelism, orthogonal, machine tool offset and roundness error. These error components must be measured in order to determine the resultant error. The geometric errors of the lathe are dependent upon thermal and loading conditions. For example, the bearings in the spindle grow due to the thermal gradient caused by the machine's use.

Objective of Thesis

The goal of this project was to characterize a two axis vertical lathe to ensure it will produce a more accurate part. This research was divided into several sectors to achieve this goal. The first sector was known as error measurement, which involves a quantitative description of the machine behavior that affects the finished part. Sensitive aspects of the two axis machine must be measured for these errors. These errors included linear, straightness, and angular errors through movement of the tool, along with thermal behavior. A ball bar was also used to examine machine errors along a circular path, which proved useful for the circular profile of the test part. The next sector involved tool path correction with G Code compensation. Once these machine tool errors were determined, the next step was to correlate these errors to achieving a better part. A correctional G code algorithm was created using a developed homogenous transformation matrix (HTM) and then implemented into the two axis vertical lathe via software. Test parts that exposed the machine tool errors were applied to verify the characterization of the lathe. Test parts were created with and without the G Code compensation. The dimensional accuracies of the test parts will then be compared to determine the improvements with the G Code. A Coordinate Measurement Machine (CMM) will be used to accurately determine the dimension of the test parts.

CHAPTER II

BACKGROUND

Overview

The accuracy of a finished part is directly related to the accuracy of the machine tool. It is very costly to remove all the errors by machine design alterations. Therefore, instead of vainly attempting to eliminate all the errors, this study offers a process to predict the machine tool errors and compensate for them. The area of machine error compensation has been extensively researched over the years. Slocum (1992) suggests research in error compensation seeks to determine the difference between the desired and the actual tool path and then adjust the tool path. The deviation from the nominal tool path is a result of thermal errors and geometric errors. Thermal errors generally come from the thermal deformations of the machine elements caused by heat sources that exist in the machine structure, such as ball screws, spindle, etc (this genre of errors is discussed later). Geometric errors are caused by inaccurate motions of machine elements such as carriages, work tables, etc. Determining the geometric errors involves precision measurement equipment. After an initial discussion of each piece of equipment, an investigation of the use of each and their results is presented through published papers.

Measuring Instruments

A machine tool's positioning accuracy can be enhanced by measuring the six degrees of freedom for each axis according to Ulmer (1997).

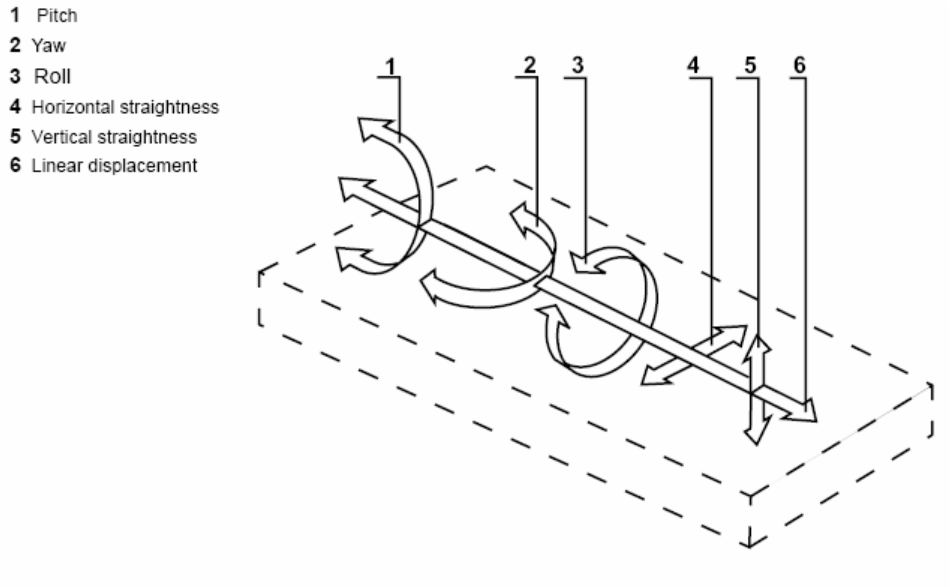

Figure 1-Six Degrees of Freedom (HP Manual)

There are several types of interferometer sensors. A brief explanation of the fundamental physics of wave and light properties is needed to understand the usefulness of a laser interferometer. A laser interferometer is an instrument used to determine positioning accuracy. Interferometers make measurements based on the concept of wave interference; it measures a relative change in tool path length by superimposing two wave forms. Perhaps it is easiest to picture two waves traveling parallel to each other with the same frequency, amplitude and velocity; however a phase angle causes a lag between the waves et al Slocum (1992). These two waves can be represented by the following equations:

$$Y_1 = A\sin(kx - \omega t - \phi) \tag{2.1}$$

$$Y_2 = A\sin(kx - \omega t) \tag{2.2}$$

.

This means that at any time the waves are ϕ/k apart, where k is the inverse of the wavelength. The superposition of these two waves is:

$$Y = 2A\cos(\frac{\phi}{2})\sin(kx - \omega t - \frac{\phi}{2}). \tag{2.3}$$

If ϕ is set to zero, meaning there is no phase angle, then the superposition of the wave is just twice the amplitude of the original waves. This is call constructive interference; whilst destructive interference occurs when the phase angle is π causing the amplitude of the superimposed wave is to be zero.

Figure 2 shows the beam path and set up used to determine the velocity of a moving target.

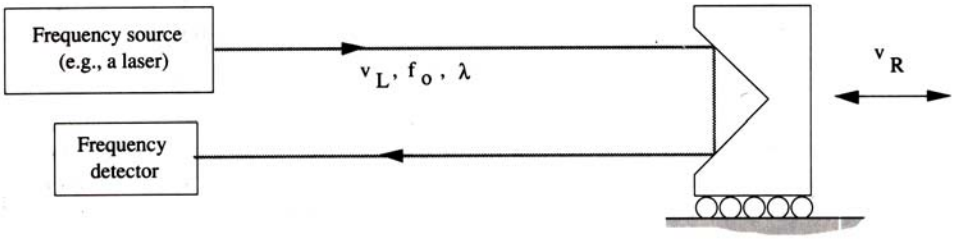

Figure 2- A typical laser and photo detector setup (Slocum 1992)

Several equations were developed to relate the displacement of the retroreflector to the change in phase. It is assumed that the light source is fixed and the velocity of the mechanical components is very small compared to the speed of light (3 x 10^8 m/s). Therefore the distance traveled by the retroreflector is given by (2.4)

$$\Delta x = \frac{\Delta\phi\lambda}{4\pi}, \tag{2.4}$$

where $\Delta\phi$ is the phase change and λ is the wavelength of light. A photo detector is a device that measures the phase difference between the laser beam as it leaves the

interferometer and reflects back. Thus, displacement measurements could be made in a machine tool if this retroreflector was attached to the moving element.

For example, linear displacement measurements along an axis could be made using the set up in Figure 3 and the previously discussed theory.

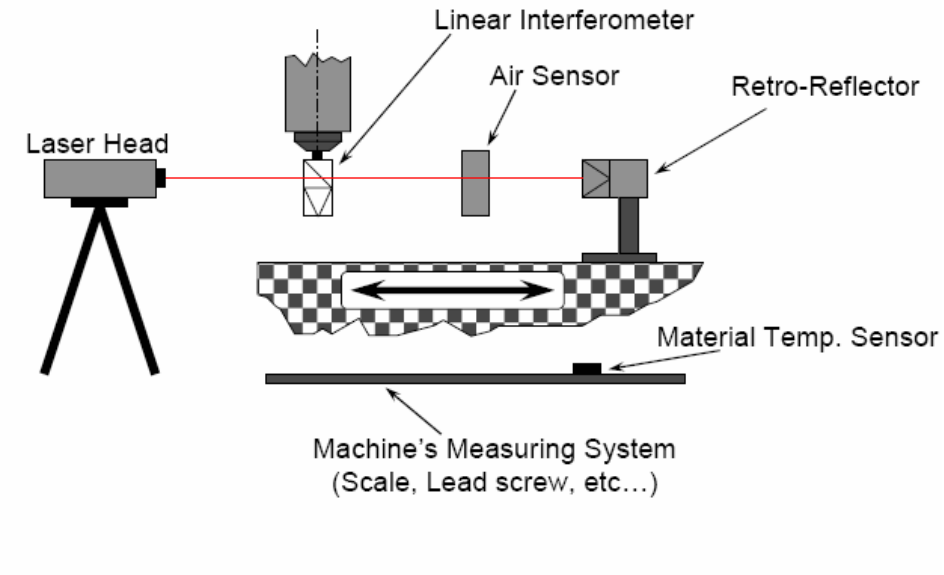

Figure 3- Laser interferometer Setup for linear displacements (Kurfess)

The laser beam is split into a reference beam and a measurement beam as shown in Figure 3 (the optical setup depends upon the axis of interest and type of measurement). If the paths differ by any integer multiple of the wavelength or by half an integer number of wavelengths then constructive or destructive interference occurs respectively. A counter inside the interferometer counts the number of peaks and relates this to a relative position measurement to within half a wavelength of light. An HP 5529A laser interferometer was used to make the following measurements: linear displacement error (translational error movement of a machine element along its axis of motion), angular errors (rotational

errors caused by geometric inaccuracies of the slideways), straightness (translational error of a machine element in the two orthogonal directions not on its own axis of motion), parallelism (expressed as a small angle) and squareness (Slocum 1992).

The HP 5529A laser interferometer is used in conjunction with a set of standards to serve as a guideline. The HP 5529A software allows for several different standard outputs to use for analysis. One of these standards is ASME B5.57M, Methods for Performance Evaluation of Computer Numerically Controlled Lathes and Turning Centers (ASME 1997). This Standard establishes requirements and methods for specifying and testing the performance of CNC lathes. It also allows for performance comparison between machines by general machine classification and treatment of environmental effects. This guideline represents a minimum requirement to ensure conformance to accuracy and repeatability. More specifically criteria such as the default line of measurement for the laser interferometer experiments is in the work zone parallel to each machine linear axis direction, measuring intervals of no longer then 25.4 mm, and two complete back and forth cycles for each linear axis. The manual for the HP interferometer and Standards for Machine Performance coincide with each other and used in Chapter IV. Aforementioned was the several output types available for use in the analysis section of the laser interferometer. An example of the full data set for positioning deviations of an axis (bi-directional) for ASME B5.57M is shown in

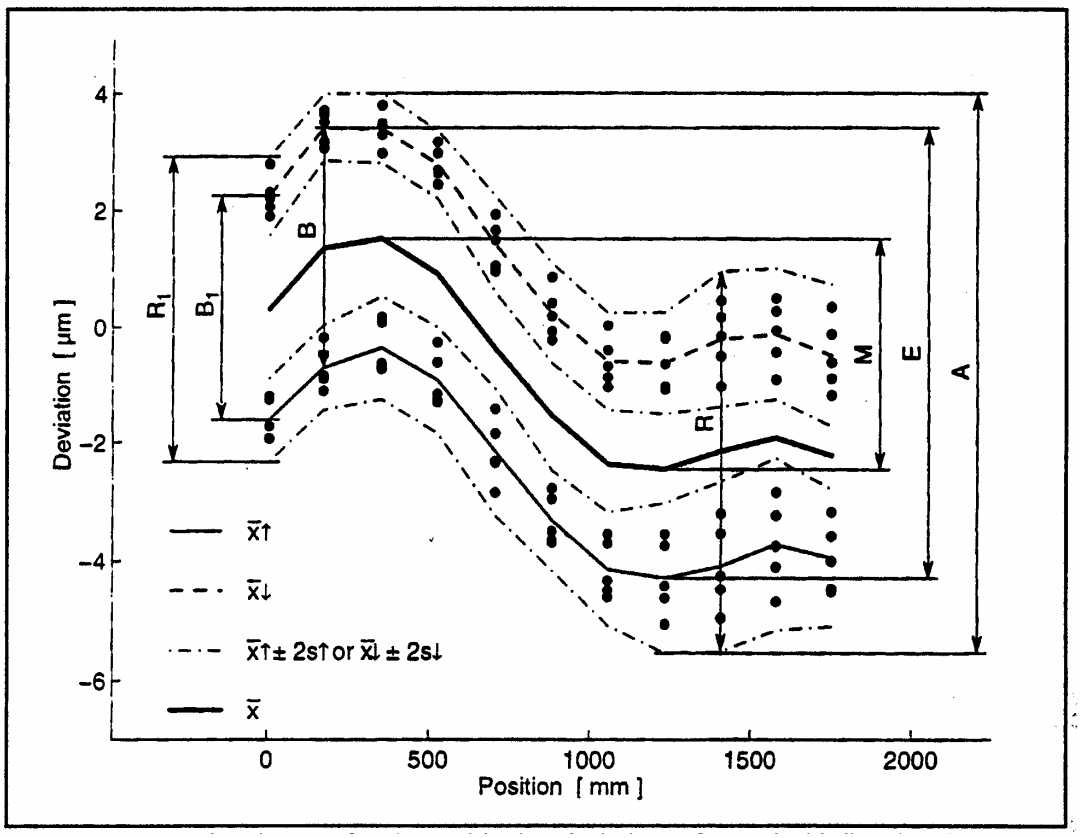

Figure 4- Example of ASME B5.57M output for analysis

The laser ball bar (LBB) was designed to measure volumetric errors of machine tools quickly by direct measurement of the spatial coordinates of the tool with respect to the machine table et al Ziegert (1994). It is important to mention that the experimental procedures for a laser ball bar and a ball bar using an LVDT (linear variable differential transformer) are very similar. An LVDT ball bar was used in the scope of this research however literature on the laser ball bar is readily available. LVDTs use the principle of electromagnetic induction to sense linear motion et al Slocum (1992). Procedures for the laser ball bar were more detailed and readily available; therefore they will be presented in

this discussion. A ball bar consists of two precision spheres connected by a telescoping rod that incases a LVDT as shown in Figure 5.

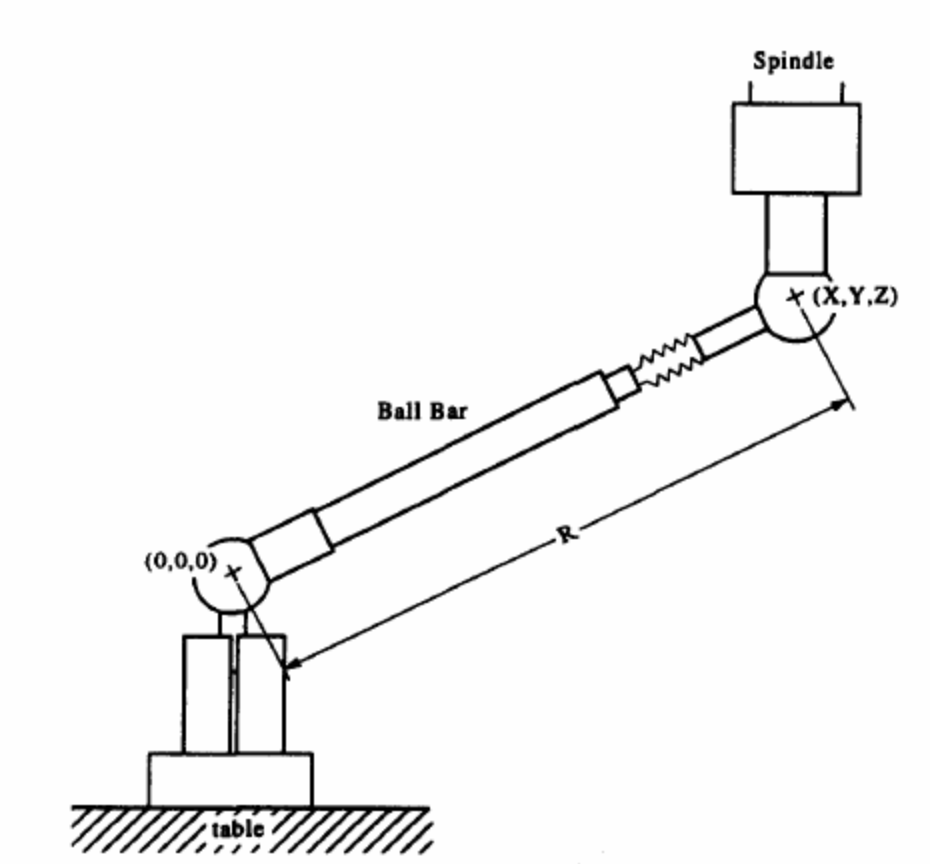

Figure 5- Schematic of Ball Bar (Pahk 1997)

One sphere is attached to the spindle while the other is attached to the tool holder. The tool holder is then commanded to move in a circular pattern. The LVDT can measure the relative displacement between the two spheres because the change in voltage is proportional to the change in length. The error is then determined by the difference of the commanded position and the actual position determined by the LVDT. Zeigert (1994) states this significantly reduces the measurement time because a rigid body kinematical error model was used to estimate the volume accuracy. Furthermore, the ball bar can be

used to measure translational, axis alignment, tilt and spindle errors. Therefore, the ball bar has been proven to play a significant role in measuring machine tool error. Reference Bryan (1982) is an excellent source for a more detailed explanation of laser ball bars and other various kinds of ball bars (such as telescoping and fixed).

Reversal Technique

The reversal technique is a method to determine the misalignment between optical (such as mirror flatness errors) components of the laser interferometer setup for straightness measurements. The reversal technique provides a method to eliminate errors in the measurement set up. An explanation of this technique was taken from Slocum (1992) where the author specifies how to find the straightness of the z-axis independent of the test arbor (the specific case explained here is for straightness along the z-axis; however this technique is adaptable to numerous measurements) Two sets of measurements are required to apply the reversal technique. A set of data is collected at the proper measuring interval for the z-axis. The optical pieces are then "reversed" or rotated by 180^o and the data is collected in the same manner again. The first and second measurements are represented by equations (2.5) and (2.6) respectively:

$$m_1(z) = a(z) - s(z) \tag{2.5}$$

$$m_2(z) = a(z) + s(z) \tag{2.6}$$

where m_1 (z) and m_2 (z) represents the data acquired at position 1 and 2 respectively, a (z) is the non-straightness of the optical pieces and s (z) is the straightness of the z axis. Substituting equations (2.5) and (2.6) and solving for s (z) yields:

$$s(z) = \frac{-m_1(z) + m_2(z)}{2} \tag{2.7}$$

Equation (2.7) provides the straightness of the z-axis without the error associated with the test arbor. The reversal technique can be applied to most test cases such as parallelism; however these cases can be more difficult because there are several errors involved in such an error measurement.

Thermal Errors

Machine tool error is not solely dependent upon geometric errors. The thermal behavior of the machine is also extremely important to understand. This behavior can be partially described in terms of the time constant (the amount of time it takes the machine to reach thermal steady state). The thermal time constant is a quantity that broadly describes the machine tool as a system. Slocum suggests a method to determine the temperature profile of machine elements from which the thermal behavior of the machine can be determined. Essentially, displacement errors were taken as the machine warmed up, then a single variable nonlinear least squares curve fitting technique was used (specifically, z-axis) as shown in (2.8)

$$\delta_z(z) = a_0 + a_1 T + a_2 T^2 + a_3 T^3 + a_4 T^4 . \tag{2.8}$$

This equation describes the behavior of machine tool error under thermal variance. This reference also provided useful insight for temperature acquisition, such as the optimum position to measure temperature.

A more detailed examination of thermal errors is required. Yun (1999) provides a method for estimating the machine tool error cause by thermal errors of a feed drive system. The feed drive is divided into two thermally changing elements: the ball screw and the guideway. The thermal behavior for both elements are developed separately, a modified lumped capacitance method and genius education algorithm was used to

develop the thermal model of the ball screw, while the finite element method is used for the guideway. The thermal expansion of the ball screw and guideway is then added together to predict the linear positioning error of the cutting point in the machine. These estimated thermal errors are then compared to the experimental errors of the CNC lathe. The accuracy of the proposed models (through experiments) was 3.79 μm. Another important conclusion is that the guideway accounted for 22.7% of the total thermal error. Yun explains in detail how to find and compensate for the thermal errors of the guideway and ball screw.

There are many other subsystems in the machine tool besides the ball screw and guideway. Another such subsystem of primary importance is the machine's spindle. Yang determines the thermal effects on the spindle. This paper proposes a "novel method for completely measuring and analyzing the thermal errors of a 3-axis machine tool using only one ball bar system" et al Yang (2004). A hemispherical ball bar test is applied to a synthesized volumetric model via a helix trajectory. The thermal errors can be measured by means of the change in ball bar measurements before and after thermal distortion. A capacitance sensor system is used to measure thermal errors and spindle drift errors in order to verify the accuracy of the ball bar measurements. Spindle drift is a motion through a nominal axis of rotation of the spindle caused by thermal deformations of the spindle components and support structure. The thermal errors measured by the ball bar system were almost identical to the spindle drift errors measured by the capacitance system (the difference was within 6 μm). Thus a novel idea was devised by accurately measuring the thermal errors of a spindle in a 3 axis machine with a ball bar system.

Furthermore, there has been extensive research on evaluating both thermal and geometric errors in spindle error motion, error model development and error compensation thereof. Choi (2003) examined the spindle motion errors (along with geometric and thermally induced errors) and concluded that an error model with spindle errors shows a better agreement between simulated and experimented roundness data. This was achieved through the implementation of a homogenous transfer matrix (a more detailed explanation of an HTM will be provided later) and a spindle error measurement system as shown in Figure 6:

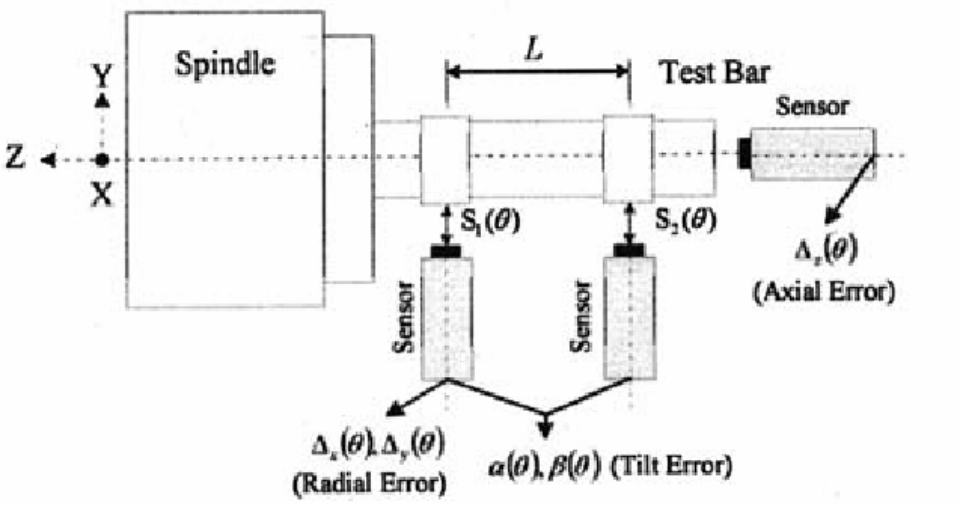

Figure 6- Spindle Error Measurement System (Choi 2003)

Simulated part profiles using the HTM were created and compared to cut parts that were measured on a roundness tester. The simulation results based on the error model without the spindle errors underestimates the error values when compared to the measured values.

Another paper that evaluates geometric errors due to thermal rise from the spindle can be found et al Tseng (2002). Instead of an HTM, a multivariable regression was used

to formulate the thermal errors from the spindle. This paper also describes the proper locations for temperature acquisition. Other phenomenon that affects the nominal position of the tool tip is tool wear, cutting forces and vibrations.

Tool Wear

Tool wear changes the functional point (the point at which the tool interacts with the work piece to provide material removal). The tool wear is a function of its material make, the material to be cut and the cutting parameters. Zhou (2001) describes the affect tool wear has upon the profile accuracy of the work piece. The cutting point moves about the edge of the cutting tool when contouring the profile (in our case, a circular profile will create the sphere). Tool wear causes the loss of the original profile accuracy of the cutting edge. To complicate matters even more, the tool wear is usually non-uniform due to several phenomena. Most of the factors are based upon the physical and mechanical properties gradients of the tool material. This paper suggests the implementation of a rotary table to the two axis lathe for tool normalcy as a solution to the uneven tool wear. The relationship among tool offset and machined form accuracy was also studied. The tool offset is the horizontal component of tool decentration with respect to the spindle axis. The tool height error is the vertical component. Essentially, several test parts were machined with varying tool offsets. The results demonstrate that the tool offset can influence the form accuracy (on the order of 40 μm), while the tool height offset influences the form accuracy a great deal less.

Fixturing

According to Lee (2004), the machining of a chucked cylindrical workpiece involves degradation in machining accuracy, such as out-of-roundness. This decrease in machine tool accuracy is inevitable due to deviation in the radial compliance of the chuck caused by the position of jaws with respect to the direction of the applied force. The illustration of out of roundness is shown in Figure 7.

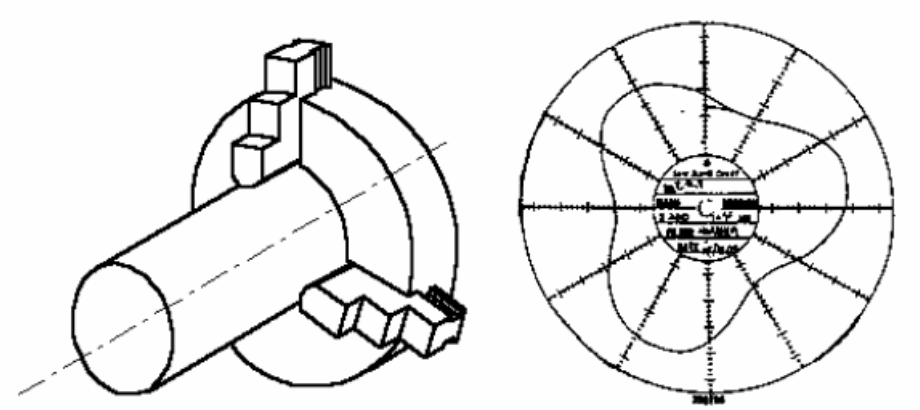

Figure 7- Cutting of cylindrical workpiece with 3 jaw chuck and out of roundness due to the chuck

Lee (2002) proposed using a high-speed tool drive with a linear motor to compensate for machining errors that derived from the chuck. This method is applied to improve workpiece roundness. A relation between roundness and chucking conditions were examined. This relationship was then used to predict the cutting depth variation and the roundness profile. A compensated path was constructed once the predicted path was determined. The roundness was improved by 50% after the compensation was applied.

Tool Setting Station

Tool set up error is present if the cutting tool in not coincident with the work piece's rotational axis at the vertex of the generated curve et al Zhou (2001). In this paper, the effects of tool setup accuracy on surface distortion were investigated. This paper investigates the affect of tool offset on profile accuracy for diamond turned non-ferrous components. The affect of tool offset is shown in Figure 8.

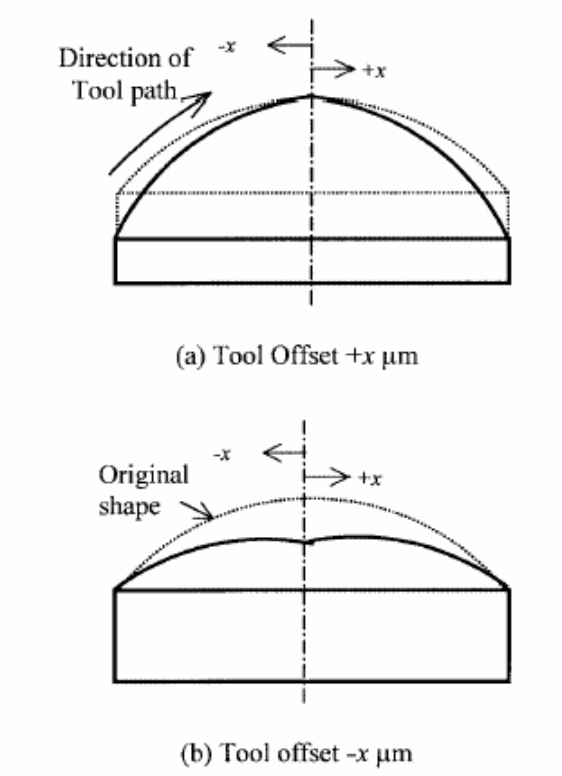

Figure 8- The effect of tool offset on convex spherical surfaces (Zhou 2001)

Cutting tests were performed on a two-axis diamond turning machine. Spherical mirrors were turned with varying preset tool offsets. The relationship among machined form accuracy, tool offset, and tool height was determined based on experimental and

analytical results. The analytical results of the paper can be described through Figure 9 and equation(2.9):

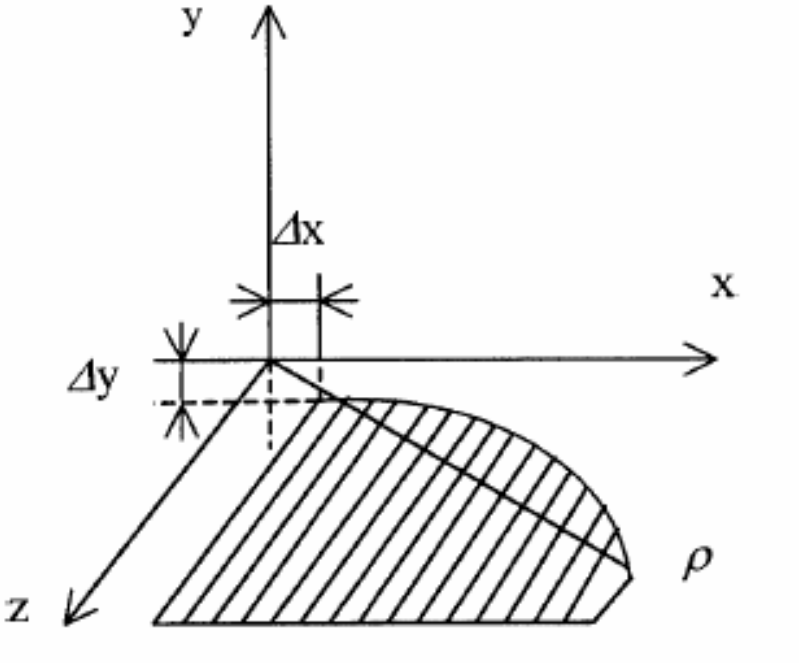

Figure 9- Cutting Geometry with tool offset error (Zhou 2001)

$$z = f(\rho) = r - \sqrt{r^2 - \left(\rho - \frac{\Delta y^2}{2r} - \frac{\Delta y^4}{8r^3} - \ldots - \Delta x\right)^2}, \qquad (2.9)$$

where ρ is a point on the part surface, Δx and Δy are the tool offset and tool height error respectively, and r is the radius of curvature of the surface. Equation(2.9) shows that the dominant factor of form accuracy is the tool offset Δx. This relationship was also verified through the aforementioned cutting tests. These results are shown in Figure 10.

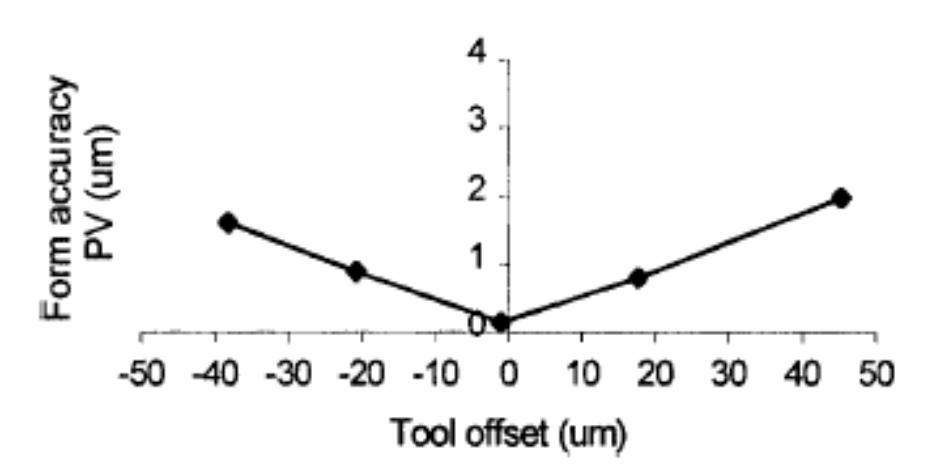

Figure 10-Variation of form accuracy, z, with tool offset (Zhou 2001)

Therefore a tool set station is implemented to determine the tool offset error and account for it. The tool-setting station is mounted to provide a reference point. The reference point is determined by permanently mounting a gage bar to one of the tool stations on the turret. An LVDT (linear variable differential transformer) is used to measure the position of the tool in the X and Z direction with respect to this reference point.

Cutting Forces and Vibrations

The vibrations involved in a machining process can play a major role on the work piece, mainly with respect to its surface finish. These vibrations are primarily caused by structural vibrations and friction. The structural vibration is dependent on the cutting process. Much research has been conducted to determine the vibrations associated in the machine tool due to cutting force. Thomas (2003) provides detailed methods in determining the amplitude of these vibrations through the means of an accelerometer and FFT. The cutting force analysis includes the steady state forces, random cutting forces, and harmonic cutting forces. The cutting tool was provided with strain gages and a tri-

axial accelerometer to measure accelerations in feed, cutting directions, and in the thrust directions.

Homogeneous Transformation Matrix (HTM)

A homogeneous transformation matrix (HTM) must be created to transform the actual tool path to the desired tool path. Slocum provides a detailed method in defining the spatial relationship between the tool point and the work piece through the use of a HTM. It is easiest to first present the HTM and then explain it:

$$R_{T_n} = \begin{bmatrix} O_{ix} & O_{iy} & O_{iz} & P_x \\ O_{jx} & O_{jy} & O_{jz} & P_y \\ O_{kx} & O_{ky} & O_{kz} & P_z \\ 0 & 0 & 0 & P_s \end{bmatrix} \tag{2.10}$$

The first three columns represent the orientation of the rigid body's X_n, Y_n, Z_n axes with respect to the reference. The last column represents the rigid body's coordinate system's origin with respect to the reference frame. The subscripts can be explained as follows: the first represents the desired reference frame while the second represents the original reference frame. The case for simultaneous motions in the work space can be represented as a combinational method. The HTM's of the translations and rotations of the coordinate system along each principal axis are multiplied in series with the error terms of each axis. For brevity purposes, only the results will be shown, the derivation can be found on pages 62 to 66 of reference Slocum (1992). The resultant error in position with respect to the desired position will be:

$$E_n = \begin{bmatrix} 1 & -\varepsilon_z & \varepsilon_y & \delta_x \\ \varepsilon_z & 1 & -\varepsilon_x & \delta_y \\ -\varepsilon_y & \varepsilon_x & 1 & \delta_z \\ 0 & 0 & 0 & 1 \end{bmatrix} \tag{2.11}$$

This error is with respect to a reference frame at the origin. Therefore the actual HTM for linear motion is RT_nE_n:

$$R_{T_{nerr}} = \begin{bmatrix} 1 & -\varepsilon_z & \varepsilon_y & a+\delta_x \\ \varepsilon_z & 1 & -\varepsilon_x & b+\delta_y \\ -\varepsilon_y & \varepsilon_x & 1 & c+\delta_z \\ 0 & 0 & 0 & 1 \end{bmatrix} \tag{2.12}$$

Where a, b, c are offsets in the x, y, and z direction respectively. Using the same methodology, the axis of rotation errors will be:

$$R_{T_{nerr}} = \begin{bmatrix} \cos\theta_z & -\sin\theta_z & \varepsilon_y & \delta \\ \sin\theta_z & \cos\theta_z & -\varepsilon_x & \delta \\ \varepsilon_x \sin\theta_z - \varepsilon_y \cos\theta_z & \varepsilon_x \cos\theta_z + \varepsilon_y \sin\theta_z & 1 & \delta \\ 0 & 0 & 0 & 1 \end{bmatrix} \tag{2.13}$$

The previous derivations assumed that the second order effects were negligible. This will be the case for the scope of this research because we do not seek nanometer performance levels. Therefore an HTM of similar appearance will be developed for the machine tool used in this research.

Tool Path Correction

There has been extensive research in tool path correction via error compensation NC code. A number of methods for the prediction and compensation of the desired tool path have been proposed. The common objective of each method is defining the error in the nominal relationship between the tool and the work piece. Kiridena and Ferriera (1994) developed a method for a three-axis machining center using a rigid body kinematic model. They developed a quasi-static error model that is a function of the error component of each axis. Anjanappa (1988) developed two methods for error

compensation of cutting force under the rigid body assumption. This paper addressed the development and experimental validation of a cutting force-independent tool path error correction methodology.

One method involves the machine controller altering the machine code based upon compensation, while the other describes how to tilt and translate a magnetic bearing spindle for real-time correction. Of more relevance is Wang, Liu, and Kang's (2002) error compensation model. Since the nominal cutting path is given in a form of NC code, the compensation software identifies the coordinates of the cutting trajectory and uses them as inputs for error predictions. It is assumed at this point that the causes of error at the tool tip are found (including geometric errors of the axis, deflections caused by static and dynamic cutting forces and thermally induced deformations).

A finite element model is implemented to provide the error at points within a defined workspace. This work space is divided into smaller three dimensional elements. The error and stiffness at arbitrary positions in every element can be interpolated once the local nodal points of these elements have been defined for errors and stiffness. This transition is accomplished through the use of shape functions and interpolation methods. It is noted that if the errors are compensated once, the tool will not reach the desired position, therefore the software must be recursive. These iterations are performed until the actual and desired positions are very close (defined by a predetermined tolerance on the position error). The following equations correspond to this iterative process:

$$U_c(I) = U_d + \sum_{i=1}^{I-1} \delta(i) = U_c(I-1) + \delta(I-1) \tag{2.14}$$

$$U_a(I) = U_c(I) + \Delta(U_c(I)) \tag{2.15}$$

$$\delta(I) = U_d - U_a(I). \tag{2.16}$$

Where δ(I) is the difference between the actual and desired position, U_c is the compensated position, and U_a is the actual position. Figure 11 provides the software scenario

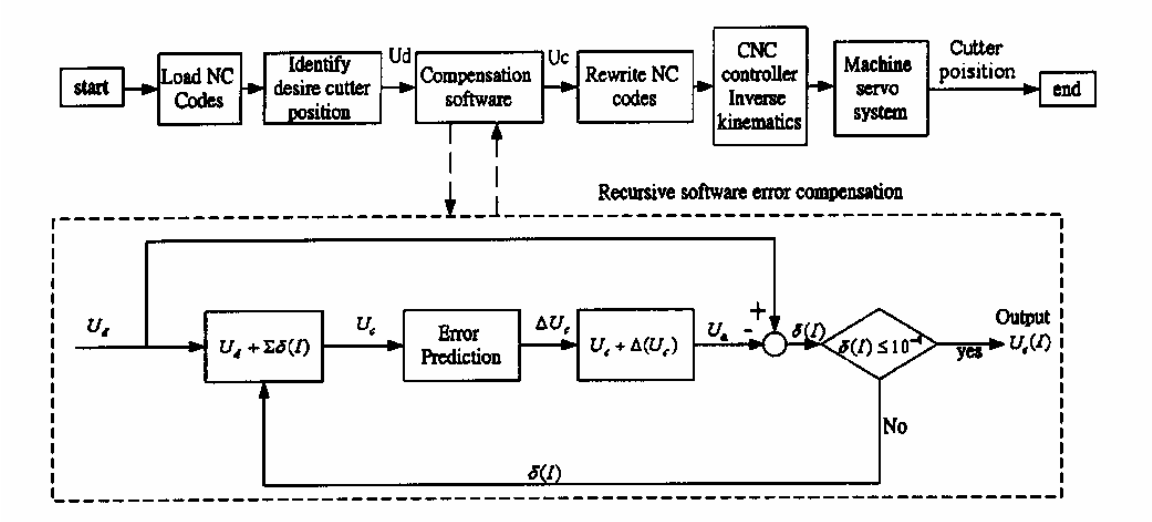

Figure 11- Software compensation schematic (Anjanappa 1998)

The NC program provided the desired positions of the cutter by interpolation of the cutter trajectory. A C^{++} identifying and rewriting system was used to develop and extract the nominal positions of the cutter for error prediction and correction. When this was determined, the software updates the NC program with the error-compensated position.

Experiments of practical cutting with and without the software were performed to verify the software. It was shown the machining accuracy in the Δx path was improved from 254.4 μm to 22 μm and from 159.6μm to 22.7μm in the Δy direction. This paper also noted that the resolution of the workspace is an important parameter. Increasing the amount of sampled points increases the prediction accuracy, but causes a larger

computation time. Therefore the number of sampled points should be based on accuracy requirements.

CHAPTER III

EQUIPMENT

Okuma Howa Vertical Lathe

A CNC vertical lathe requires a spindle to rotate the work at speeds reaching 3000rpm, while simultaneously requiring the machine tool to be positioned in such a manner to remove material and produce an accurate part. This researched used the Okuma Howa Vertical Lathe (shown in Figure 12).

Figure 12- Okuma Howa V40R

The work volume specifications of this machine are presented in Table 1. It is quite obvious that this lathe is vertical due to the configuration of the spindle and tool turret. The specifications of the spindle are provided in Table 1.

Table 1- Specifications of the Okuma Howa Lathe (Okuma Website)

MAIN Spindle Direction	Vertical	
X-axis Travel	10.43''	264.92 mm
Z-axis Travel	17.72''	450.08 mm
X-axis Thrust Force	1,257 lbs	
Z-axis Thrust Force	2,698 lbs	
X-axis Ballscrew Diameter/Pitch	1.57''/0.47''	39.88/11.94 mm
Z-axis Ballscrew Diameter/Pitch	1.97''/0.47''	50.04/11.94 mm
X-axis Positioning	0.0006''/3.94''	0.0152/100.08 mm
X-axis Repeatability	0.0001''	±0.00254 mm
Z-axis Positioning	0.0009''/11.81''	0.02286/299.9mm
Z-axis Repeatability	±0.0002''	±0.00508 mm
Minimum Input Increment	0.0001''	0.00254 mm

Laser Interferometer

A laser interferometer was required to determine the linear and angular errors of the axes of the vertical lathe. An HP5529A laser interferometer was used to determine these errors. Figure 13 shows the laser interferometer system mounted on a tripod. The specifications of the laser interferometer are displayed in Table 2.

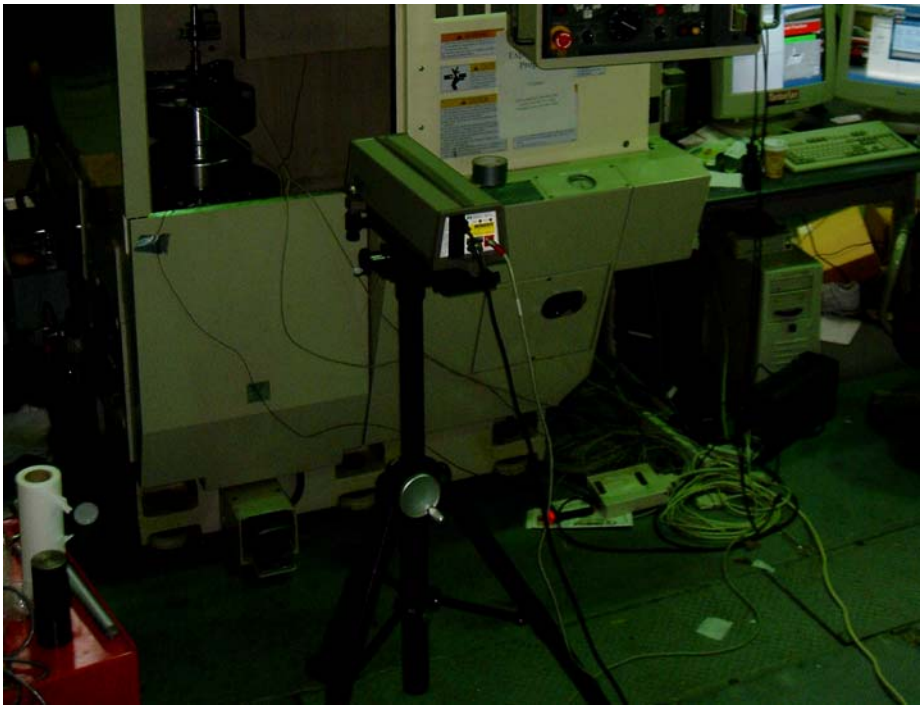

Figure 13- Laser Interferometer on tripod

Table 2- Laser Interferometer Specifications (HP)

Characteristic	Specification
Type	helium-neon with automatically tuned Zeeman-split two-frequency output
Warm-up time	less than 10 minutes (typically 4 minutes)
Operating temperature	0° to 40° C (32° to 104° F)
Power requirements—laser head	100 to 120 Vac, 48 to 66 Hz and 400 Hz; 220 to 240 Vac, 48 to 66 Hz; 50 W during warm-up,
Vacuum wavelength Wavelength accuracy	632.991354 nm ± 0.1 ppm
Short-term (1 hour) wavelength stability	± 0.002 ppm typical
Long-term (lifetime) wavelength stability	± 0.02 ppm typical
Maximum output power	1 mW
Beam diameter	6 mm (0.24 in)
Beam centerline spacing	11.0 mm (0.43 in) input to output aperture
Safety classification	Class II laser product conforming to U.S. National Center for Devices and Radiological Health Regulations 21 CFR 1040.10 and 1040.11

Renishaw QC10 Ball Bar

Resolution	0.1 µm (4 µin)
Ballbar Sensor Accuracy	± 0.5 µm (at 20 °C) ± 20 µin (at 68 °F)
Maximum Sample Rate	250 values per second
Extension Bars Available	50, 150, 300 mm (1.97, 5.9, 11.8 in)
Operating Range	0-40 °C (32-104 °F)

Coordinate Measurement Machine

A coordinate measurement machine (CMM) was used to inspect the test parts. A CMM is a metrology apparatus that uses a touch-trigger probe to acquire data about the part. The Brown & Sharp MicroVal Pfx CMM (Figure 14) is a vertical bridge type machine which was operated in direct computer control. The specifications of the machine are presented in Table 3 (Brown & Sharpe 1991).

Figure 14- Coordinate Measurement Machine (CMM)

Table 3- Specifications of the Brown & Sharpe Microval PFx CMM

Specifications	Metric
Repeatability B89 5.3.3.1 Band	0.003 mm
Volumetric Accuracy B89 5.5.2 Band	0.010 mm
Linear Accuracy B89 5.4.3 Band	0.005 mm
VDI/VDE U1	3+3L/1000
VDI/VDE U2	3+3L/1000
VDI/VDE U3	3+4L/1000
Resolution	0.001 mm
Display Range	± 9999.999 mm
Throughput	40 hits/minute
Tunnel Diameter	0.3 mm
Range XYZ**	457 x 508 x 406 mm
Length	1093 mm
Width	940 mm
Height on Base	2388 mm
Weight (complete system)	727 kg
Weight (machine only)	205 kg
Weight (granite work table)	114 kg
Weight (machine stand)	341 kg
Weight (computer)	68 kg
Shipping weight (2 boxes)	841 kg
Part weight capacity	227 kg
Part size capability (Y,X,Z)	750 x 559 x 452 mm

** Machine range when using 76.2 mm long probe

CHAPTER IV

METROLOGY PROCEDURES

The previously described equipment requires specific procedures and guidelines in order to obtain proper results. The purpose of this section is to provide a condensed version of these procedures for each of these metrology tools.

Interferometer

Basic Guidelines

The HP 5529 heterodyne interferometer was used under specific procedures to ensure correct measurements were made. There are a set of guidelines that should be adhered to before making a new measurement; they are as follows (HP Manual).

- Determine the travel limits for each axis you will make measurements on.
- Determine the start position for each axis. Also, determine which direction is positive and which is negative.
- Determine if the controller requires incremental or absolute errors
- Determine the machine's least programmable resolution unit.
- Determine which format the Agilent 10747A Metrology Software should use for its output.
- In determining the measurement interval, choose an interval that is not a multiple of the pitch of the lead screw. This is so periodic errors are accounted for.

These guidelines were applied to the software setup that accompanied the interferometer. These guidelines were applicable to each of the measurement types, both linear and angular. The basic principles remained constant while only the optical set up changed. Measurements were only made in the sensitive directions of the machine and with in the appropriate work volume.

Interferometer Software and Sensor Setup

The HP5529A used the provided software package to acquire data. There are several parameters that require the users input. The environmental conditions affected the accuracy of the laser interferometer. These environmental conditions consisted of air temperature, air pressure, and relative humidity. These conditions were compensated for by inputting the value of each parameter into the software package via a dialogue box, "Set Up Environmental Conditions". These values can be entered in manually by the operator or acquired continuously through the optional air and material sensors. These sensors were placed according to strict guidelines to ensure that the software compensation can accurately adjust the measurement values for each experiment:

- Place the air sensor as close to the path of the actual measurement as possible. The sensor must not be placed directly below the laser beam because it will act like a heat source and distort the measurement.
- The humidity switch should be placed to the closest relative humidity of the room enclosing the machine tool.
- Place the material sensors in positions corresponding to technical calibration codes such as ANSI B-5 (refer to Figure 15 for example).

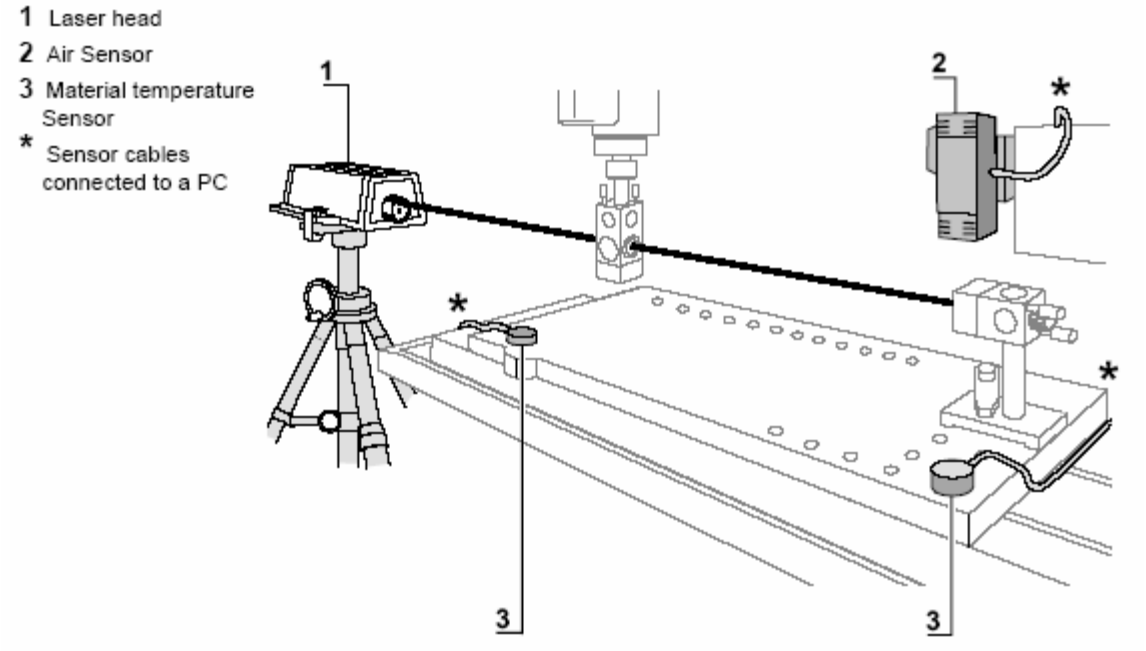

Figure 15-Example of proper sensor placement (HP)

Mounting and Aligning Optics

The origin of the laser beam is the laser interferometer, therefore the laser head should be close to the same height as the optics. The placement of the optics followed these two guidelines:

- Mount one optic on the tool turret and the other optic on the spindle. The interferometer assembly must be between the retroreflector and the laser head.
- For measurements along an axis perpendicular to the laser beam (with respect to the original beam path), mount the interferometer assembly on a stationary part of the machine.
- An interferometer assembly consists of the combination of an interferometer and a retrorefelctor (these optical components are shown in Figure 18). A retroreflector was placed upon an interferometer such that

one of the arrows on the interferometer label pointed toward the retroreflector (as shown in Figure 16).

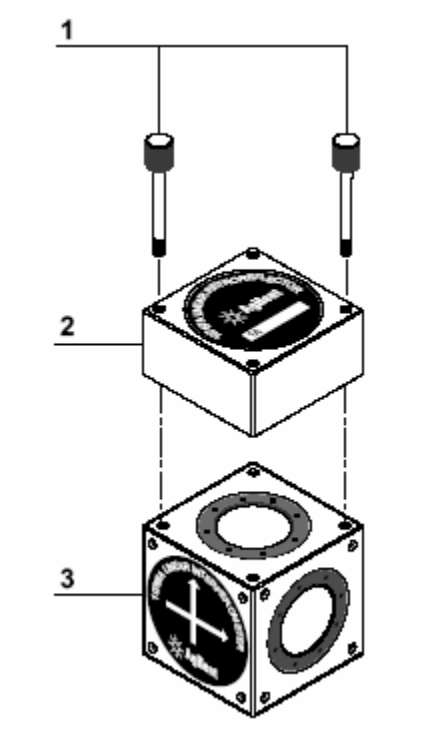

Figure 16- Interferometer assembly (HP manual)

This assembly was then mounted on the machine using posts, bases, and height adjusters such that the arrow that does not point to the retroreflector pointed away from the laser head. The optics was mounted according to their specific optical configuration (these configurations are shown in the following sections because they are dependent on the measurement of interest).

The next crucial step (and also most time consuming) was to align the optics. The alignment process requires the laser heads upper port to be set to the small aperture (as shown in Figure 17).

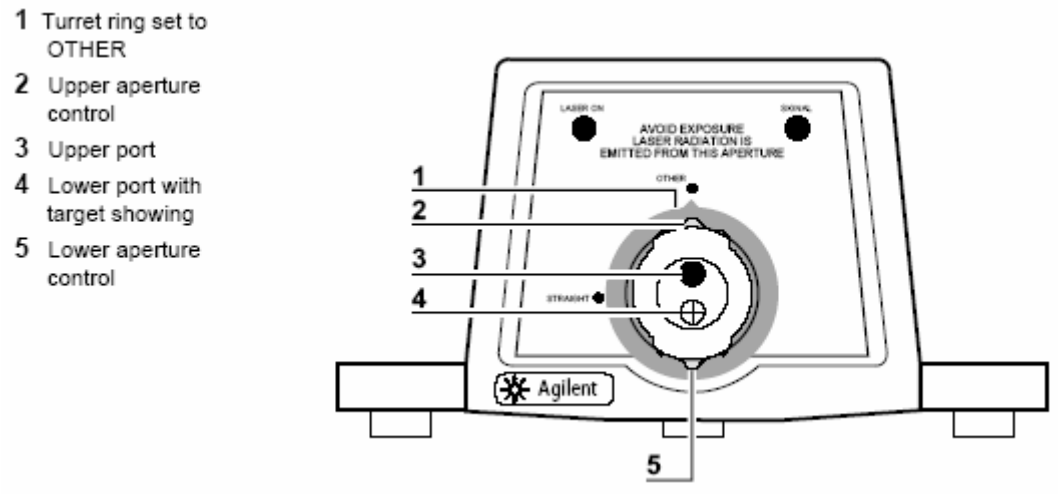

Figure 17- Front view of the laser head (HP manual)

The lower port should be rotated such that the target is showing and the laser head's turret ring should be set to other. The laser head unit itself should be adjusted so that the laser beam enters the lens of the interferometer and the return beam is near the laser head. The goal of this alignment was achieved when the exiting laser beam and the entering laser beam are coincident. This was achieved by moving the laser head or moving the optical components (specifically, the interferometer assembly). The returning laser beam appeared as a dot on the front of the laser interferometer. Sometimes the optics was initially misaligned enough that returning beam will not even appear on the front. It was helpful to take a sheet of white paper and impose it over the front of the laser interferometer with the surface of the paper perpendicular to the return path. Of course a hole of proper size was cut so the exiting laser beam can travel through the optical set up.

The retroreflector was moved as close to the interferometer as possible (this will be the start position). The retroreflector was adjusted so that the return beam was centered on the target covering the laser head's return port. The scope of this procedure

was for short range measurements (less then 355.6 mm) because the work volume of importance never exceeded this value in any dimension.

Displacement Measurements

There are two main classes of measurements: displacement and angular. The previous section that consisted of optical alignment and initial guidelines was accommodated to displacement measurements; however it will be sufficient for angular measurements. The displacement measurements included straightness and linear measurements. Each measurement required a specific set of optical components and proper configuration of these components. For example, linear measurements required a linear retroreflector and a linear interferometer. The linear and optical components are shown in Figure 18 and Figure 19.

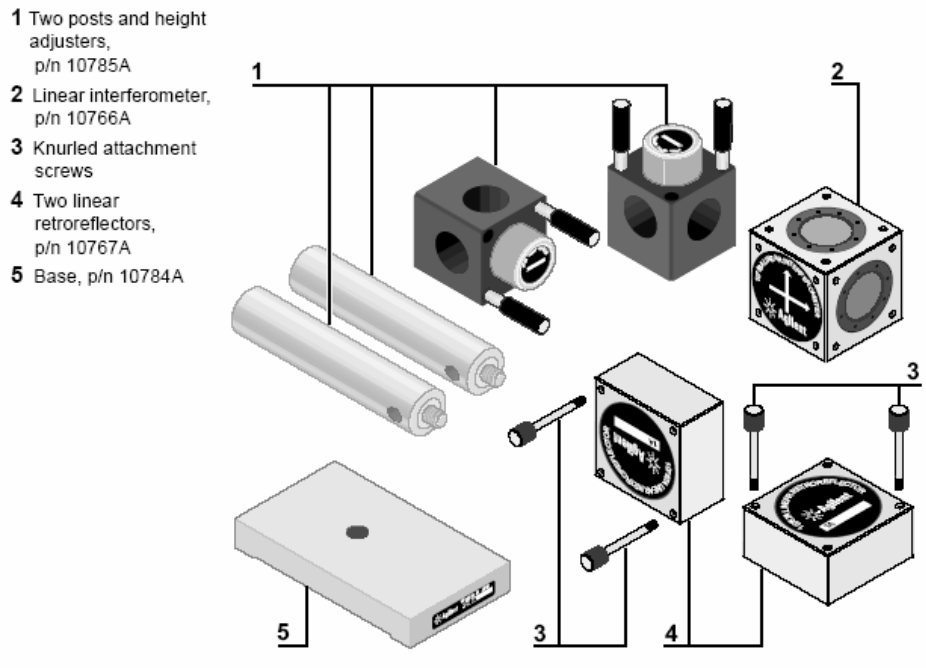

Figure 18-Required hardware for linear measurements (HP manual)

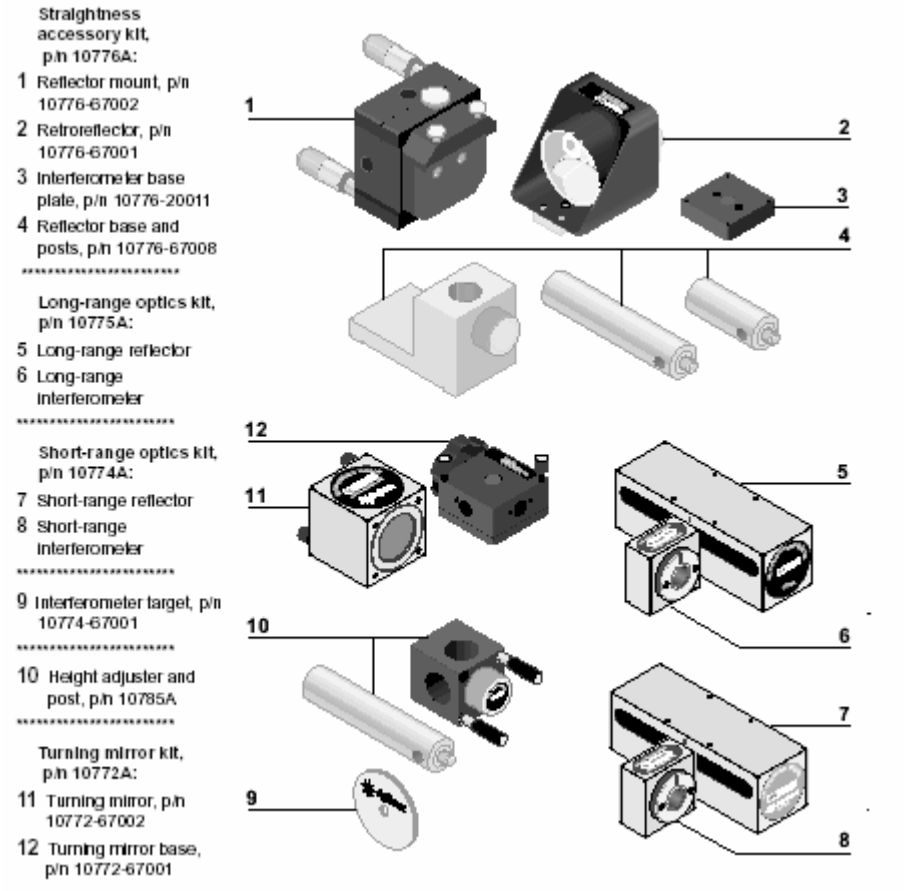

Figure 19-Required hardware for straightness measurements (HP manual)

An appropriate optical configuration must be implemented once the proper components have been determined. Figure 20 shows a generic arrangement of the optical components for a typical beam path in displacement error measurements.

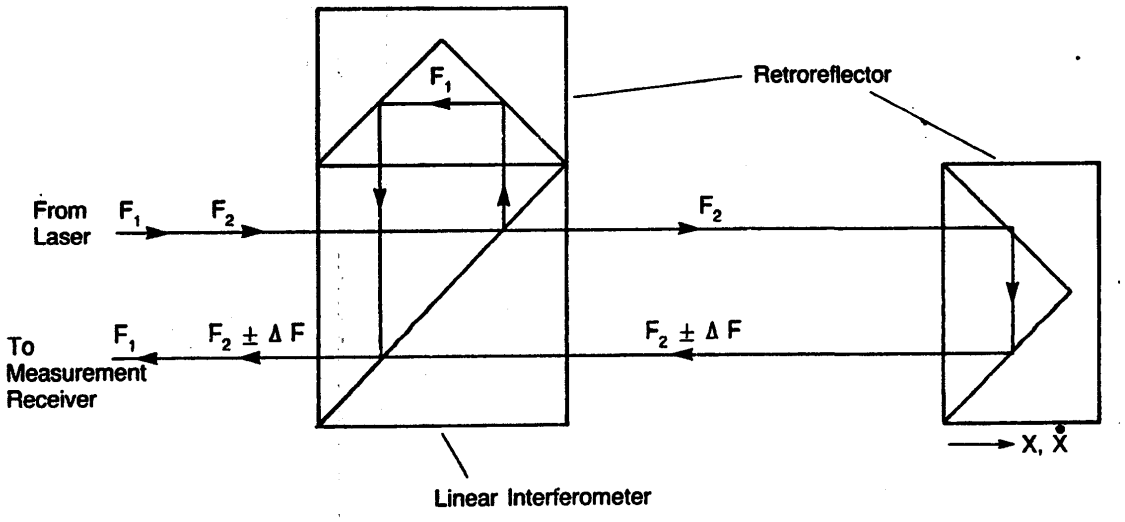

Figure 20- Optical configuration for displacement measurements (Donmez 1985)

Generally speaking, it is now easy to visualize how displacement measurements are made. For example, picture the retroreflector in the right of Figure 20 mounted to the end of a vertical tool turret. The tool turret was moved along the x-axis and data determined by the interferometer and software set up was collected. A schematic for straightness measurements is shown in Figure 21.

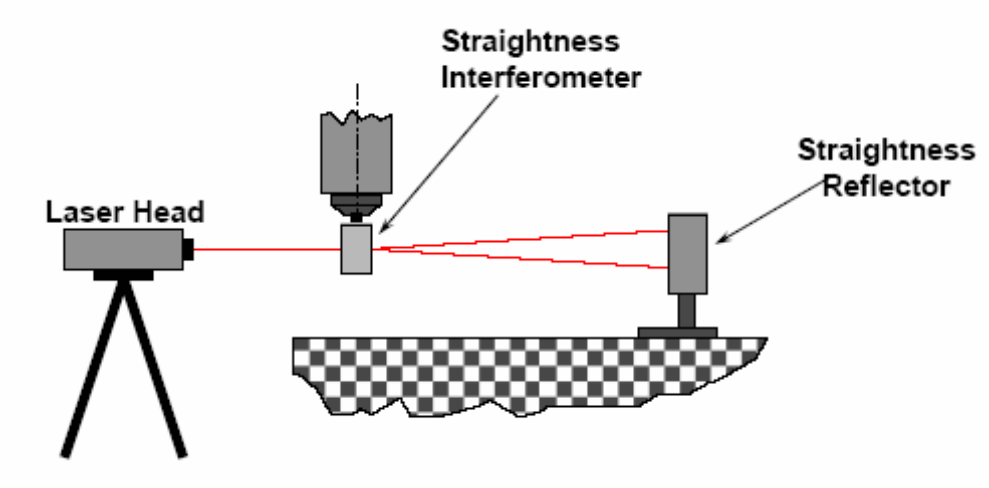

Figure 21- Schematic of beam path in straightness measurements (Kurfess)

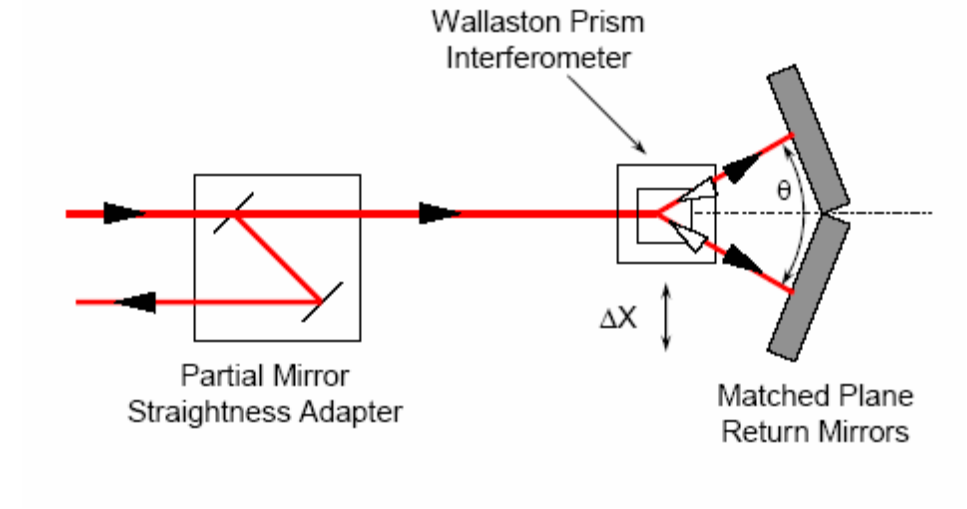

Figure 22- Straightness measurement (Kurfess)

Angular Measurements

Angular measurements contained similar protocols that were used for displacement measurements. The difference between displacement and angular error measurement is that different optical components are mounted on the spindle and tool

turret. An angular retroreflector was mounted on the tool turret. The typical beam path for angular error measurements is shown in Figure 23.

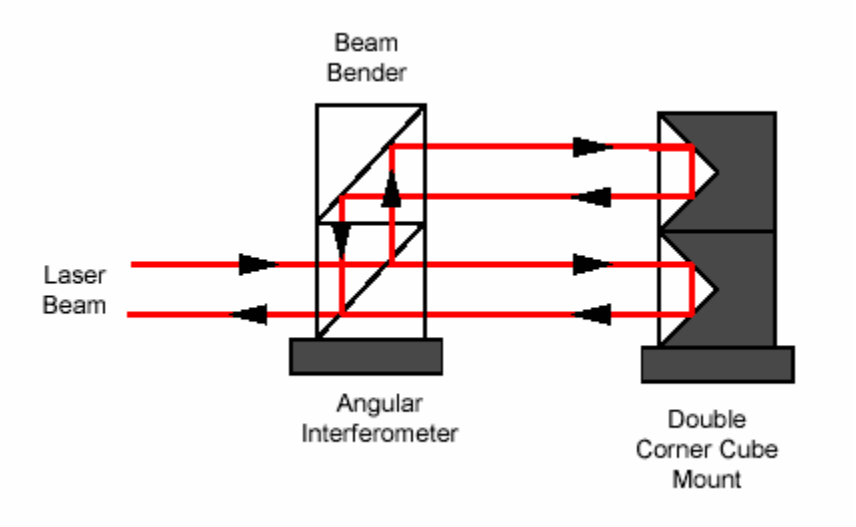

Figure 23-Optical configuration for angular measurements (Kurfess)

Ball Bar

The ball bar was a much simpler metrology tool to operate then the laser interferometer. The ball bar system used was the Renishaw QC10 ballbar system which is shown in Figure 24.

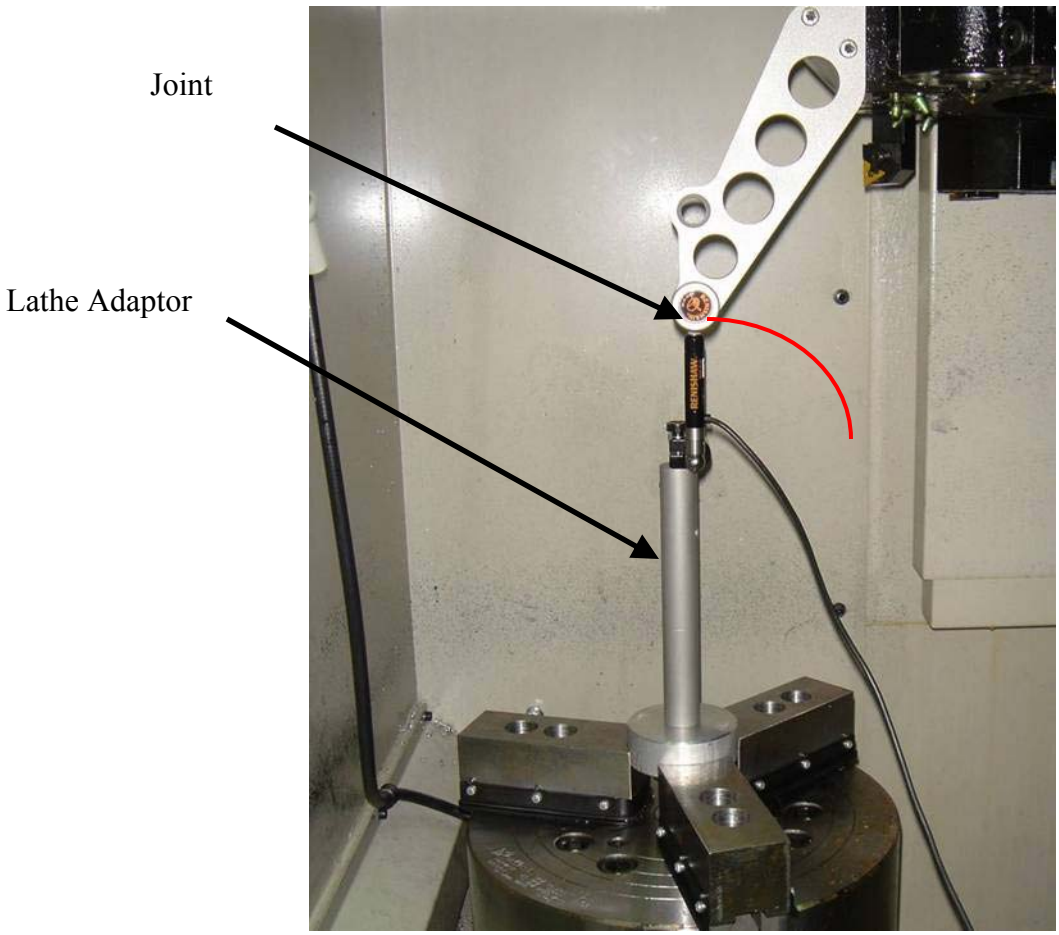

Figure 24-Ball Bar system setup

The Renishaw QC 10 ball bar system was designed for a horizontal lathe, thus a vertical lathe adaptor was required in order for implementation in the machine tool. Essentially (as previously discussed) the machine tool moved in a desired arc with nominal radius set to the length of the ball bar. The ball bar then recorded deviations from the nominal while the ball bar rotated around a fixed sphere. This sphere was the center of the radius of the path the machine tool followed. Therefore the tool offsets programmed into the machine tool are equal to the center of this sphere. To accomplish this, the end of the lathe adaptor is brought to close proximity of the sphere. There is a mechanical element that interfaces

the lathe adaptor to the sphere called the joint. The joint can be screwed into the lathe adaptor to touch the sphere and then unscrewed to allow for the machine tool to travel without disturbing the position of the sphere. Thus the lathe adaptor was connected to the sphere and the tool offsets are recorded. The interfacial element was then unscrewed and the lathe adaptor was brought to the feed in position. This was the position shown in Figure 24. The ball bar was first calibrated then attached on one end to the sphere and the other end to the interfacial element. The data collection program was then executed and the machine tool moved in a radius of 100mm at a feed rate of 39.37 mm/min. The collected data and plots are shown in the results section.

CHAPTER V

THERMAL ANALYSIS

This chapter outlines the ever so important thermal study of the machine. Thermal errors from temperature rise can contribute 40-70% of the precision errors in a turning center et al Tseng (2001). The thermal time constant of a machine presents crucial information on when the machine has reach thermal steady state. Thermal deformation of the machine is negligible once this state has been achieved. This analysis provides insight as to when experiments should be executed. For example, if machine tool errors are to be compared between a cold and hot state, then experiments will need to be run when thermal steady state has been achieved. The term cold refers to the initial thermal state of the machine tool; while hot refers to the thermal steady state of the machine tool.

The thermal behavior is of a first order model et al Palm (1999). The temperature for the warming up period can be described by the following equation:

$$T_{warm} = T(1 - e^{-t/\tau_w}) + T_{atm} \tag{5.1}$$

where T is the system gain, τ_w is the time constant and T_{atm} is the offset temperature. The time constant represents the amount of the time system requires to achieve 62.5% of thermal steady state. Similarly, the temperature for the cooling down period can be described by the following equation with T (0) in this case being the steady state temperature and τ_c is the amount of time required to reach 62.5% of steady state:

$$T_{cool} = T(0)e^{-t/\tau_c} + T_{atm} \tag{5.2}$$

Intuitively speaking, one may think that the thermal time constants for the warming up period and cooling down period should be the same. In this situation different thermal behaviors were exhibited during heating then cooling. Figure 25 and Figure 26 show a simplified schematic of the mechanical system (i.e. spindle or axis slide) during heating and cooling respectively.

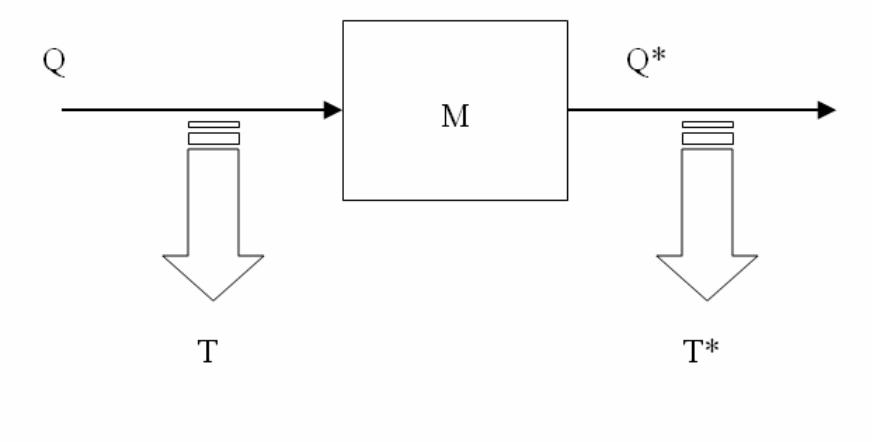

Figure 25- Schematic of system for heating

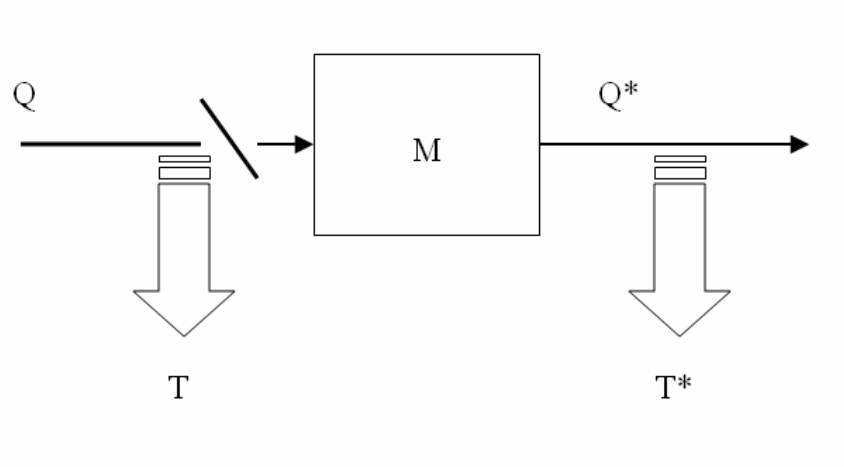

Figure 26-Schematic of system for cooling

M represents the lumped system that contains the temperature of interest (spindle or slide), Q represents the heat into the mechanical system and Q* the heat out of the mechanical system. T represents the heat that does not make it to the mass because of the environment and T* represents the heat into the environment after it is transferred into the lumped system M. The heating process includes a heat source that sheds some heat into the environment before it reaches the lumped mass. The heat that is conducted into the mass is then transferred to the environment. The cooling process involves the heat source Q to terminate and thus the "stored" heat in the lumped mass M dissipates into the environment. So in the first case there is a heat source that transferred some of its heat to the lumped mass, M while in the second case Q is equal to 0 and the heat stored in the mass is dissipated into the environment. This explains why b_w will differ from b_c.

The experimental setup basically involved placing a thermal couple in locations of interest around the machine. More specifically, a T type thermal couple was connected to a DAQ board, which in turn was connected to a computer where LabView ™ was used to collect temperature data. This data was then stored in a personal computer file. A temperature reading was recorded every second while the machine was warmed up then cooled down at the termination of the warm up period. The locations of interested are shown in the following figures. These locations were chosen because they develop the thermal behavior of the machine most accurately. These locations also contributed the most to the thermal change of the machine.

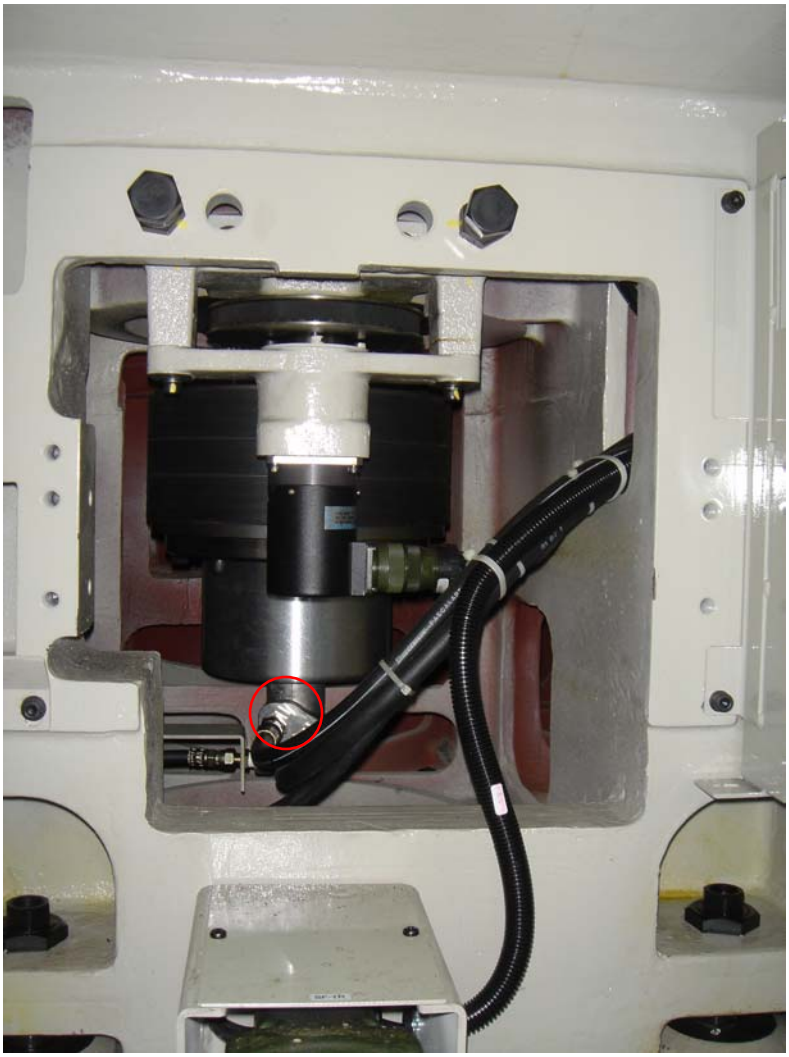

Figure 27- Thermocouple placed on the spindle housing

Of course the thermocouple could not be placed on rotating portions of the spindle. Therefore, it was placed as close as possible to the rotating elements of the spindle (reference Figure 27). The experimental spindle speed was chosen to be 1000 rpm. Also, the spindle speed does not influence the thermal time constant (the time constant represents the amount of time it takes a system to reach a certain percentage of a final value). Varying the spindle speed varies the temperature range; however it does not vary

the time to reach a percentage of its final value. Temperature data was collected while the spindle was at a speed of 1000 rpm for four hours. The spindle was then stopped, commencing the cooling period and cooling data was then collected. This experiment was repeated several times and the average of the values were plotted in Matlab™. The program cftool was used to fit a curve to the data. This program required a type of fit to use with the data.

Due to the nature of the experiment, the sampling rate chosen was 1 Hz. The actual temperature would not fluctuate significantly between data points at this sampling rate. Unfortunately there was a large amount of noise in the system. An oscilloscope was used to determine the source of the noise. When the thermocouple was hooked directly to the oscilloscope the reading was a clean tight signal that did not fluctuate as significantly as the signal in Labview™. Thus, the electrical noise must be located in the A/D card. The oscilloscope was used to verify this.

Temperature data were acquired for the spindle using a low pass filter. The following figure shows warm up and cool down data with the respective curve fits for 1000rpm spindle speed.

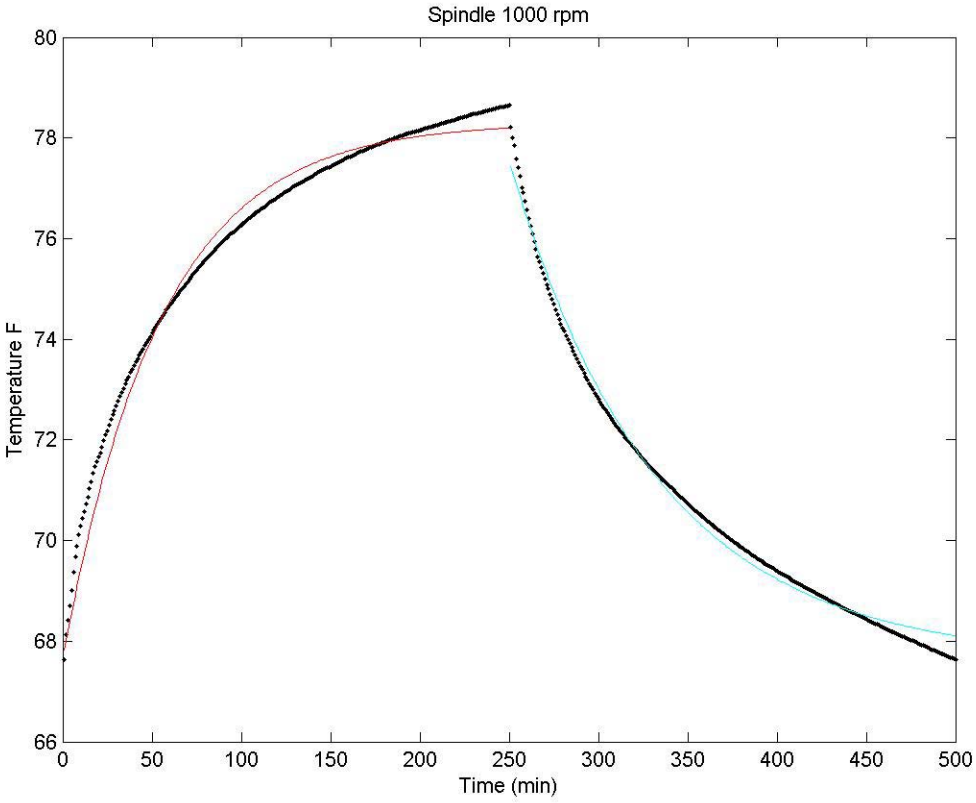

Figure 28- Warm up and cool down data of the spindle for 1000 rpm

(5.3) and (5.4) represent the warm up and cool down temperature versus time for the spindle respectively:

$$T_{warm} = 9.913\left(1 - e^{-\frac{t}{54.59}}\right) + 67.64 \tag{5.3}$$

$$T_{cool} = 9.91e^{-\frac{t}{81.97}} + 68.05 \tag{5.4}$$

Therefore, it takes the machine 54.29 minutes to achieve 62.5% of thermal steady state and 81.97 minutes to achieve 62.5% of the steady state temperature on cool down.

The previous text described the thermal behavior of the spindle. The following text will conclude the thermal analysis of the machine tool with results of temperature data collected from the z and x axis slides. These are two very important points of thermal interest because they dominate the thermal behavior of the machine tool. Figure 29 shows the location of the thermal couple for the z axis.

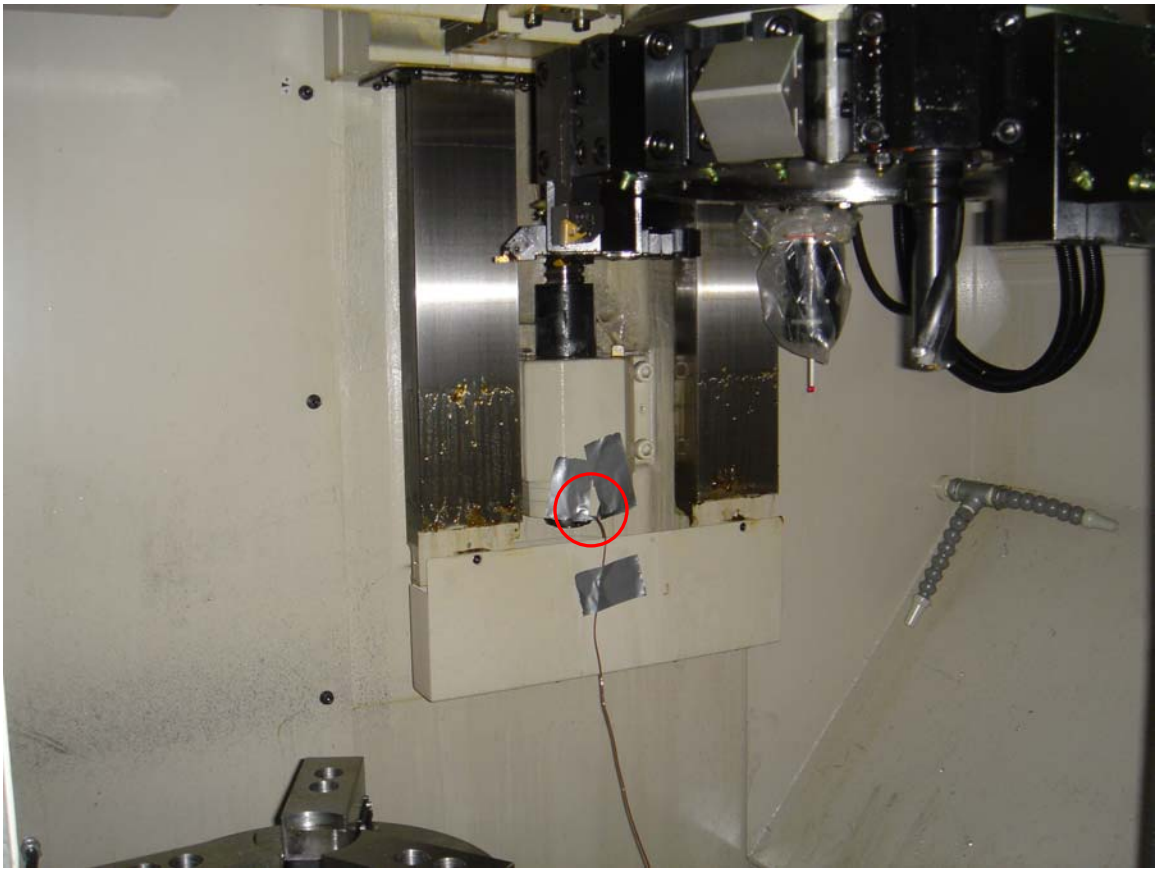

Figure 29- Location of thermocouple for the z-axis

The data collection scheme followed the same process as that for the spindle temperature data collection. Of course in this case the feedrate was varied, which is synonymous to

the spindle speed in the spindle temperature data collection. The following figure shows the thermal behavior of the z-axis for a feedrate of 2.54 m/min (100 in/min).

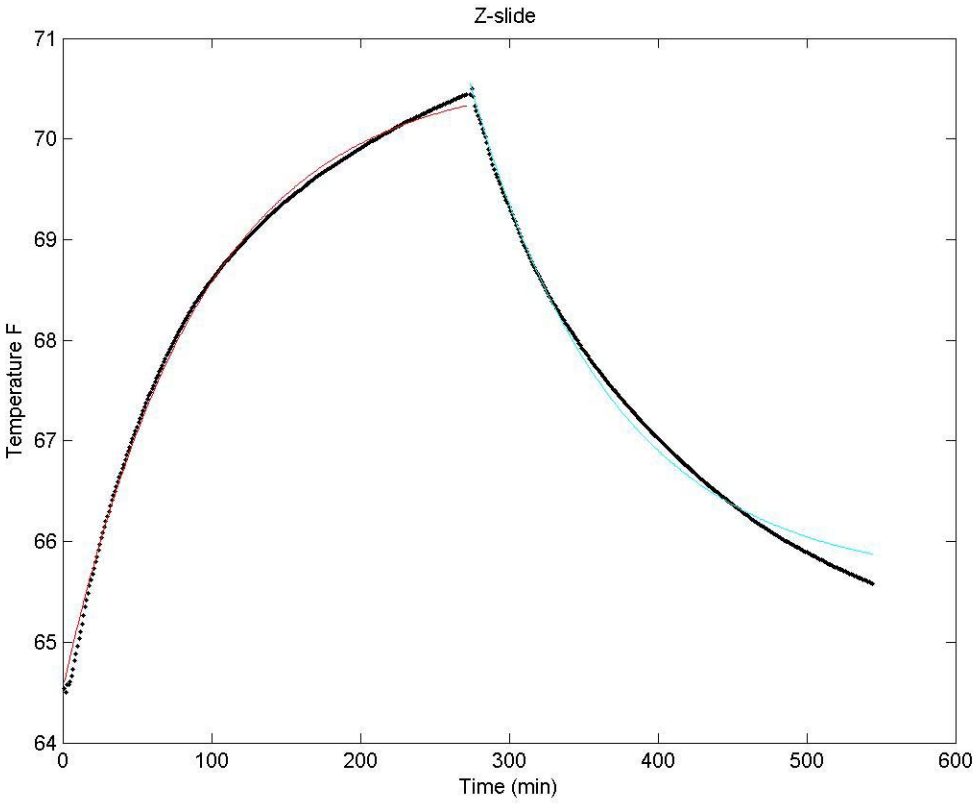

Figure 30-Warm up and Cool down behavior for the z-axis (f=2.54 m/min)

(5.5) and (5.6) represent the warm up and cool down temperature versus time for the z axis slide respectively:

$$T_{warm} = 6.12\left(1 - e^{-\frac{t}{92.59}}\right) + 64.53 \tag{5.5}$$

$$T_{cool} = 5.01e^{-\frac{t}{95.24}} + 65.28 \tag{5.6}$$

The time constants for warm up and cool down are 92.59 minutes and 95.24 minutes respectively.

The cross slide was much more difficult to locate a point of thermal interest that was accessible. The ball screw and bearing for the x-slide were in a location that prohibited a thermal couple to be properly mounted.

CHAPTER VI

BALL BAR RESULTS

Experimental Results-Ball Bar

The ball bar system was used according to the aforementioned protocols. The part program used in conjunction with the ball bar system caused the ball bar to rotate two complete revolutions at a federate of 39.37 mm/min in two directions. Thus, the ball bar was feed in from an initial position and then rotated counterclockwise for two rotations. The ball bar was then feed out and feed in again for a clockwise rotation to occur for two revolutions. Figure 31 and Figure 32 show the results of the ball bar experimental tests via Renishaw's software application. The cold state means the ball bar was used a significant amount of time after the most recent use of the machine tool.

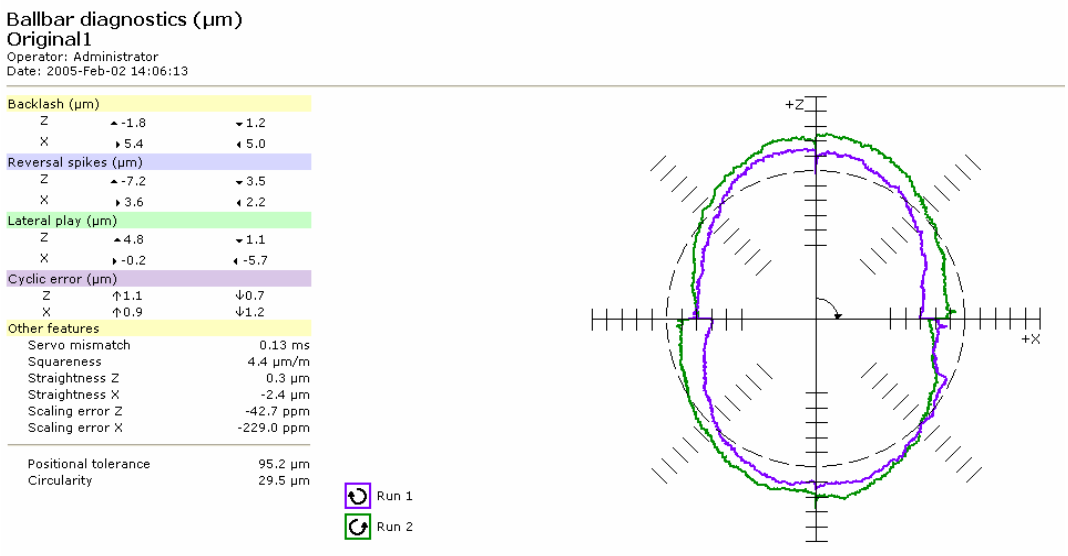

Figure 31- Ball Bar Errors for cold state 5µm/div

The term hot state means that the machine tool was warmed up so that it achieved thermal steady state. The manner in which the machine tool was warmed up is that the spindle was turned on for 2 hours at a speed of 1000 rpm (which corresponds to the thermal analysis that suggest thermal steady state will be achieved at this point). Figure 32 shows the results of the ball bar for thermal state.

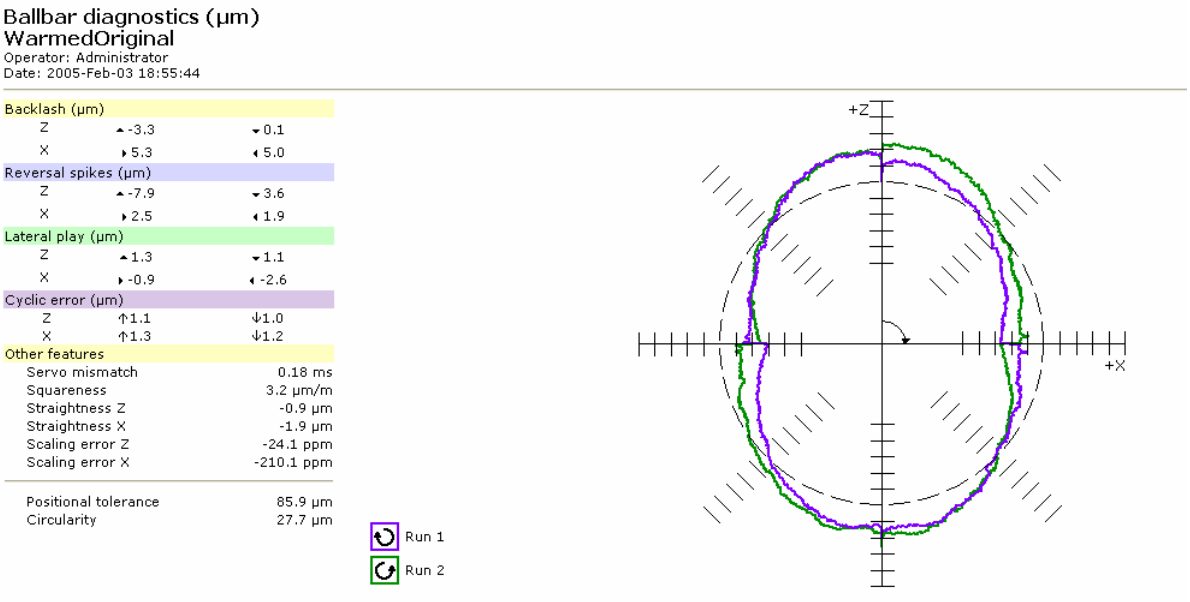

Figure 32- Ball Bar errors for hot state (5 µm/div)

Ball Bar Compensation Case Study

A case study was conducted during this research. A question was raised to suggest that the ball bar data could be used solely to correct for an arc made by the

machine tool from 0 ^{o} to 90^{o}. More generally speaking, could the error measurement from the ball bar significantly compensate the actual tool path to the desired tool path? Thus, the errors from the ball bar results in Figure 31 were obtained. This data were used to create offsets at each sample point. This would ideally cancel out the error at each point however the ball bar results are not absolutely repeatable. The following schematic in Figure 33 shows the hypothetical tool paths.

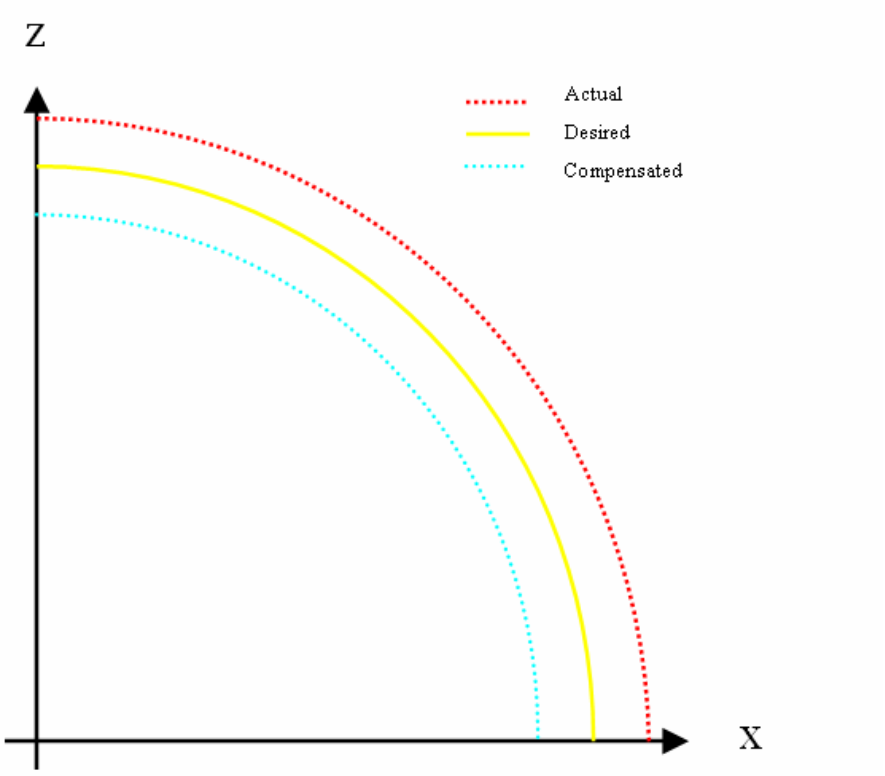

Figure 33 Schematic of tool paths

The desired tool path is known along with a good approximation of the actual tool path (from the ball bar system); therefore a compensated path was constructed. The following equation describes this construction at each point P along the tool paths.

$$P_{Compensated} = P_{desired} - P_{Actual} \tag{5.7}$$

Each data point was properly offset to created compensated data. The data was then fit to a new circle using MetroloGT and used to create a new Gcode using the alter radius and center.

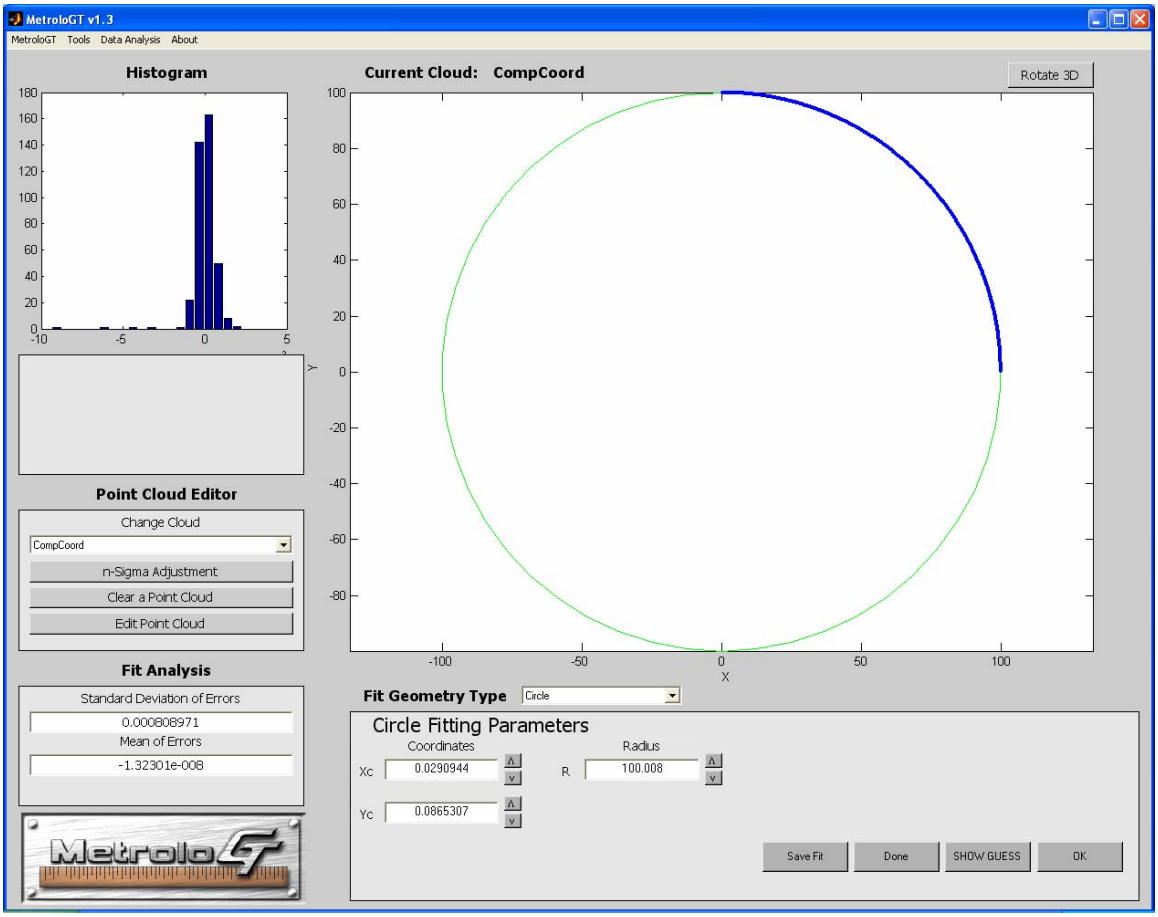

Figure 34- MetroloGT circle fit for 0° to 90°

Essentially, the center point of the arc was shifted to the center of circle fit in MetroloGT and the new radius was altered in the Gcode. The ball bar system was used again with the compensated code. The polar plot of the nominal, original and corrected tool path is shown in Figure 35.

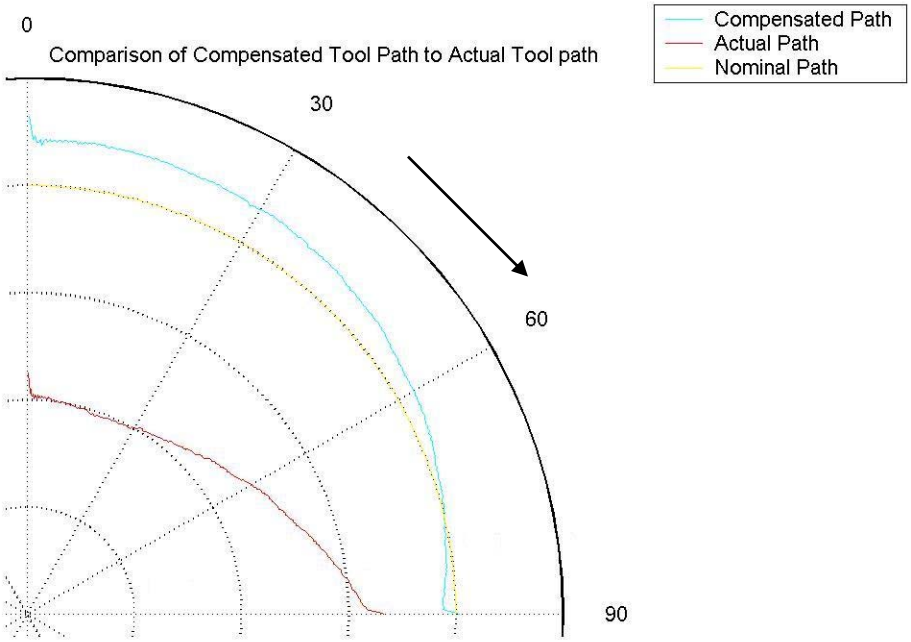

Figure 35- Results of Case Study for the first quadrant 0.05mm/div (CW direction)

Figure 35 clearly demonstrates that the compensated tool path marginally corrects the machine tool errors. The root of the sum of the squares of the errors for the original data and corrected data were also taken to shown the improvement in machine tool errors.

$$SSQ = \left[\sum_{i=1}^{N} (P_i)^2 \right]^{1/2} \tag{5.8}$$

The magnitude of the error for the original data from 0^{o} to 90^{o} was 1.6658 mm and for the compensated data 0.284 mm.

A series of ball bar tests were conducted with the uncompensated part program to verify the repeatability of the test. The four tool paths are plotted with the nominal tool path in Figure 36.

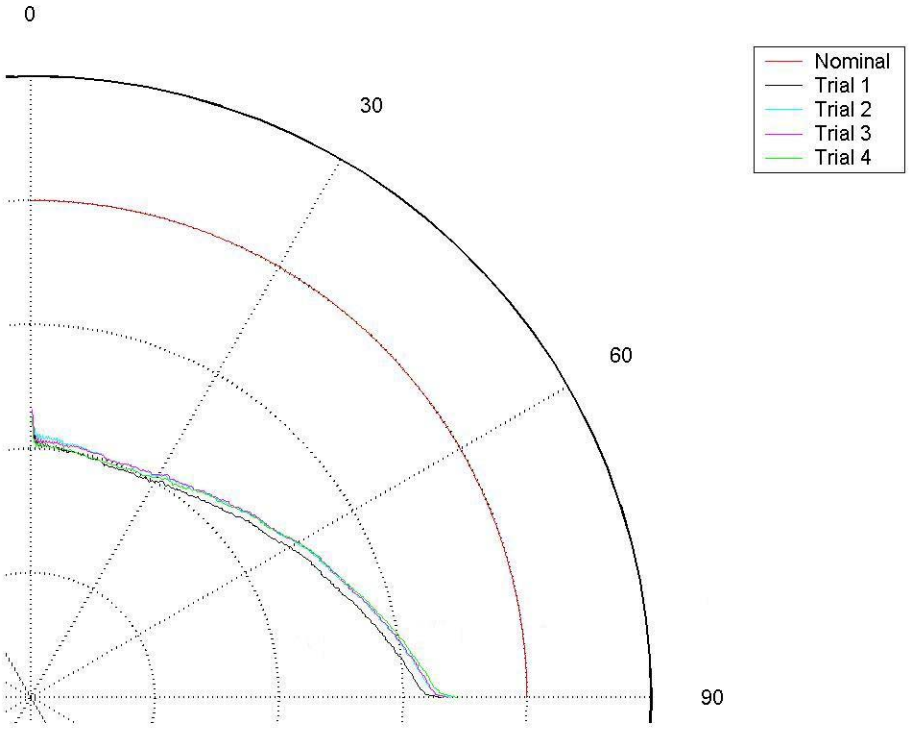

Figure 36- Repeatability of ball bar tests

The next step was to try to compensate the tool path for a complete circle. Again, the data from the original ball bar test was used to construct a compensated tool path. This time the tool path was constructed via different modes. These modes consisted of fitting the compensated tool path to a circle; to two half circles; and finally four quarters of a circle. These modes are discussed in sequential order. The x and z components of the

compensated tool path was imported into MetroloGT. A circle was fit to this data and the ball bar was manipulated to move with the new origin and radius. These results are shown in Figure 37.

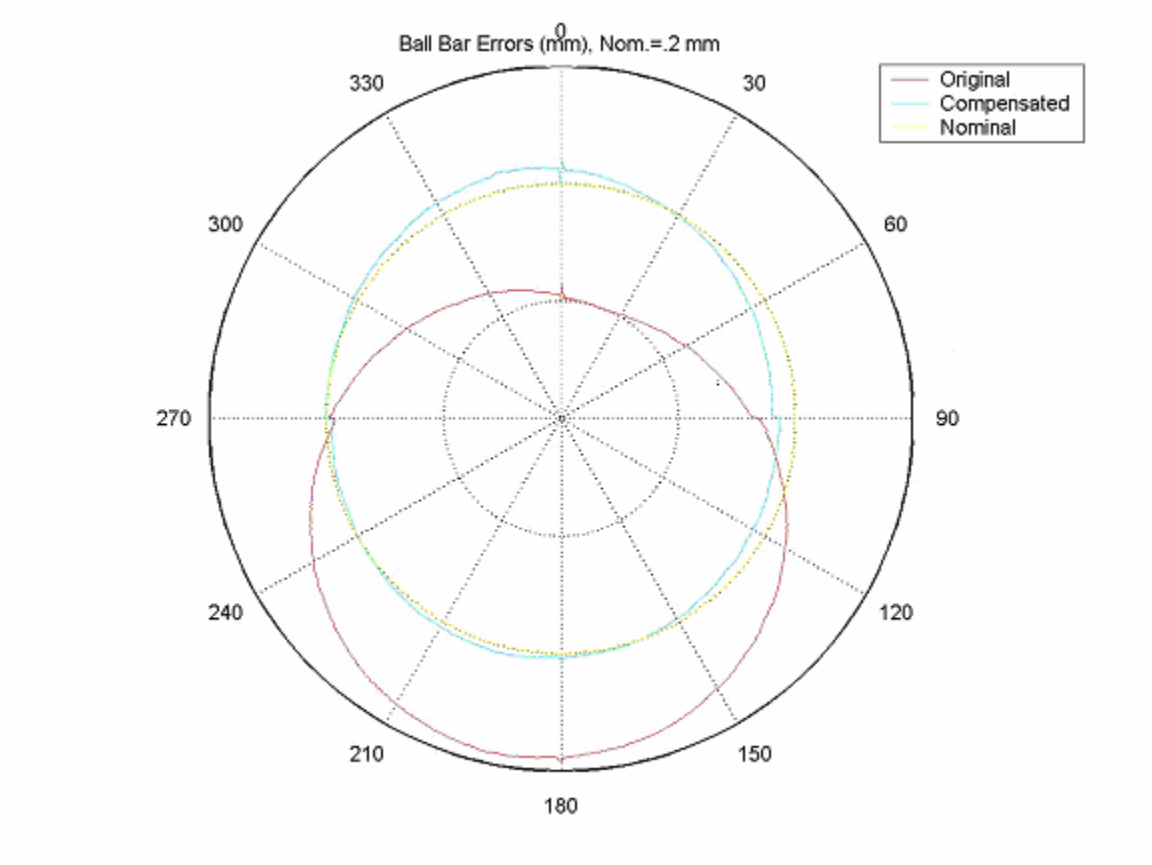

Figure 37- Results for circle fit (.1mm/div)

This plot shows that the compensated path follows the nominal much closer then the original actual tool path. The actual tool path is off center and of an incorrect radius. In reference to Figure 31, it is evident that the first and second quadrants of the graph contain mostly negative errors while the third and fourth quadrant contains mostly positive errors. Therefore, it would be more accurate to fit two half circles (or 180^{o} arcs)

to the data in MetroloGT and use the result to construct the compensated tool path. The results of this are shown in Figure 38.

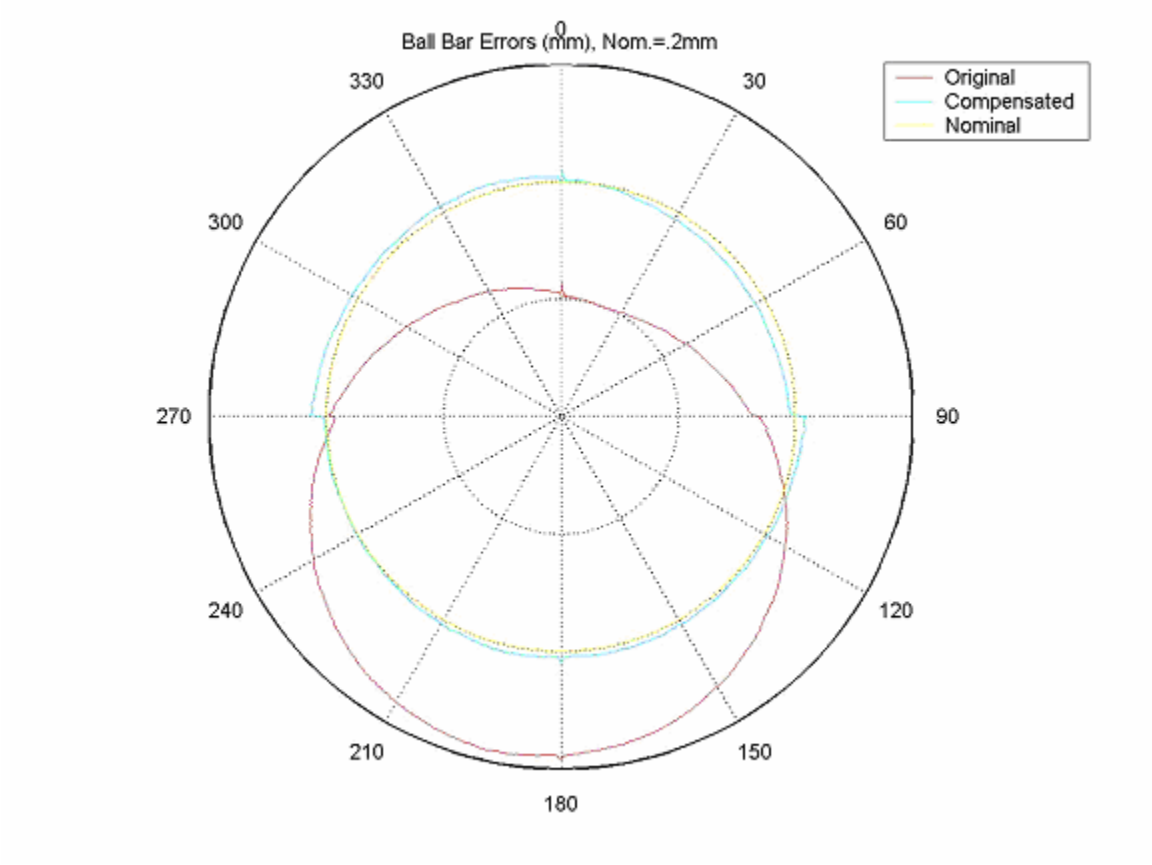

Figure 38- Results for two semi-circular fit (.1mm/div)

The final mode consisted of taken the original data for each quadrant and "piecing" together a compensated tool path from each quadrant into a circle. For example, the errors from the first quadrant were used to fit a 90^{o} arc which was pieced together with a fit of a 90^{o} arc in the second quadrant and so on. The results are displayed in

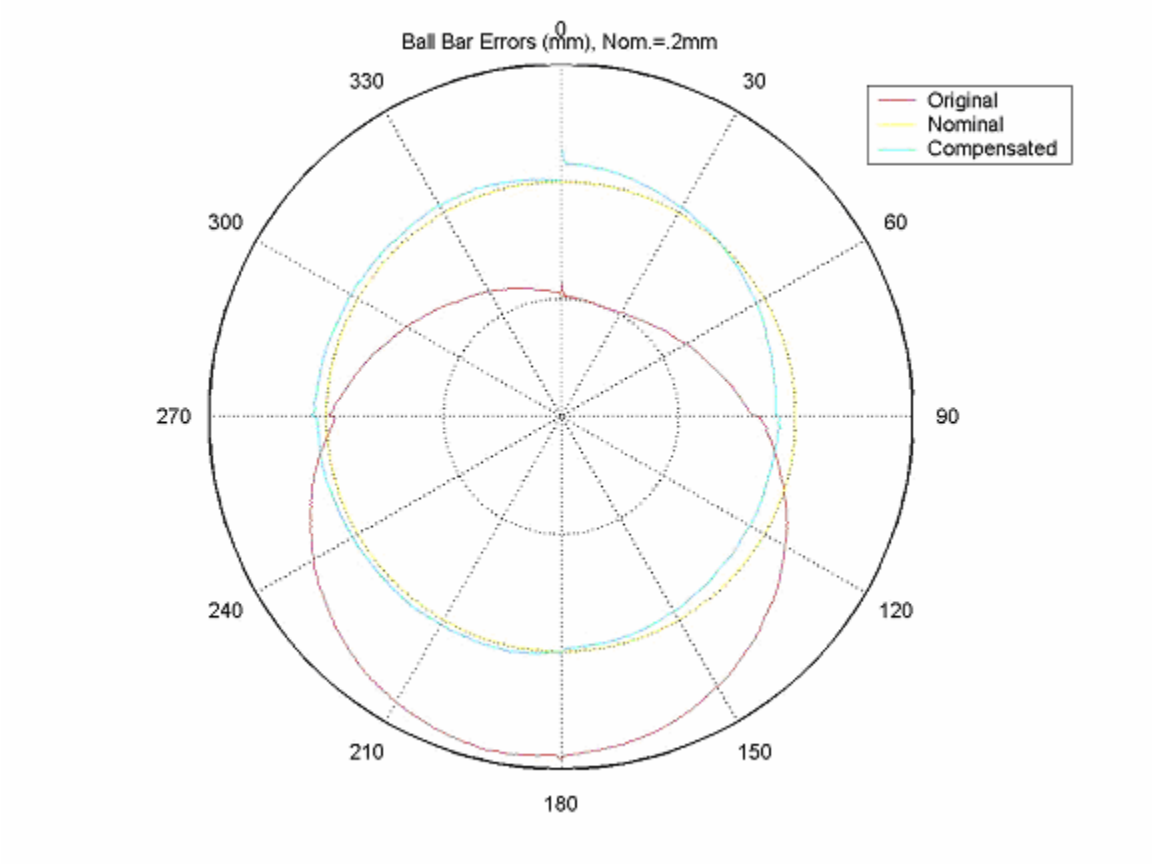

Figure 39-Results for 90 degree arc fit (.1mm/div)

The results of the fitted data from MetroloGT are displayed in Table 5.

Table 4- Coordinates of results of curve fit modes

Mode	Quadrant	X (mm)	Z (mm)	R (mm)
Original		0	0	100
	1	0.0291	0.0865	100.0080
90 degree arcs	2	0.0057	0.0815	100.0110
	3	0.0104	0.1100	100.0200
	4	0.0215	0.1000	100.0100
180 degree arcs	1 and 2	0.0175	0.0733	100.0240
	3 and 4	0.0131	0.1100	100.0220
Circle	1,2,3,4	0.0153	0.0930	100.0110

The previous figures display the compensated, actual, and desired tool path for each data fitting mode, however a quantitative assessment was required. The root of the sum of squares of the error provided this assessment. Table 5 shows the root of the sum of the squares of the errors for each fitting mode along with the errors for the original 360 degree data.

Table 5- Results of different compensation modes

	Root of Sum of Squares (mm)	Percent Improvement
Original Errors	2.70	-
Circle	0.35	86.86
Hemi	0.22	91.78
Quad	0.28	89.49

Table 5 concludes that the best way to construct the compensated tool path was with two semicircles.

The robustness of the software compensation was required to verify the results. In other words, the machine was manipulated to reach thermal steady state (using results from the thermal section of this text), and then the same compensation scheme was applied. The spindle was run at 1000 rpm for two hours and a ball bar test was conducted with the compensated coordinates. Figure 40 shows the consequences of the first quadrant after steady state is achieved.

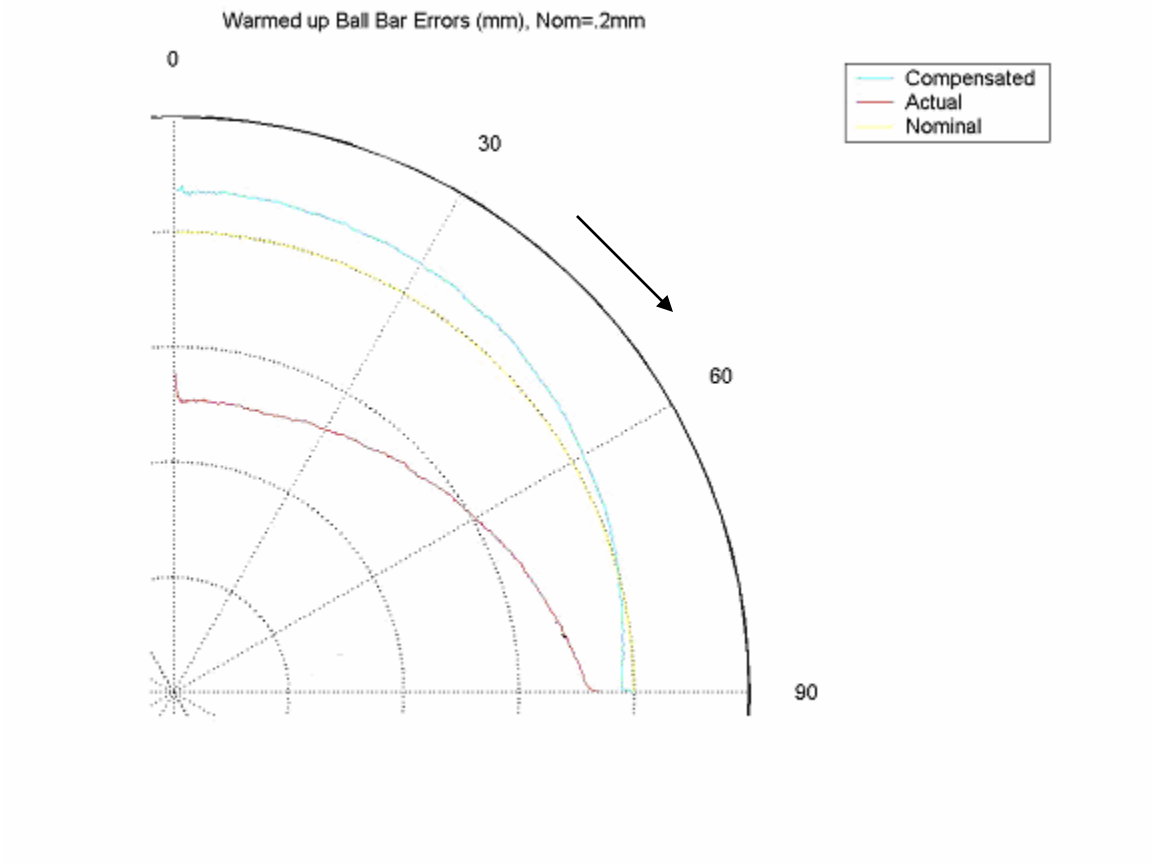

Figure 40 Results of compensated quadrant 1 for robustness CW (.05mm/div)

Thus, the compensated tool path was more accurate then the actual tool path even when the machine is at thermal steady state. Furthermore, the root of the sum of the squares of the errors for the compensated tool path (0.233mm) is nearly 5 times smaller then the actual tool path (1.139 mm). In order to verify the robustness of the other quadrants a compensated tool path using the semi-circular fits were used. Figure 41 shows the results of using the ball bar compensated tool path at a warmed up machine tool state.

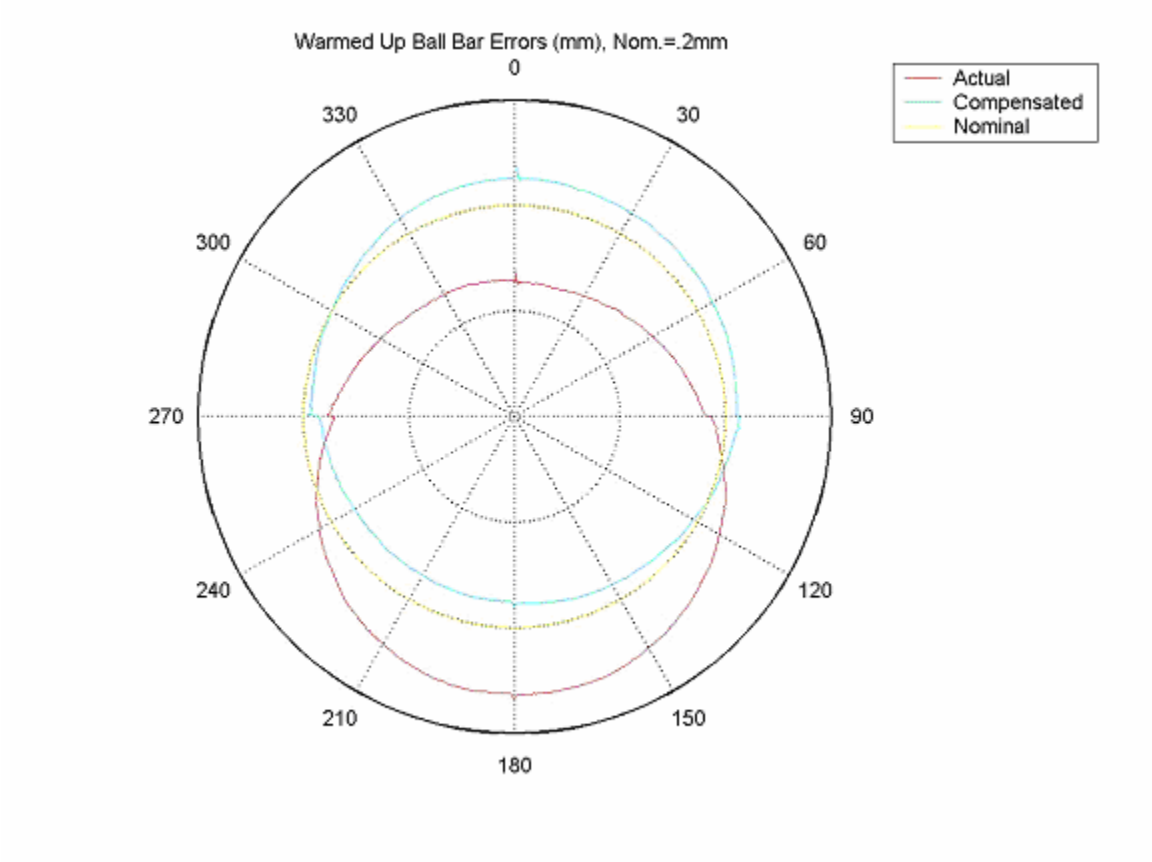

Figure 41-Results of semi-circular fit for robustness

Finally, the root of the sum of the squares of the errors for the actual tool path and compensated tool both was 1.998 mm and 0.732 mm respectively.

The results from this case study were then applied to the test part. The original ball bar program used for the previous section required a radius of 100mm. The test part required a radius of 31.75 mm (1.25) inch to be cut, while the ball bar followed a radius of 100 mm (3.937 inches). Therefore a ratio of the radii was used to construct a compensated tool path for the test part. Essentially, the original ball bar program measures the machine tool error over a 100 mm range for each slide. Thus, the x-slide travels 100 mm and the z-slide 100 mm. A 31.75 mm circular profile requires each slide

to travel over a range of 31.75 mm. Therefore, the ratio of the distance the slides moved in the original ball bar test to the distance the slides move in the test part will be used. Figure 42 demonstrates the concept of this ratio.

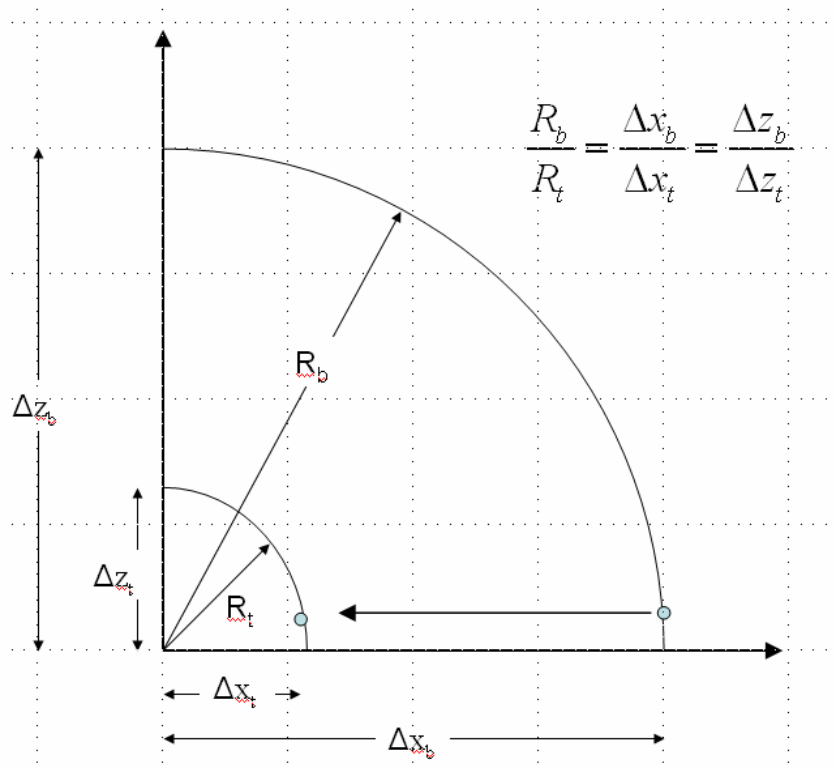

Figure 42- Demonstration of Ratio from Ball Bar test program to test part

A circular profile was cut with the original tool path for one part, while the other part was cut with the compensated tool path. A CMM was used to verify the results which are discussed in Chapter VIIII.

CHAPTER VII

INTERFEROMETER RESULTS

Linear Results

The accuracy of a machine tool is generally defined by the errors involved in the movement of the positioning axes. An HP5529A laser interferometer was used to collect data for linear displacement along the x and z-axis. The optical setup used for the z axis linear measurement is shown in Figure 43.

Figure 43- Optical setup used for Z-axis linear measurements

An explanation of the coordinate reference frame is required. When the tool turret moves down and moves left in Figure 43 it moves in the negative z direction and negative x direction respectively. This is the convention used when relating the experimental results to the coordinates of the work volume. Also for z linear measurements, (for the sake of this section) the turret always starts at an aforementioned initial position on both axis and then undergoes motion away from the spindle as shown in Figure 44.

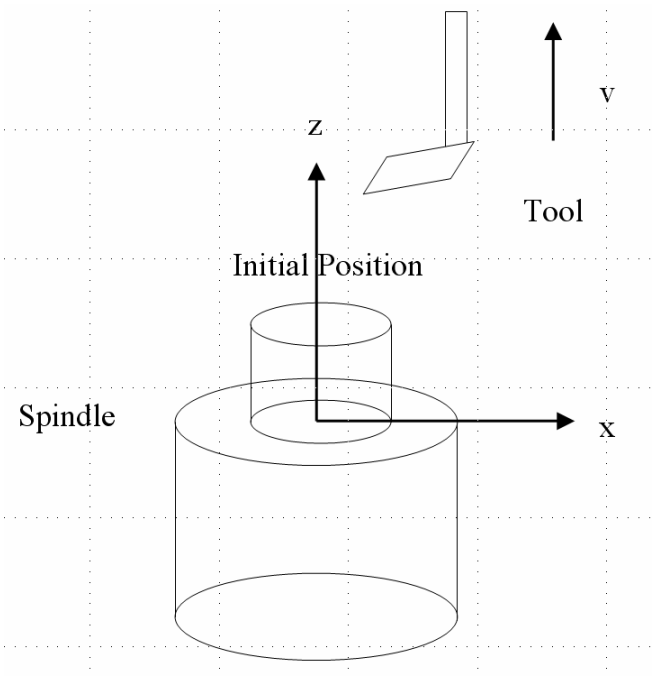

Figure 44- Initial Position location of laser interferometer measurements

The linear results consisted of a long range and short range test. The short range had a higher resolution closer to the potential workpiece volume while the long range had less resolution, but over a longer range. The long range provided a trend over a greater distance, while the short range provided a more accurate description near the potential work volume. The tool was moved in along the z axis in 6.35 mm (0.25 inch) increments over a distance of 177.8 mm (7 inches) for 3 cycles. The results for each run are shown in Figure 45.

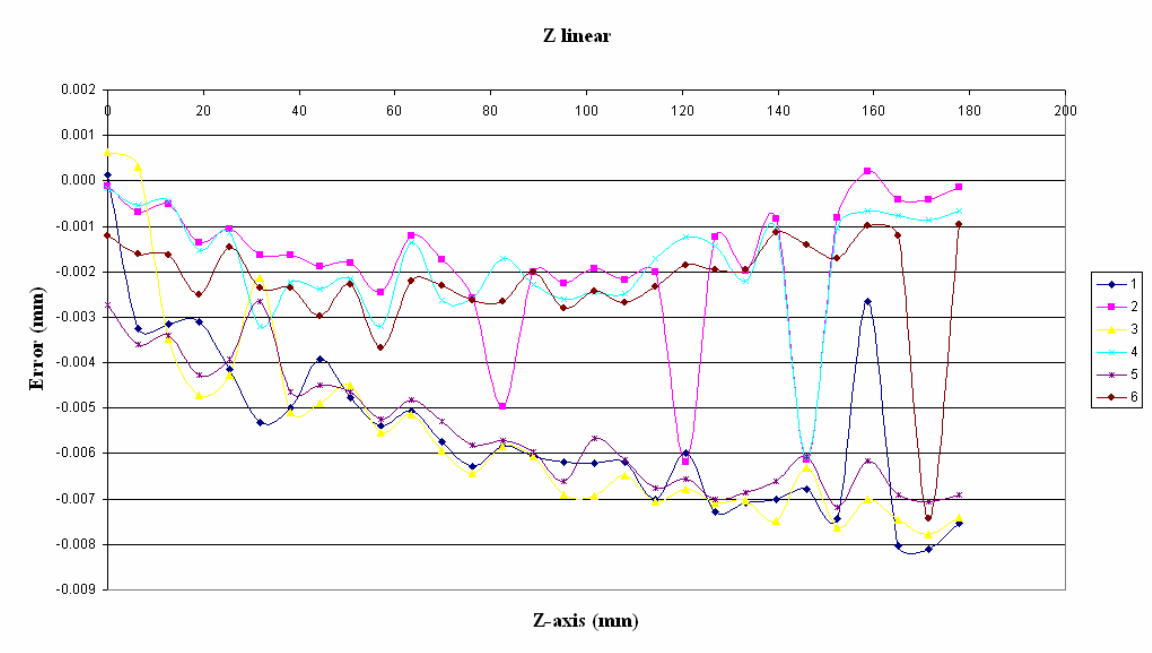

Figure 45- Results of linear Z-axis measurements for 177.8 mm (7 inch) travel

A short range measurement along the positive z-axis was made consisting of 12.7 mm (0.1 inch) increments over 50.8 mm (2 inches) of travel. The initial position of the tool turret was at -127 mm (-5 inches) which corresponds to 0 on the plot in Figure 46.

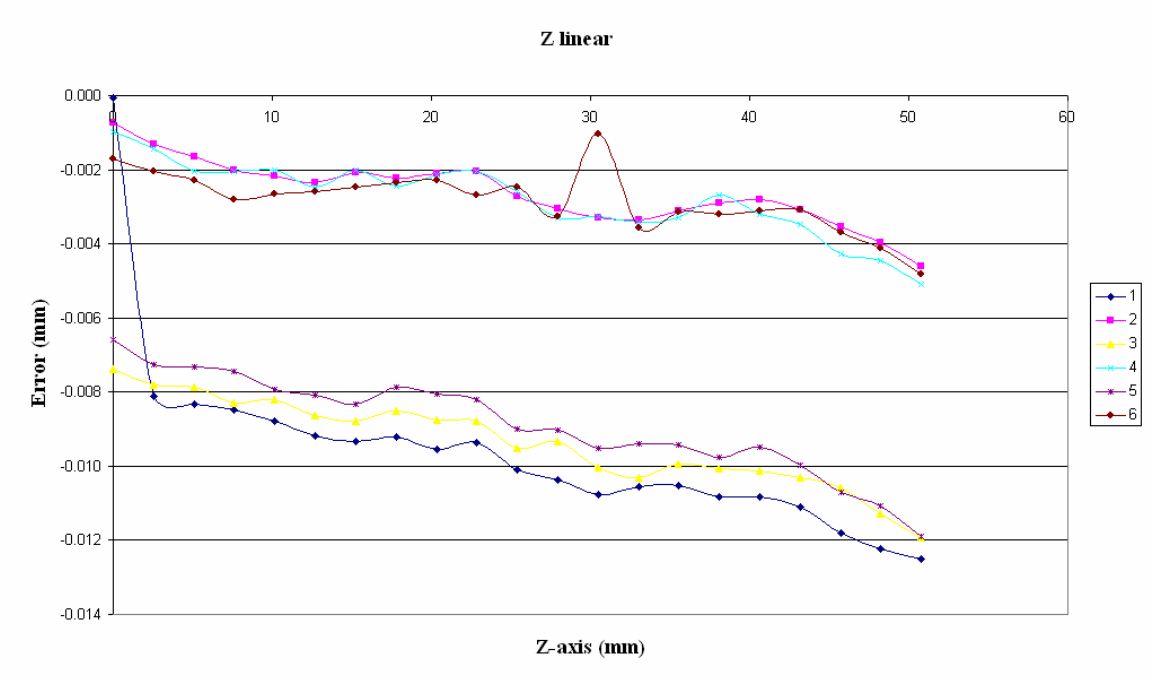

Figure 46- Results for linear Z-axis 50.8mm (2 inch) travel

The same method was used for x axis linear measurements. The starting position of the tool turret was at 0 then moved under diametric notation to -228.6 mm (-9 inches) (thus from right to left for 114.6 mm (4.5 inches)).

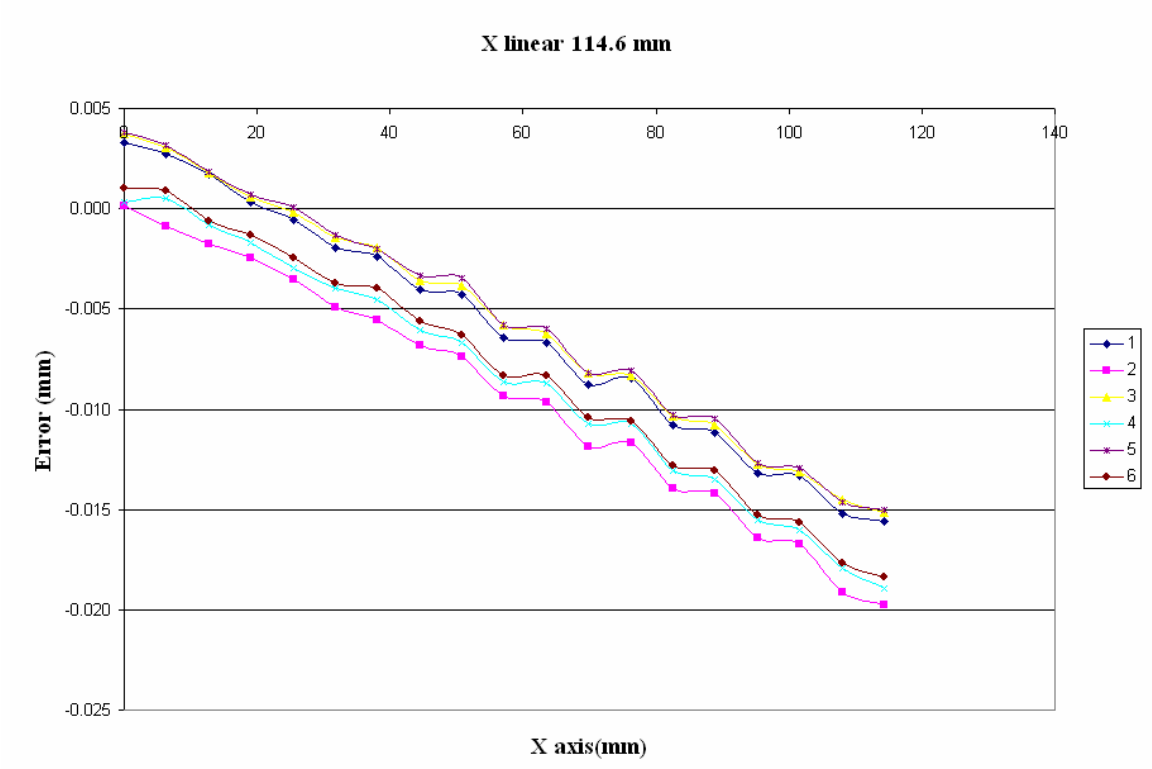

Figure 47- Results for linear X-axis 114.6mm (4.5 inch) travel

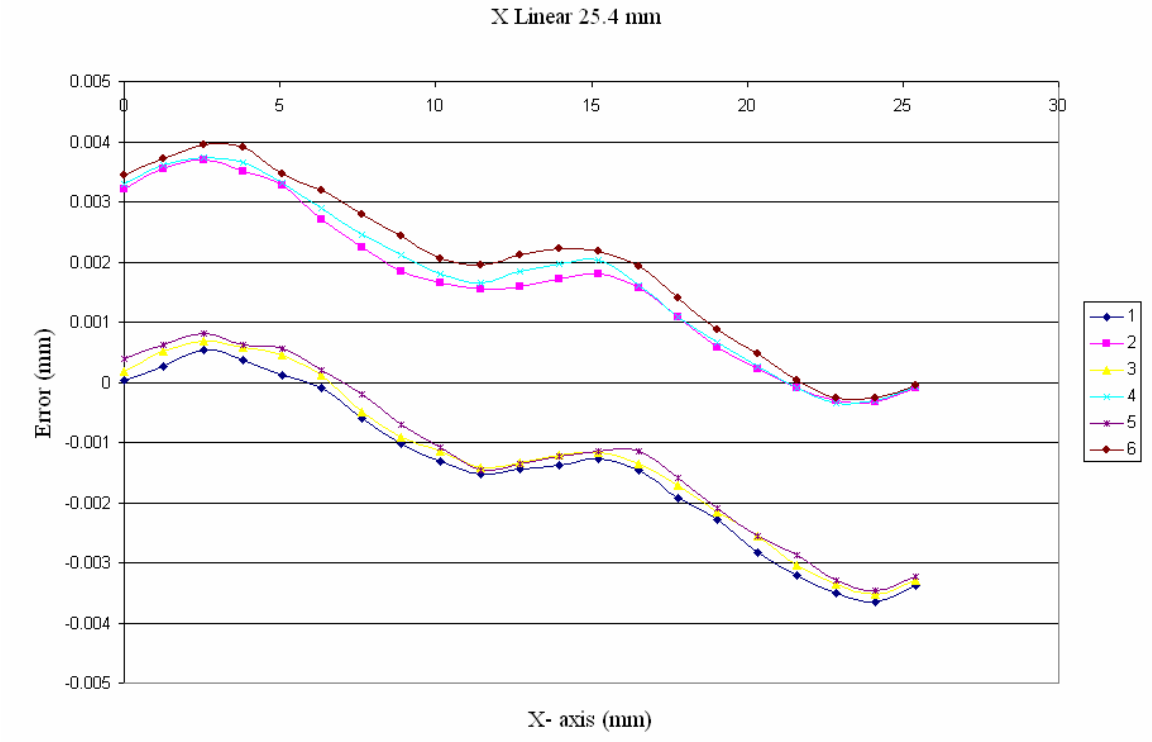

Figure 48- Results for linear X-axis 50.8mm (2 inch) travel

Figure 45 and Figure 46 showed the z linear positioning error while Figure 47 and Figure 48 showed the linear positioning error of the x-axis. The magnitude of the z-axis linear errors is on the order of .01 mm while the order of the x-linear positioning errors is on the order of .05 mm for a travel of 25.4 mm. This relative magnitude of the z linear errors being twice as large as the x linear errors is in correlation with the machine tool specifications. These linear plots also suggest that the machine tool does not reach the desired position when the travel of the tool is in the direction to the spindle. There is also a sinusoidal behavior in the previously mentioned plots. The phenomena behind this are owed to the ball screw pitch of 11.93 mm. The pitch is the amount of linear motion traveled by the lead screw for ever rotation of the ball screw. Thus, the period of the plots is equal to the pitch of the ball screw. This phenomena is evident for each error measurement, therefore the following figure is provided to show this behavior graphically.

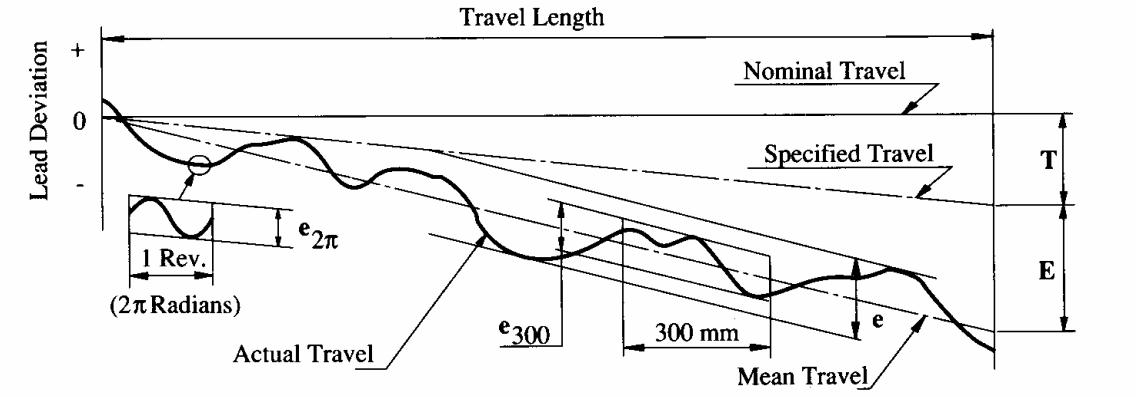

Figure 49- Illustration of ball screw pitch affect on linear motion (Slocum, 1992)

The actual displacement of the nut relative to the screw shaft is the actual travel and e is the maximum width of variation due to the pitch of the ball screw.

Straightness Results

The next set of experiments yield straightness results for the x and z axis which is the ability of the machine to move along an axis of interest, in this case the x and z axis. Straightness is the deviation from true straight-line motion. Just to re-iterate, the machine of interest is a 2-axis lathe, therefore straightness in the x and z direction with respect to y is neglected because the y-axis can not be compensated for and thus is considered insensitive. Figure 50 shows the optical setup for vertical straightness along the x axis.

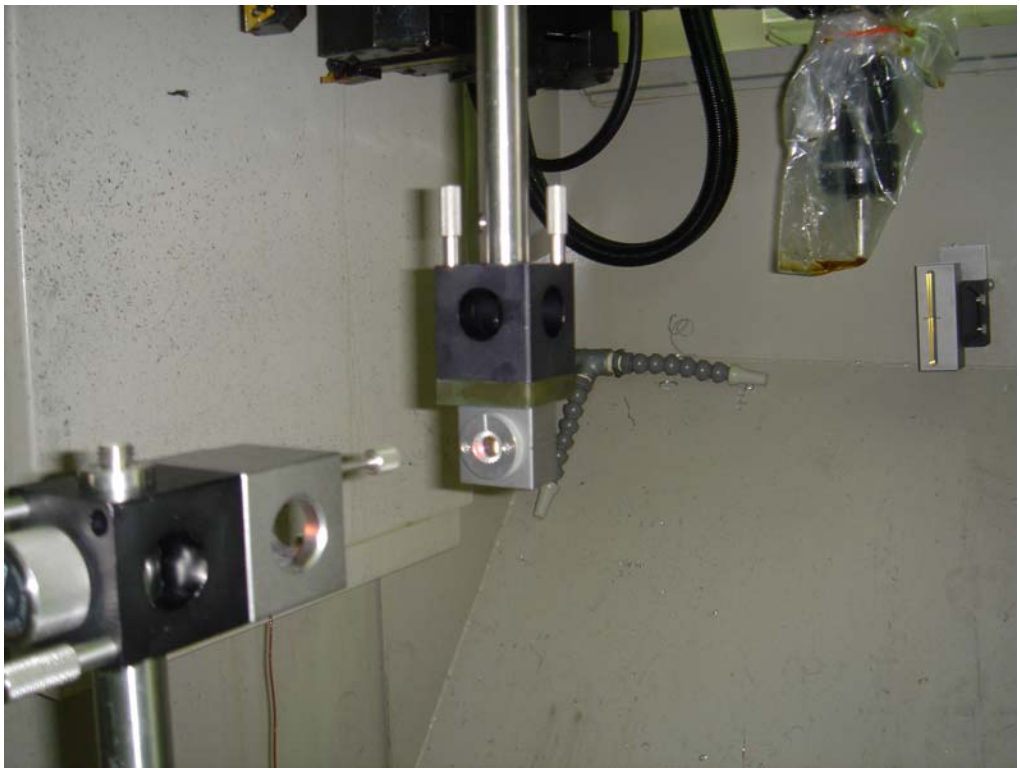

Figure 50- Optical Setup for X-straightness in the vertical direction

Unfortunately, the optical setup shown in Figure 50 allowed for machine vibration to drastically affect the results of the measurement. In this configuration the reflecting

mirror is mounted on a thin wall that is susceptible to vibration. There for the optical configuration in Figure 54.

Figure 51- Optical Configuration for vertical X-axis straightness

Figure 52 shows the results of the vertical straightness along the x axis. The initial position translates to the machine tool origin and a positive error corresponds to motion of the x-axis along the positive z-axis.

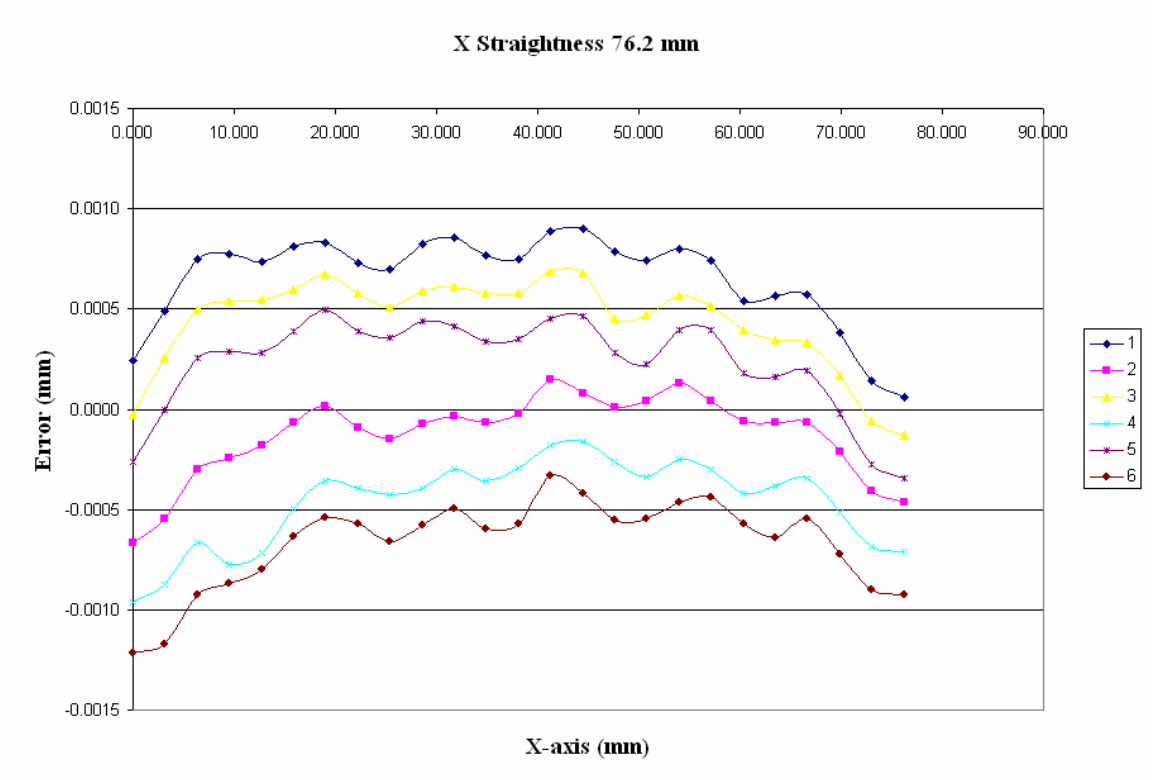

Figure 52- Vertical X straightness Results for 76.2 mm (3 inch) travel

There is sinusoidal behavior in the plot in Figure 52 due to the periodicity of the ball screw. The pitch of the ball screw is 11.94 mm (0.47 inches). Figure 53 shows the vertical X straightness results for 25.4 mm (1 inch) of travel.

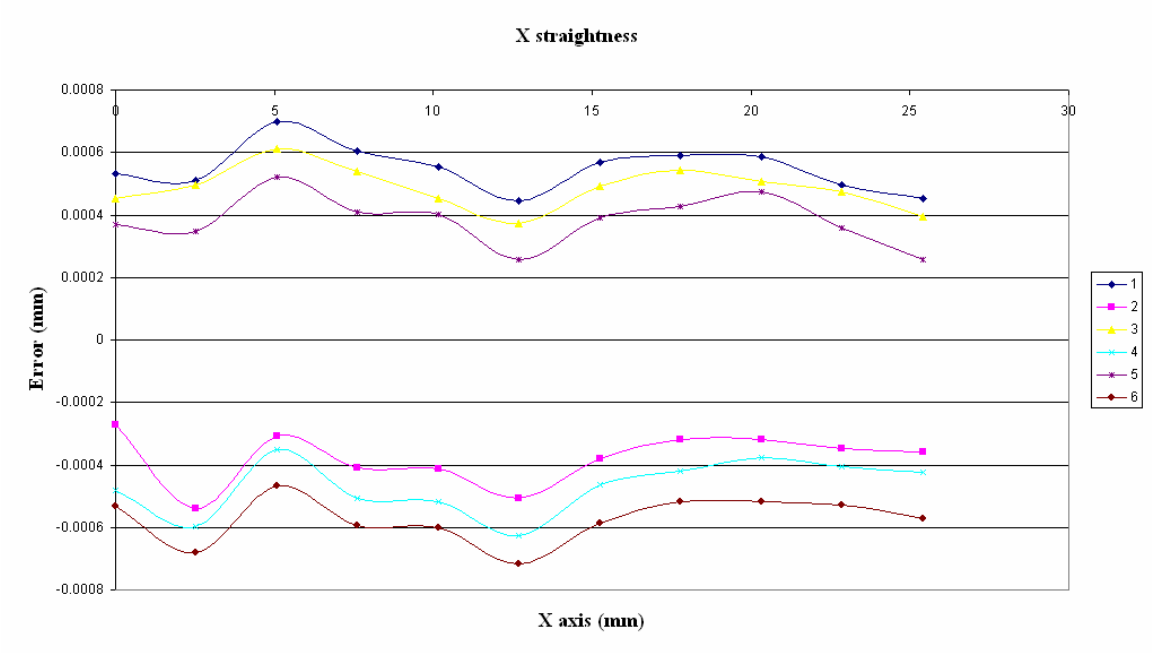

Figure 53-Vertical X straightness results for 25.4 mm (1 inch) travel

Similarly, the optical setup for the horizontal straightness along the Z-axis and the results are illustrated in Figure 54 and respectively. A positive error corresponds to the positive x-axis.

Figure 54- Optical configuration for horizontal straightness along the Z-axis

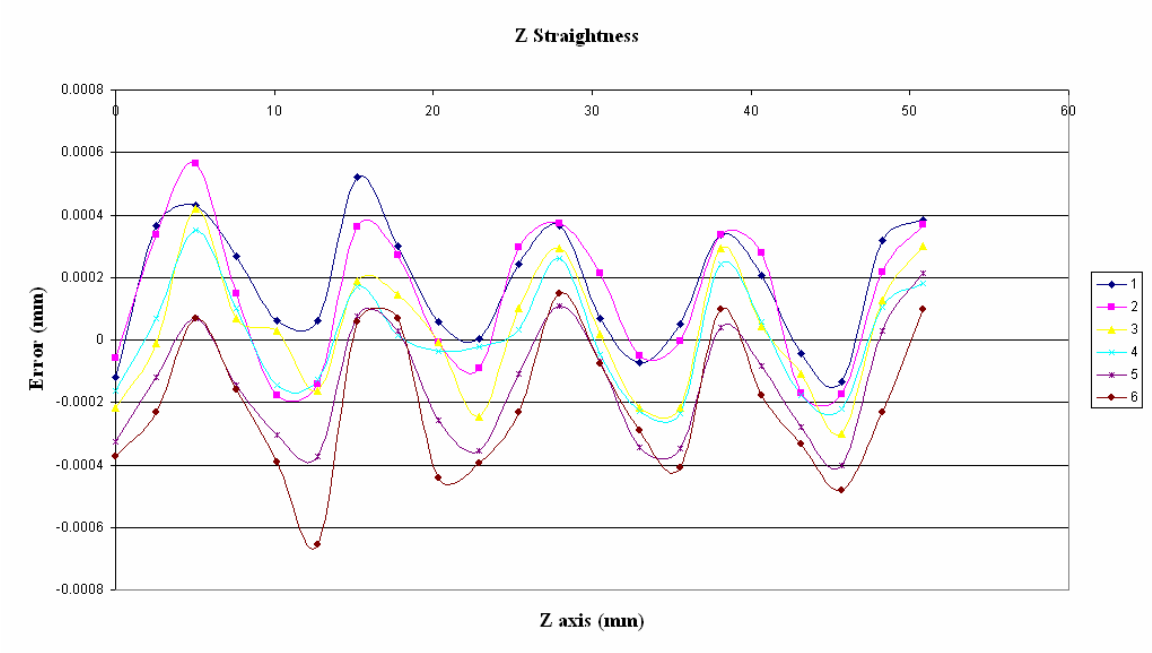

Figure 55- Results of horizontal straightness along the Z- axis 50.4 mm (2 inches)

The magnitude of the z straightness errors is about 0.0005 mm and for x straightness errors of about 0.0006 mm for the same range. Referring back to the linear displacement errors, the straightness errors are about 10 times smaller in magnitude. The straightness errors are also smaller then the minimum input increment of the controller (0.0254 mm). Therefore the straightness errors will not play a significant role in the HTM error compensation.

Angular Results

Finally, the laser interferometer and proper optical configurations were used to measure the yaw along the Z axis and the pitch along the X axis. Once again, a short

range and long range test were conducted for the same reasons as the linear measurements. The configuration for the pitch along the X axis is shown in Figure 56 (the same configuration for yaw along the Z is used, however rotated 90^{o}).

Figure 56- Optical configuration for pitch along the X-axis

The results for the pitch along the x axis for short range (50.4 mm (2 inches) starting at -203.2mm (-8 inches) to -304.2 mm (-12 inches) in terms of the machines co-ordinates)

and long range (152.4mm (6 inches) diametrically from 0 to 304.2 mm (-12 inches)) are shown in Figure 57 and Figure 58 respectively. The x-axis of the plot corresponds to the x-axis of the machine tool and a positive error corresponds to a counterclockwise rotation in the xz plane.

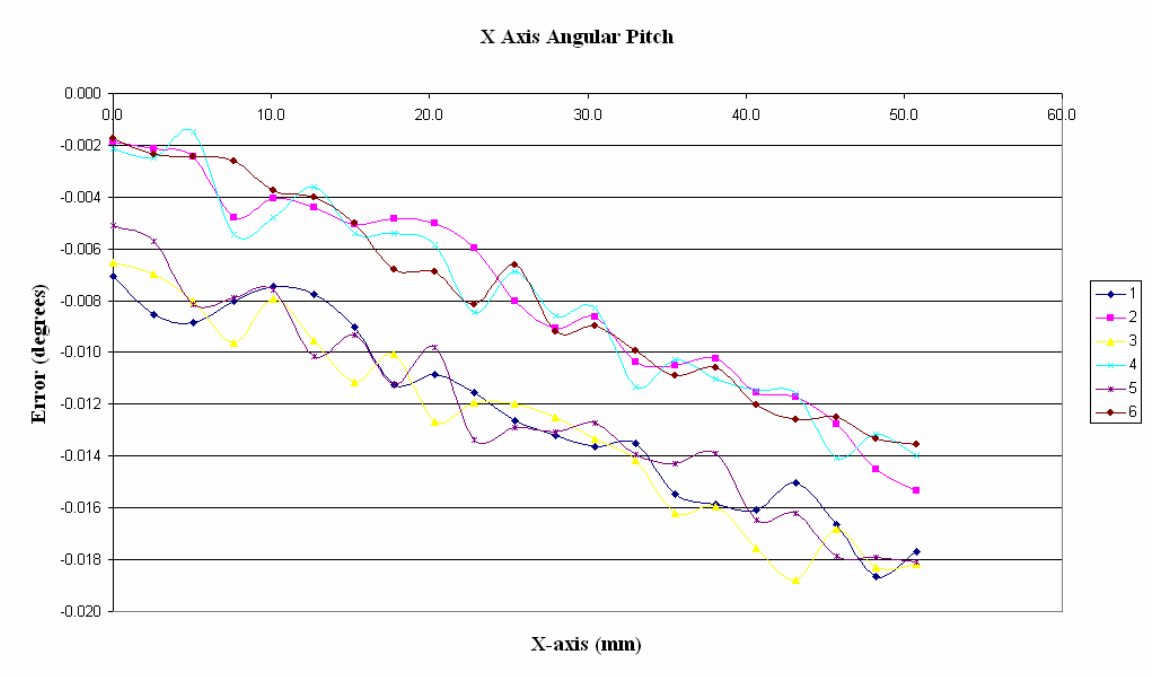

Figure 57- Results of pitch along the X axis for 50.4 mm (2 inch) range

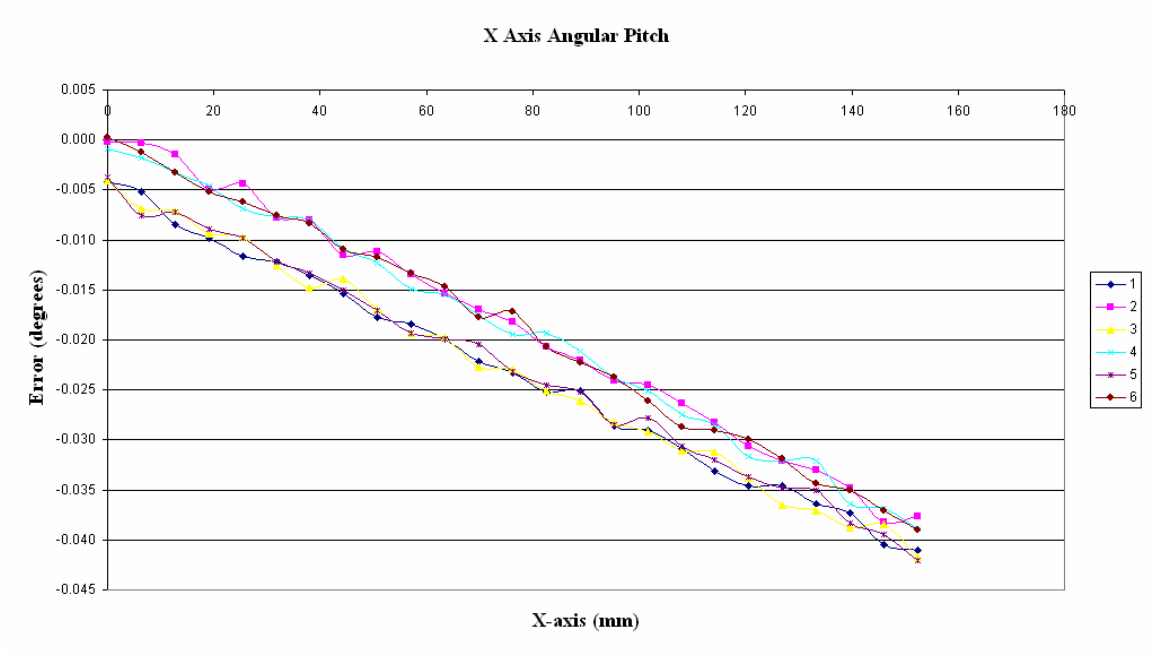

Figure 58- Results of pitch along the X axis for 152.4mm (6 inch) range

The magnitude of the X-axis pitch errors is on the order of 0.01 degrees with 0.04 degrees being the maximum. The largest travel for the angular measurement was about 160 mm. The amount of travel for 25.4 mm will provide an angular error of about 0.005 degrees. A quick calculation to determine the severity of these errors is as follows:

$$\delta = l * \sin(\theta) = 25.4 * \sin(0.005) = 0.0022mm$$

The minimum input increment is 0.00254 mm; therefore the angular errors are on the order of being negligible by the HTM compensation program. The same deduction follows for the Z-axis yaw.

The results for yaw along the z axis for short range (50.4 mm from -127 mm to -177.8 mm) and long range (177.8 mm from 0 to -177.8) are shown in

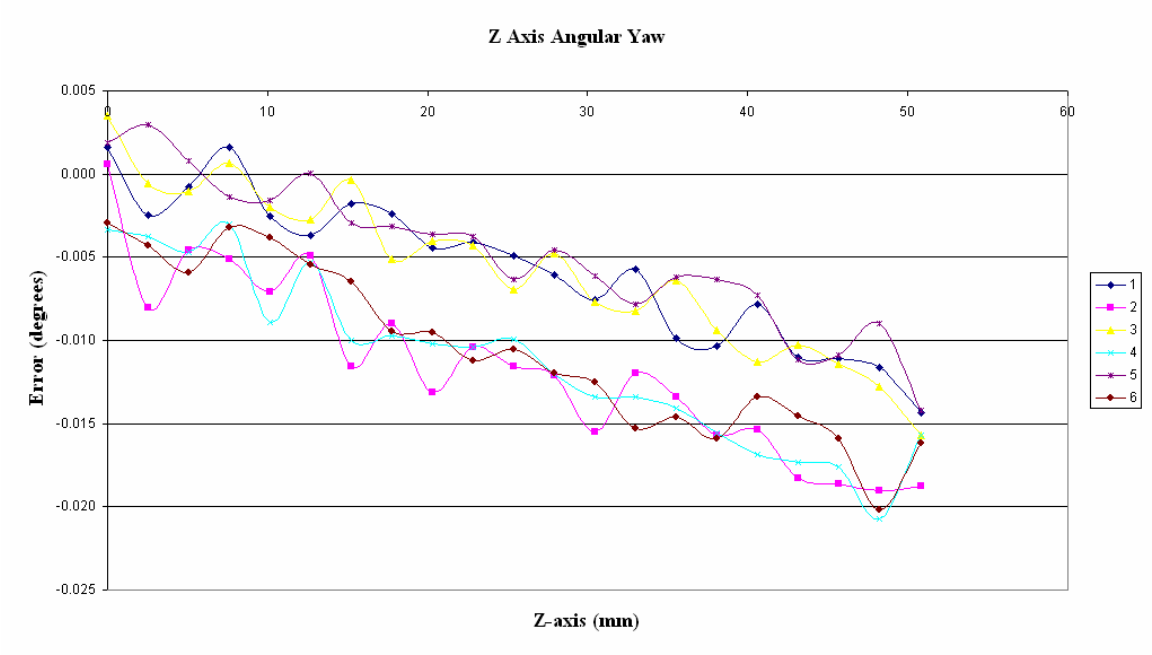

Figure 59- Yaw along the Z-axis for 50.4 mm (2 inches)

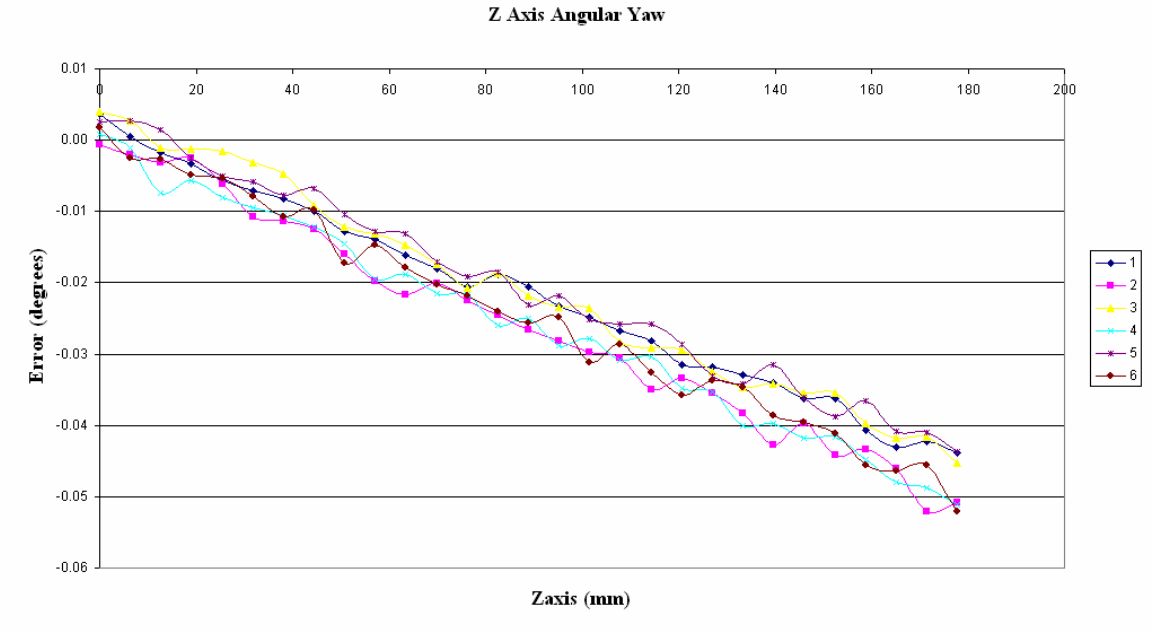

Figure 60- Yaw along the Z-axis for 177.8mm (7 inches)

Discussion of Interferometer Data

The interferometer data exhibit certain behavior. For example, the 3 trials were conducted away from the spindle and 3 trials towards the spindle. A systematic error was present in the error measurement results. This hystersis was highly reproducible and has a sign depending on the direction of approach. It is clear that backlash is causing the offset between the trials away from the spindle and the trials toward the spindle. Backlash is evident at the contact surface of the ball screws that have a pre-load. Thus the direction of the measurements affects the interferometer data. It is important to notice the magnitude of each individual machine tool error. The linear displacement errors dominate the machine tool errors. The z linear displacement errors cause the largest machine tool inaccuracies. This can be compared to the specifications of the machine which are 0.0153 mm (0.0006 inches) and 0.0229 mm (0.0009) inches in the x and z axis positioning respectively. The repeatability of the x-axis and z- axis is ±0.00255 mm (±0.0001 inches) and ±0.0051 mm (±0.0002 inches) respectively. The machine tool is less accurate in the z-direction due to the design of the machine. The z-axis holds the tool turret and the x-slide. The z-slide (50.04mm) also has a different ball screw diameters then the x-slide (39.89mm) causing the differences in positioning accuracy. The straightness and angular errors are on the order of being neglected by the HTM compensation because the minimum input increment of 0.00254 mm is close to the magnitude of these errors. There was also sinusoidal behavior due to the ball screw pitch as previously explained.

CHAPTER VIII

ERROR COMPENSATION

Homogenous Transformation Matrix

The machine tool errors measured in the previous section were implemented into an error compensation scheme. A homogenous transformation matrix (HTM) et al Donmez (1986) provides a coordinate transformation to between two coordinate systems. Donmez provided a generalized approach to develop this HTM. This paper developed the error model for a two-axis turning center. In this case, a homogenous transformation transformed the actual tool path to the desired tool path using the machine tool errors. (8.1) shows the generic form of such a matrix.

$$T = \begin{bmatrix} O_{1x} & O_{2x} & O_{3x} & P_x \\ O_{1y} & O_{2y} & O_{3y} & P_y \\ O_{1z} & O_{2z} & O_{3z} & P_z \\ 0 & 0 & 0 & P_s \end{bmatrix} \tag{8.1}$$

The first three columns represent the orientation of a coordinate frame with respect to a reference frame. The last column corresponds to the position of a coordinate frame with respect to the coordinate reference frame. P_s is a scale factor which was set to unity for this research. A general homogenous transformation matrix is of the following form.

$$T = \begin{bmatrix} O_{1x} & O_{2x} & O_{3x} & P_x \\ O_{1y} & O_{2y} & O_{3y} & P_y \\ O_{1z} & O_{2z} & O_{3z} & P_z \\ 0 & 0 & 0 & 1 \end{bmatrix} \tag{8.2}$$

(8.2) describes the relative rotation and translation between two coordinate frames. An appealing feature of the HTM is that it can be applied in series with respect to several different coordinate reference frames to achieve a resultant HTM.

The HTM is applied to the machine slides of the two axis vertical lathe. The following figure describes the axis of the machine tool of interest.

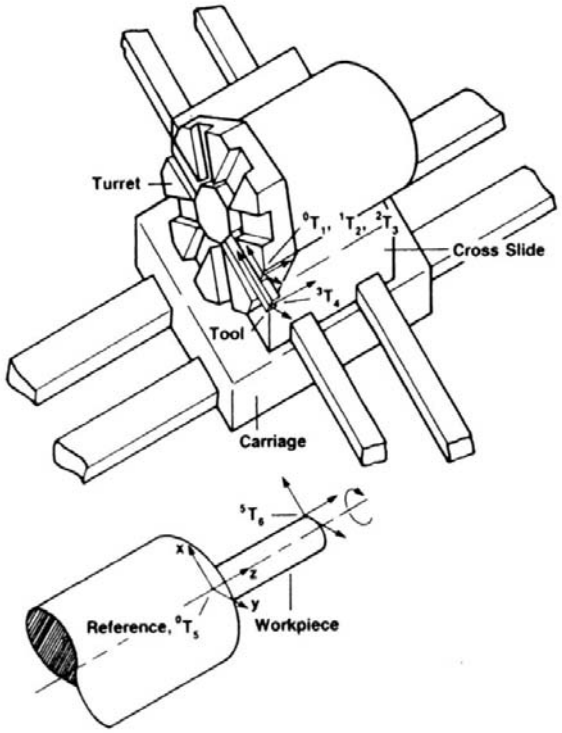

Figure 61- Coordinate frame nomenclature for machine tool (Courtesy of Donmez)

The carriage translates along the z-axis and the cross slide translates along the x-axis; therefore, an error matrix is generated for each (then applied in series to get a resultant transformation matrix).

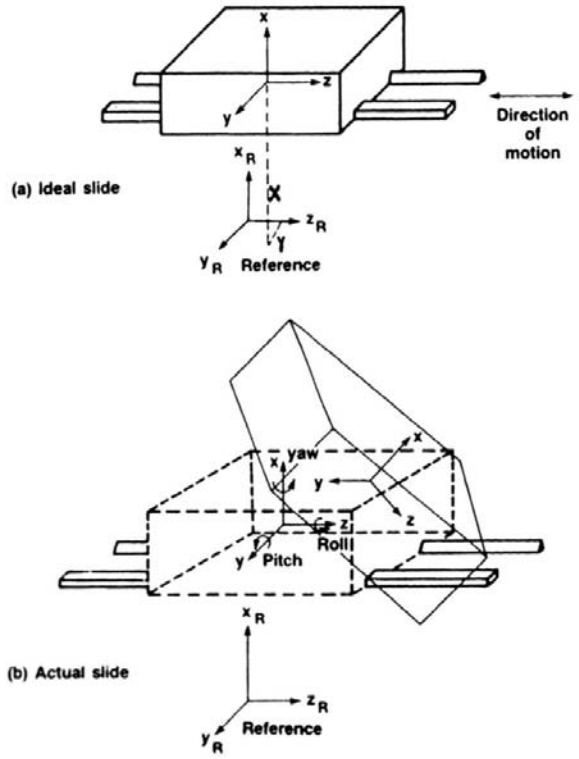

Figure 62- Roll, Pitch and Yaw associated with the x axis (Courtesy of Donmez)

Figure 62 demonstrates the rotational and translational errors of the carriage slide traveling along the z-axis. The total error motion of a slide is a combination of a rotation and a translation. The rotational error has three components about the three orthogonal

axes. These are known as roll, pitch and yaw. The general form of the rotational error matrix with assumption of small angular errors is

$$T_{rot} = \begin{bmatrix} 1 & -\varepsilon_z & \varepsilon_z & 0 \\ \varepsilon_z & 1 & -\varepsilon_x & 0 \\ -\varepsilon_y & \varepsilon_x & 1 & 0 \\ 0 & 0 & 0 & 1 \end{bmatrix} \tag{8.3}$$

where ε_x the rotational error about the x-axis is, ε_y is the rotational error about the y-axis and ε_z is the rotational error about the z-axis.

The translational error along the x axis in the z- direction is shown in Figure 63

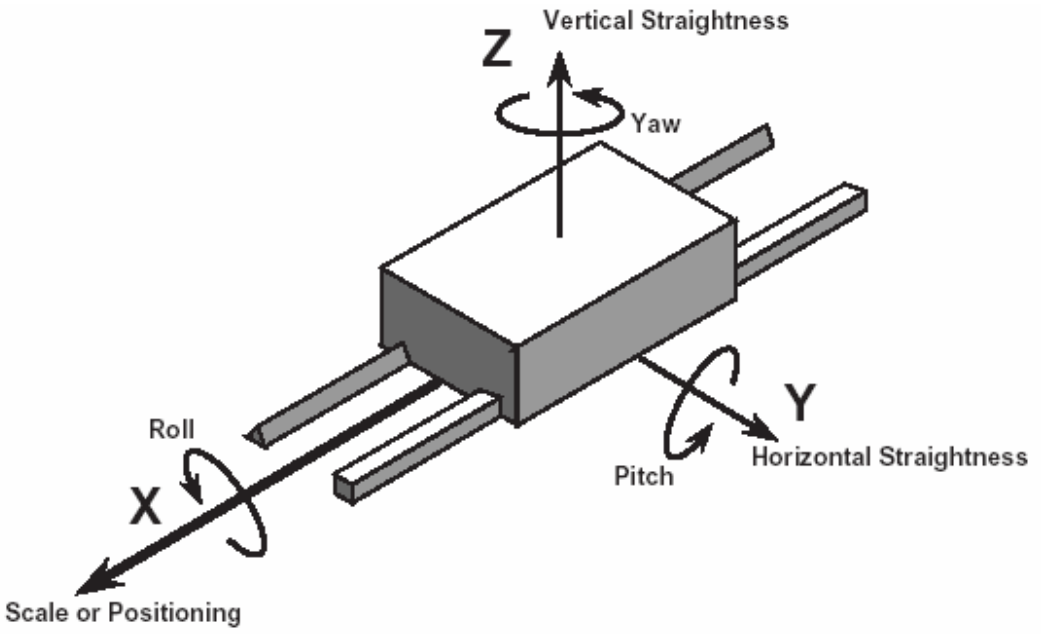

Figure 63- Schematic of straightness motion along each axis (Kurfess)

and described by (8.4)

$$\delta_x = \delta'_{Zx}(z) \tag{8.4}$$

where $\delta'_{Zx}(z)$ is the straightness along the z-axis. This straightness error is a function of z as it changes when the slide moves along the z-axis. The translational error of the carriage along the z-axis is Δz. (8.5) represents the translation error matrix for the carriage.

$$T_{trans}(carriage) = \begin{bmatrix} 1 & 0 & 0 & \delta'_{Zx}(z) \\ 0 & 1 & 0 & 0 \\ 0 & 0 & 1 & \Delta z \\ 0 & 0 & 0 & 1 \end{bmatrix} \tag{8.5}$$

The carriage contains a rotational error known as the z axis yaw, ε_x. Yaw is the rotational error of the slide around the axis perpendicular to the plane in motion. Setting all the other rotation errors in (8.3) to zero and multiplying in series with (8.5) yields

$$E_{Carriage} = \begin{bmatrix} 1 & 0 & 0 & \delta'_{Zx}(z) \\ 0 & 1 & -\varepsilon_x & -\varepsilon_x \delta'_{Zx}(z) \\ 0 & \varepsilon_x & 1 & \Delta z \\ 0 & 0 & 0 & 1 \end{bmatrix} \tag{8.6}$$

The actual position of the carriage is:

$$T_{position\_carriage} = \begin{bmatrix} 1 & 0 & 0 & 0 \\ 0 & 1 & 0 & 0 \\ 0 & 0 & 1 & z \\ 0 & 0 & 0 & 1 \end{bmatrix} * E_{carriage} = \begin{bmatrix} 1 & 0 & 0 & \delta'_{Zx}(z) \\ 0 & 1 & -\varepsilon_x & -\varepsilon_x \Delta z \\ 0 & \varepsilon_x & 1 & z + \Delta z \\ 0 & 0 & 0 & 1 \end{bmatrix} \tag{8.7}$$

The actual position of the cross slide was constructed using the errors along the x-axis. The cross slide is restricted to motion along the x-axis. The same manner that was used

for the carriage was used for the cross slide. The translational error along the z axis is a function of the x-axis position and is presented in (8.8)

$$\delta_z = \delta'_{Xz}(x) \tag{8.8}$$

where $\delta'_{Xz}(x)$ is the z straightness along the x-axis. The x-axis pitch, ε_z was substituted into (8.1). (8.9) represents the error matrix of the cross slides.

$$E_{Cross} = \begin{bmatrix} 1 & -\varepsilon_z & 0 & \Delta x \\ \varepsilon_z & 1 & 0 & \varepsilon_z \delta'_{Xz}(x) \\ 0 & 0 & 1 & \delta'_{Xz}(x) \\ 0 & 0 & 0 & 1 \end{bmatrix} \tag{8.9}$$

Using (8.9) the actual position is

$$T_{position\_cross} = \begin{bmatrix} 1 & 0 & 0 & x \\ 0 & 1 & 0 & 0 \\ 0 & 0 & 1 & 0 \\ 0 & 0 & 0 & 1 \end{bmatrix} * E_{carriage} = \begin{bmatrix} 1 & -\varepsilon_z & 0 & \Delta x + x \\ \varepsilon_z & 1 & 0 & \varepsilon_z \Delta x \\ 0 & 0 & 1 & \delta'_{Xz}(x) \\ 0 & 0 & 0 & 1 \end{bmatrix} \tag{8.10}$$

The actual position of each slide has been found. The total error matrix can also be found be multiplying in series (8.6) and (8.9)

$$E_{total} = \begin{bmatrix} 1 & -\varepsilon_z & \varepsilon_x\varepsilon_z & \delta'_{Zx}(z) + \varepsilon_z\varepsilon_x\Delta z + \Delta x \\ \varepsilon_z & 1 & -\varepsilon_x & (\varepsilon_z\delta'_{Zx}(z) - \varepsilon_x\Delta z + \varepsilon_z\Delta x) \\ 0 & \varepsilon_x & 1 & \left(\Delta z + \delta'_{Xz}(x)\right) \\ 0 & 0 & 0 & 1 \end{bmatrix} \tag{8.11}$$

Implementation of the HTM

A Matlab™ program was created to transform each point of the actual tool path to the desired tool path using (8.7) and (8.10). The desired parameter is the coordinates of the compensated tool path. The coordinates of the actual tool path can be found using (8.11)

$$P_{actual} = \begin{bmatrix} 1 & -\varepsilon_z & \varepsilon_x\varepsilon_z & \delta'_{Zx}(z) + \varepsilon_z\varepsilon_x\Delta z + \Delta x \\ \varepsilon_z & 1 & -\varepsilon_x & (\varepsilon_z\delta'_{Zx}(z) - \varepsilon_x\Delta z + \varepsilon_z\Delta x) \\ 0 & \varepsilon_x & 1 & \left(\Delta z + \delta'_{Xz}(x)\right) \\ 0 & 0 & 0 & 1 \end{bmatrix} * \begin{bmatrix} x_d \\ 0 \\ z_d \\ 0 \end{bmatrix} \tag{8.12}$$

where the x_d and z_d are the desired coordinates of the tool path respectively. The compensated tool path coordinates can be found.

$$P_{compensated} = P_{desired} - P_{actual} \tag{8.13}$$

Once the compensated tool path is known, an expression can be created to represent this data and then finally implemented into the machine tool. This expression for the

compensated path was divided into three segments. Each of the three segments contained a different machining operation: a turn, a face, and a circular profile. A test part was created to evaluate the compensated tool path for each of these tool paths (which are discussed in the next chapter). The profile of all three segments in combination is shown in Figure 64.

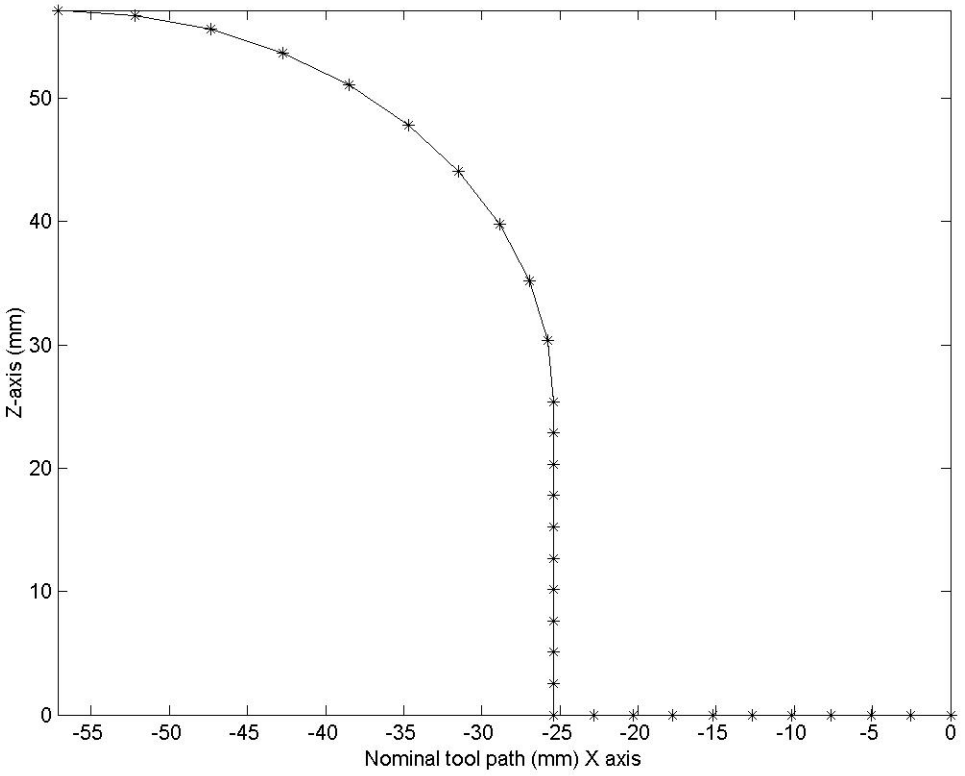

Figure 64- Nominal tool path of test part

A more detailed explanation of incorporating the errors found using the laser interferometer into the error matrix. The laser interferometer was used to take samples at

an interval of 2.54 mm (for short range). These errors must be accurately correlated to the points along the circular arc, as shown in Figure 65.

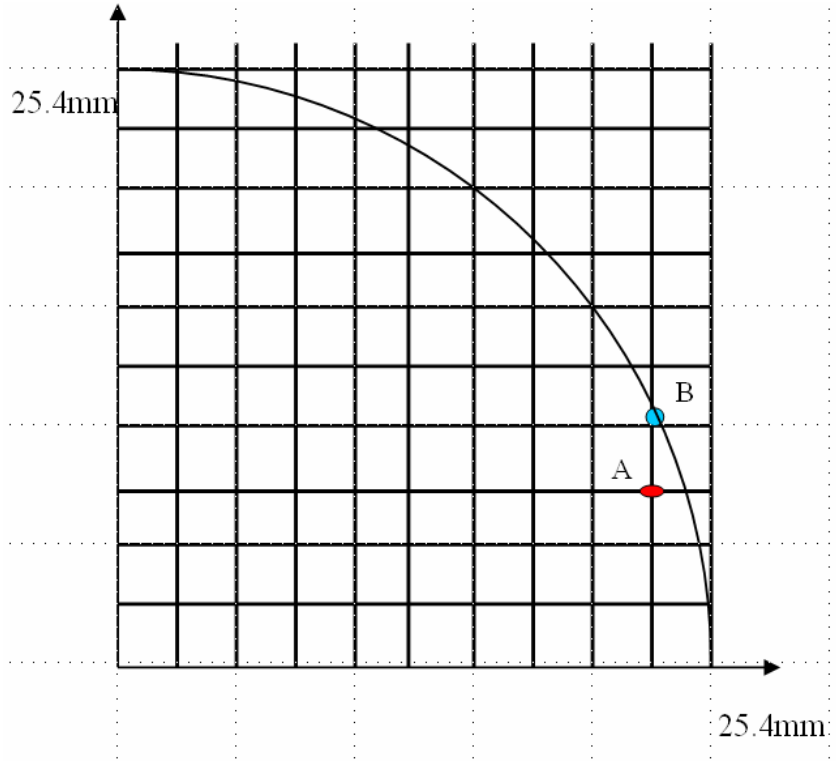

Figure 65- Mesh overlay of circular profile

The errors were measured parallel to the x axis for x measurements and z-axis for z measurements. For example, the errors at x= 2.54 mm (0.1inch) and z= 2.54 mm (0.1 inch) (the first increment) can not be directly used to transform the first point of the circular arc. Likewise, the errors at point A are known, however the errors of point B are required. Thus the Cartesian coordinates of the errors found using the laser interferometer must be transformed to polar coordinates of the circle. Table 6 presents the errors along the 25.4mm (1 inch) arc. This data was converted to appropriate coordinates along the circular arc. Linear interpolation was used to find the errors in .254 mm increments. This

generated more points that were used for shape fitting and the errors more accurately match the coordinates of the circular arc.

Table 6 Machine error results from interferometer test

x (mm)	z (mm)	Xz Pitch (deg)	Zx Yaw (deg)	X straightness (mm)	Z straightness (mm)	X linear (mm)	Z linear (mm)
25.4001	0.0000	-0.0062	0.0023	0.0005	-0.0002	0.0003	-0.0011
25.0873	3.9734	-0.0063	-0.0002	0.0005	0.0002	0.0008	-0.0018
24.1569	7.8490	-0.0066	0.0001	0.0005	0.0001	0.0003	-0.0023
22.6316	11.5314	-0.0072	-0.0021	0.0005	-0.0001	-0.0005	-0.0024
20.5491	14.9298	-0.0082	-0.0017	0.0006	0.0002	-0.0013	-0.0022
17.9605	17.9605	-0.0085	-0.0036	0.0005	0.0001	-0.0013	-0.0023
14.9298	20.5491	-0.0078	-0.0040	0.0005	-0.0001	-0.0013	-0.0022
11.5314	22.6316	-0.0095	-0.0040	0.0004	-0.0002	-0.0018	-0.0023
7.8490	24.1569	-0.0108	-0.0051	0.0005	-0.0001	-0.0025	-0.0024
3.9734	25.0873	-0.0116	-0.0059	0.0005	0.0001	-0.0033	-0.0026
0.0000	25.4001	-0.0125	-0.0061	0.0004	0.0001	-0.0033	-0.0026

These errors were then implemented into (8.11) at each increment along the arc using Matlab™. The coordinates of the compensated path were then determined using (8.13).

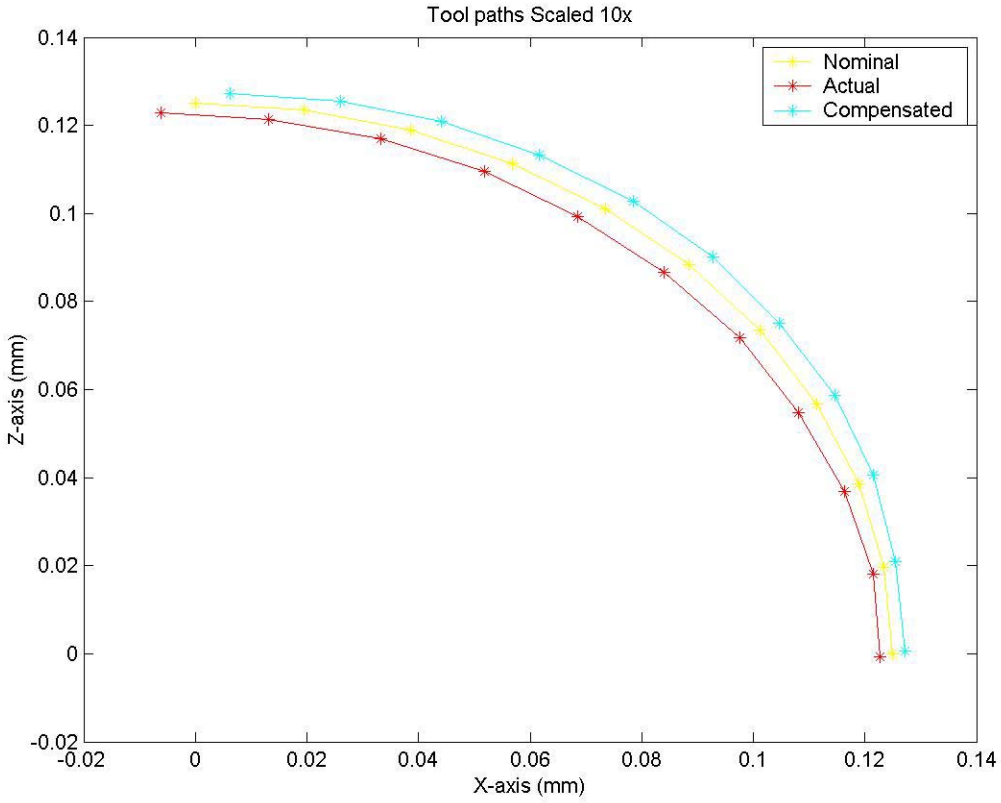

Figure 66- Actual and Corrected tool path for circular profile of 25.4 mm (1 inch) radius

Figure 66 shows the actual and compensated tool paths using the calculated coordinates from the Matlab™ program and aforementioned equations. The tool paths were magnified ten times in order to show the differences between the respective tool paths. The coordinates from the compensated tool path were used in MetroloGT to fit a circle. This Matlab™ program used a non-linear least squares fit. This type of fit minimizes the normal distance of the point cloud points to the fit. The results of the circle fit using MetroloGT is in the first column of Table 7.

Table 7- Results of Circle Fit

	Interferometer	Ball Bar
X (mm)	0.0051	0.0074
Z (mm)	0.0057	0.0220
R (mm)	25.3958	25.4021

The results from the circle fit were then implemented via G-code. The results for the HTM were then converted (using the aforementioned ration in Chapter V) in order to use the ball bar system to validate the trajectory of the compensated test part.

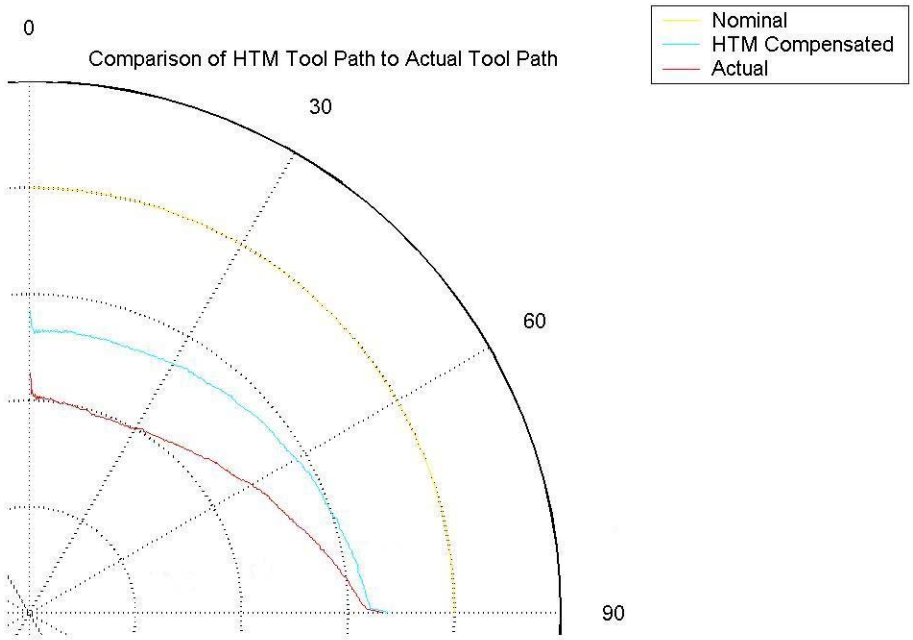

Figure 67- Comparison of Ball Bar compensation path and HTM compensation path (0.05mm/div)

Figure 67 compares the compensated tool path for the ball bar and HTM. The root of the sum of the squares error for the actual, HTM compensated and Ball Bar compensated tool path is 2.7 mm, 0.508 mm, and 0.285 mm respectively. The ball bar compensated tool path is more accurate then the HTM compensated tool path. This was expected because the ball bar system directly measures the machine tool's accuracy in following a circular tool path. The ball bar compensated program used the ball bar system data. The HTM compensated tool path is less accurate because estimation was used to correlate the interferometer increments to a circular profile. In addition, the HTM compensated tool path is more accurate then the actual tool path. This concludes the compensated tool path construction for the arc.

The other two machining operations consisted of facing off and turning by 25.4 mm (1 inch). The short range errors closest to the work volume were used for the error matrix, E. The actual tool path and corrected tool path for the facing is shown Figure 68.

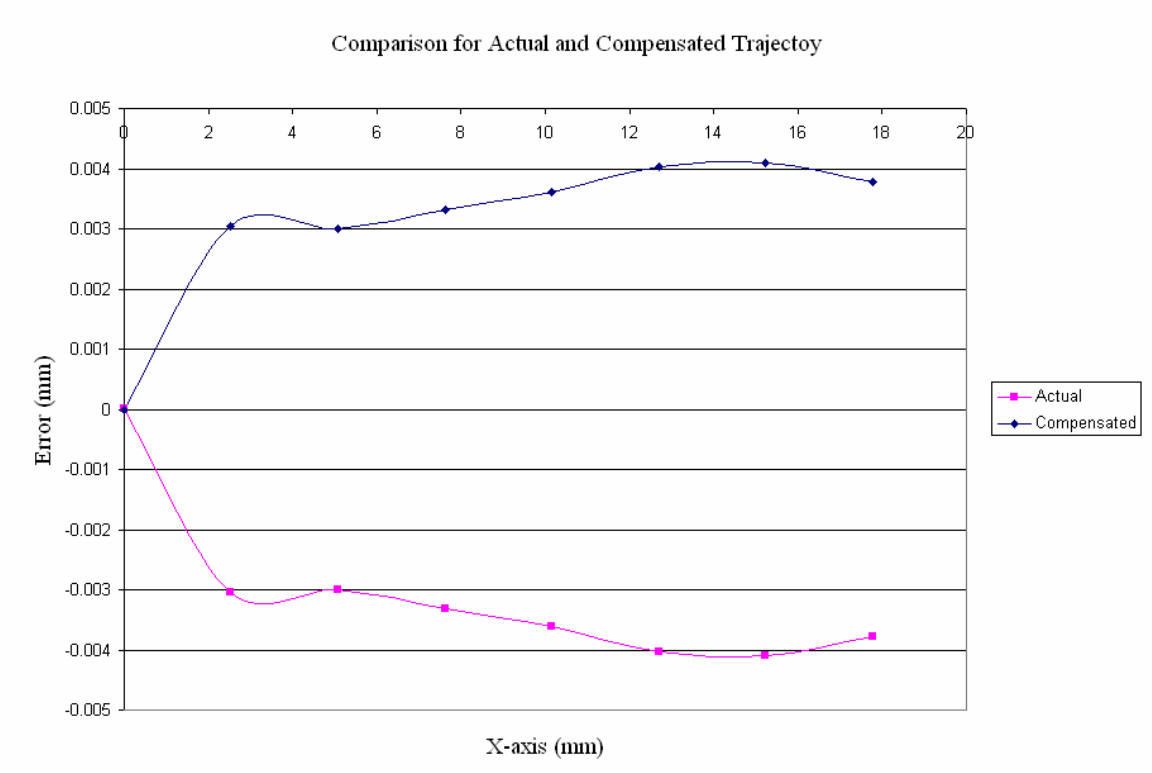

Figure 68- Actual and Corrected tool path of 25.4 mm (1 inch) face

The corrected tool path coordinates are presented in Table 8.

Table 8- Coordinates of actual and compensated tool path for facing and turning

X Comp (mm)	Z Comp (mm)	X actual (mm)	Z actual (mm)
0	0	0	0
0.0008	2.537	-0.0008	2.543
0.0005	5.0767	-0.0005	5.0833
-0.0005	7.6165	0.0005	7.6235
-0.0013	10.1562	0.0013	10.1638
-0.0015	12.6957	0.0015	12.7043
-0.001	15.2357	0.001	15.2443
-0.0015	17.776	0.0015	17.7841
-0.0025	20.3158	0.0025	20.3243
-0.0036	22.8558	0.0036	22.8643
-0.0033	25.3948	0.0033	25.4053

The compensated initial position and final position of each corrected tool path will be implemented into the G-code to create a more accurate facing. Similarly, the 25.4 mm turn is shown in Figure 69.

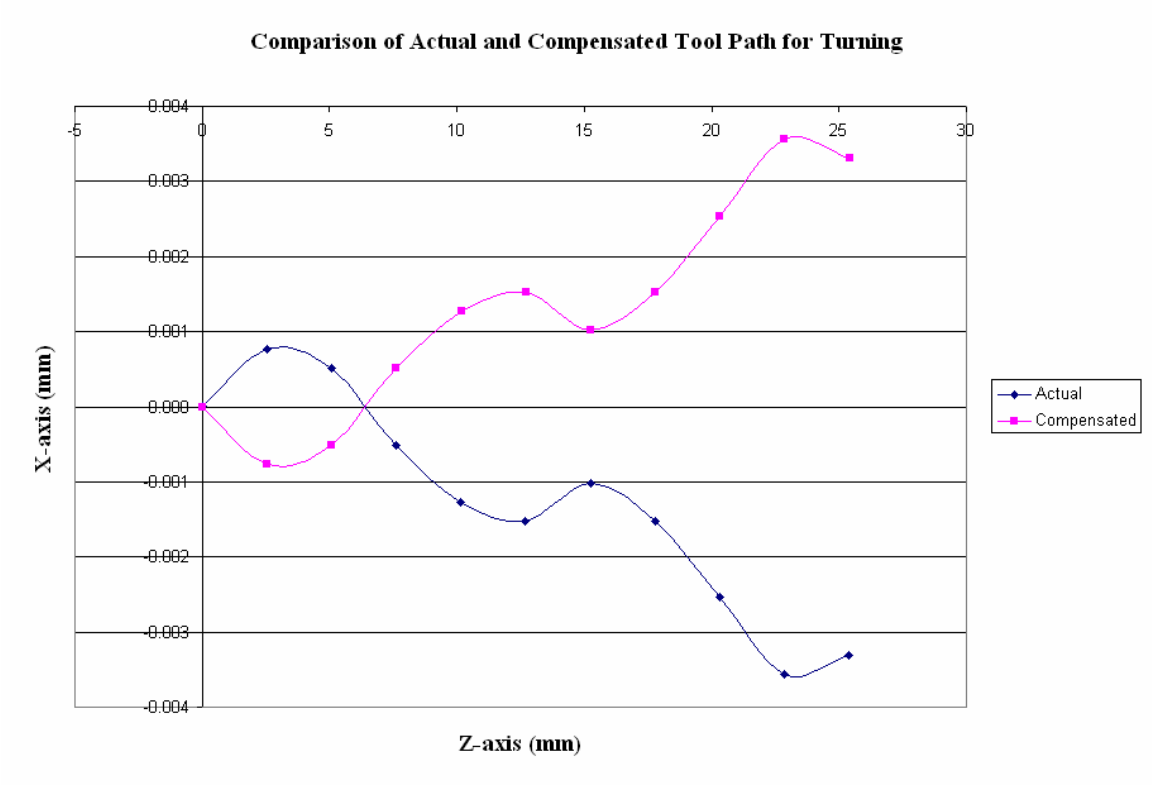

Figure 69-Actual and Corrected tool path for 25.4 mm (1 inch) turn

The compensated tool path shown in Figure 69 was implemented into the part program to correct the actual tool path. Simple G01 commands (linear travel) were used on a point to point basis every 2.54mm to generate the compensated tool path.

CHAPTER VIIII

VERIFICATION

Coordinate Measurement Machine (CMM) Results of Test Parts

Several test parts were cut to verify the performance of the compensated tool path for both the laser interferometer and ball bar respectively. These test parts consist of a 31.75 mm (1.25 inch) circular profile, a 25.4 mm (1 inch) turn and 25.4 mm (1 inch) facing separately. The CMM was used to determine the accuracy of the machined parts to an ideal CAD model. The volumetric accuracy of the CMM is 0.01 mm and the diameter of the probe used is 2mm (.0787 inches). A calculation was done to compare the surface roughness of the part to the diameter of the ball on the CMM. The purpose of this is to show that the probe of the CMM is not detecting the surface roughness which would cause an inaccuracy in the test part measurement. From Liang (2004) the peak to valley surface roughness of a part produced by a single point cutting tool with a finite-radius nose cutter is

$$R_t = (1-\cos(K_r^{'}))R + f\sin(K_r^{'})\cos(K_r^{'}) - \sqrt{2fR\sin^3(K_r^{'}) - f^2\sin^4(K_r^{'})} \qquad (9.1)$$

where $K_r^{'}$ the minor cutting edge angle and f is the feed. The radius of the nose of the tool is 0.792 mm (0.0312 inches) with a 5^o minor cutting edge angle and the federate used was 0.2032 mm (0.008 inches). Thus the peak to valley surface roughness is

$$R_t = (1-\cos(5^o))*.0312+.008*\sin(5^o)\cos(5^o)-\sqrt{2*.008*.0312*\sin^3(5^o)-.008^2*\sin^4(5^o)}$$

$$R_t = 0.00615mm = 0.000242in\,.$$

this is less then 1mm. Therefore it is expected that the CMM will not detect the surface roughness of the part. Furthermore, Figure 70 displays the comparison of the touch probe ball of the CMM to the surface finish of the part.

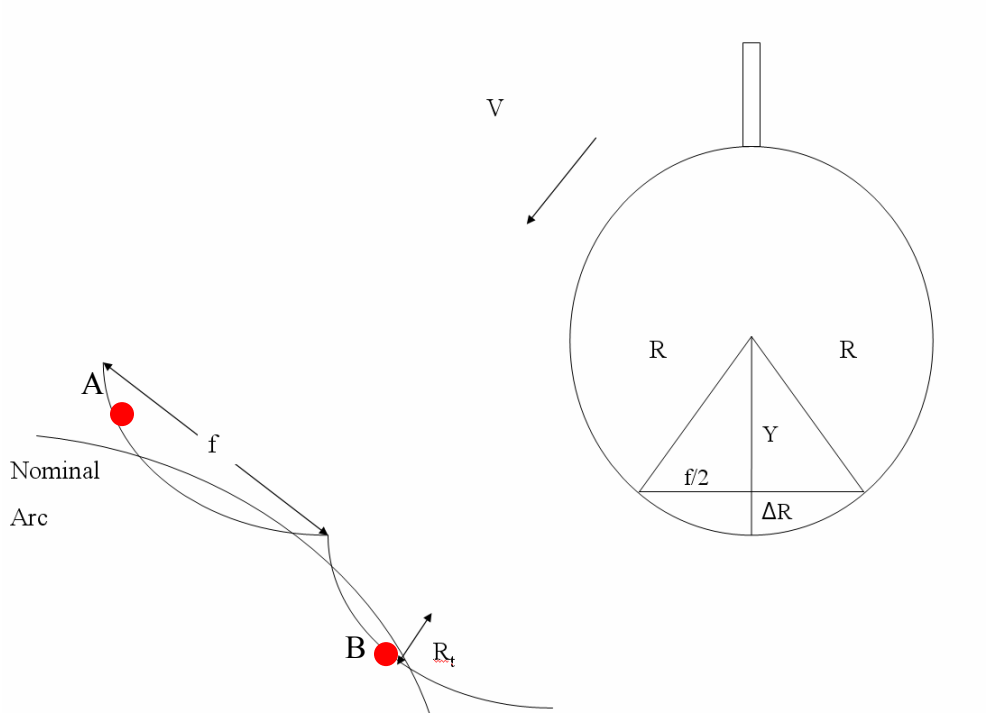

Figure 70- Schematic of surface roughness (not to scale)

The concern is that if ΔR is smaller the R_t, the CMM will detect the surface finish of the part. For example, the desire of the CMM measurement is to give equal values for point A and point B. The CMM will not detect the surface finish if ΔR is much bigger then R_t.

The radius R of the touch probe sphere is 1mm. The feed f is 0.2032 mm and R_t from (9.1) is 0.00615 mm.(9.2) determines the value of Y:

$$Y = \sqrt{R^2 - \left(\frac{f}{2}\right)^2} = \sqrt{1^2 - \left(\frac{.205}{2}\right)^2} = 0.9788mm \tag{9.2}$$

ΔR is

$$\Delta R = R - Y = 1 - .9788 = 0.0212mm \tag{9.3}$$

which is about 3.5 times larger then the peak to valley surface finish R_t. Thus, ΔR is much larger then R_t. Therefore the spread in the CMM data is not from the surface finish of the part. The source of this spread was proved in Figure 74.

Figure 71 shows the geometry of the first test part, a 31.75 mm (1.25 inch) circular profile.

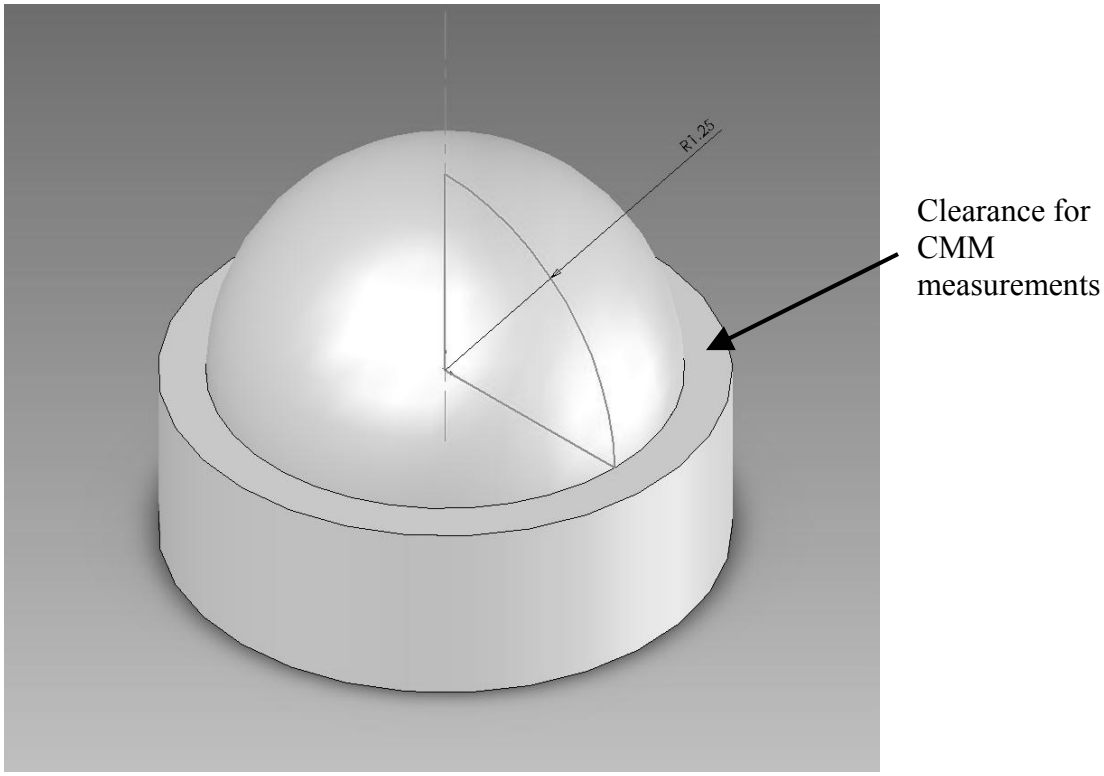

Figure 71- Ideal geometry of test part, radius is 31.75 mm (1.25inches)

The requirement of the test part was to exploit the errors in the machine tool when creating a 90 degree arc. The radius needed to be large enough for the compensated part program to be significant (the results from the 25.4 mm radius were proportioned to a 31.75mm). A radius of 25.4 mm was initially used, however the difference between compensated and uncompensated parts were not significant. The controller only has a resolution of 0.00254 mm (0.0001 inches), thus a radius of 31.75mm was selected. The "clearance" on the side of the part provides a datum for the CMM to reference the cut parts to. Three parts were cut on the machine tool using the geometry shown in Figure 71. The first part represents the original part program without any compensation. The other two parts used different coordinates and radius for the arc determined from HTM compensated data and ball bar compensated data respectively. Once the parts were cut

they were inspected using the CMM. The CAD part was imported into the CMM software to provide an ideal value at each increment (which was 0.254 mm). The radial errors are plotted versus the angle at which data were taken. The convention of the angle is shown in Figure 72.

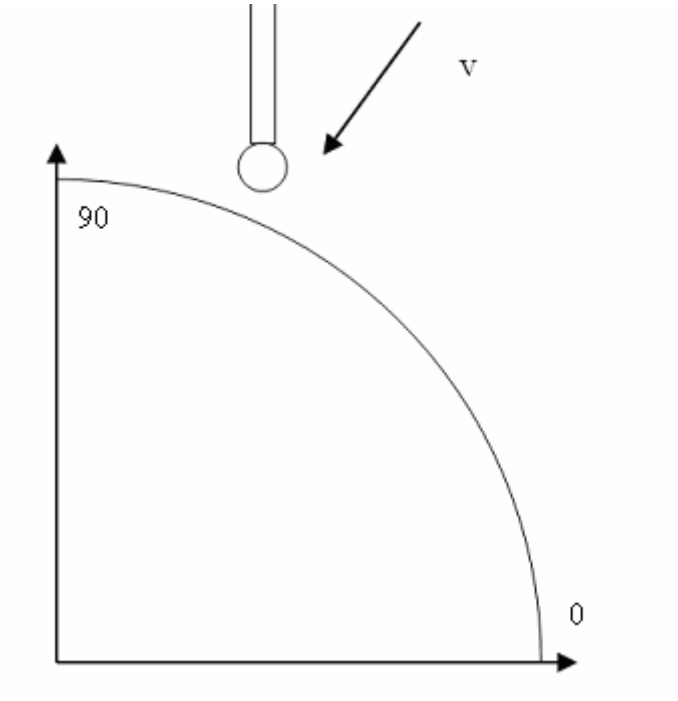

Figure 72- Angle Convention for CMM plots

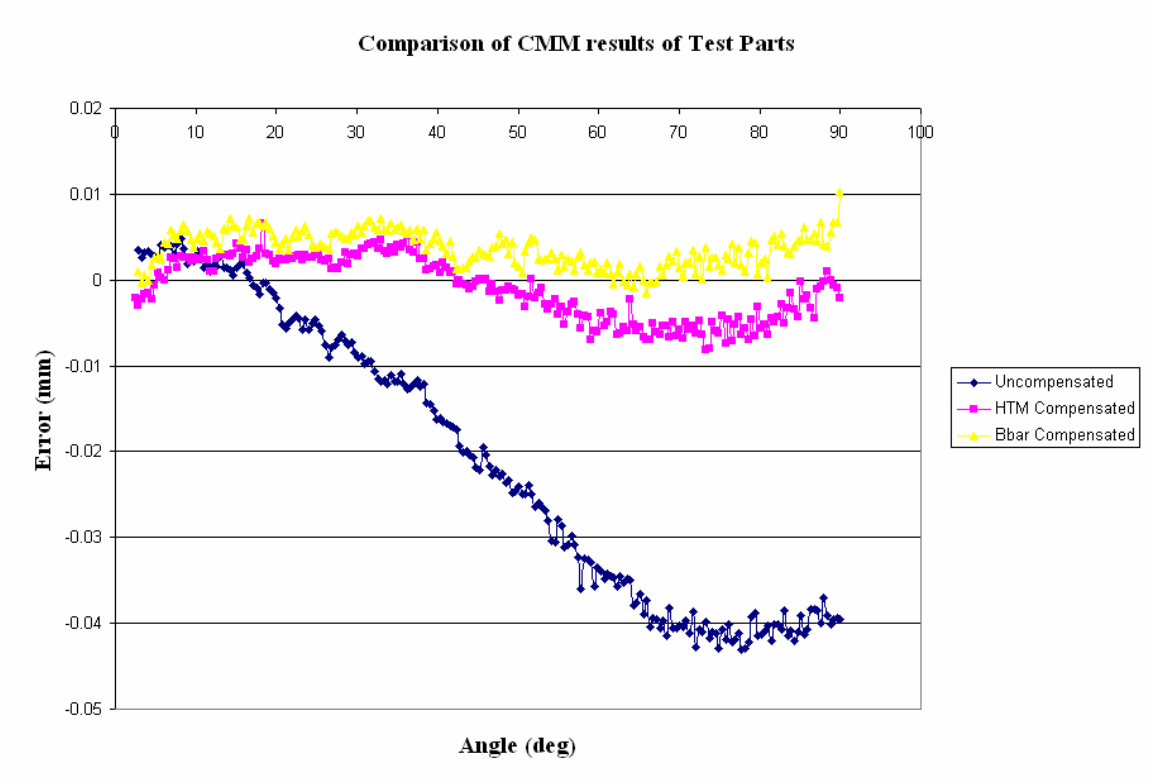

Figure 73- CMM results for test parts (0.01 in increments)

The results from the CMM inspection for each mode are shown in Figure 73. The CMM results show that the ball bar and HTM compensated tool path produced a more accurate part then the uncompensated part program. This was expected since the ball bar measurement system was used to verify the actual trajectory of each part program. The compensated part programs have positive errors from the first 45 degrees of the circular profile, and then switch to negative errors (smaller radius) for the last 45 degrees of the circular profile. The magnitude of the error for uncompensated part exceeds 0.04 mm, while the magnitude of the error for the compensated parts is on the order of 0.05mm.

There is some spread in the data of each of the plots in Figure 73. The calculation made in (9.1) rules out that the surface roughness of the part could cause this spread. Another possibility for the spread in the CMM results is due to the resolution of the CMM. Therefore a test was conducted on the CMM involving a precision sphere of radius 9.52 mm. The CMM probe was brought into contact of the sphere and data was taken at 0.0254mm increments from 0 to 90 degrees. The results of this test are shown in Figure 74.

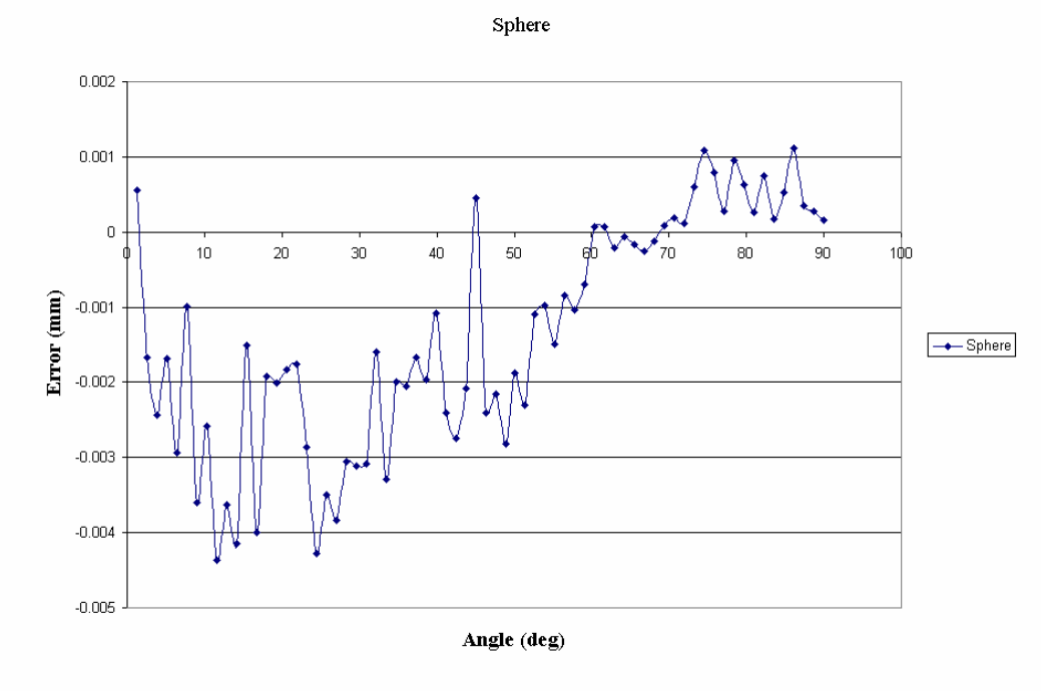

Figure 74- Test using precision sphere to verify accuracy of CMM

Figure 74 shows the errors of the precision sphere. The error band is about 0.005 mm over this volume. Therefore the results of the CMM data for the test parts are to within ± 0.005 mm.

The ball bar tests provided an accurate measurement of the trajectory of the tool path. The CMM provided an accurate measurement of the cut test parts. These two

elements were used to compare results for uncompensated, HTM compensated and ball bar compensated test parts. The nomenclature in the following text can get confusing. There is a ball bar system that determined the trajectory of the tool path for each part program. There is also a ball bar compensated test part. This means that the compensated part was derived from the ball bar error results initially found. The machine tool errors found from the ball bar test was compared to the CMM results of the uncompensated test part.

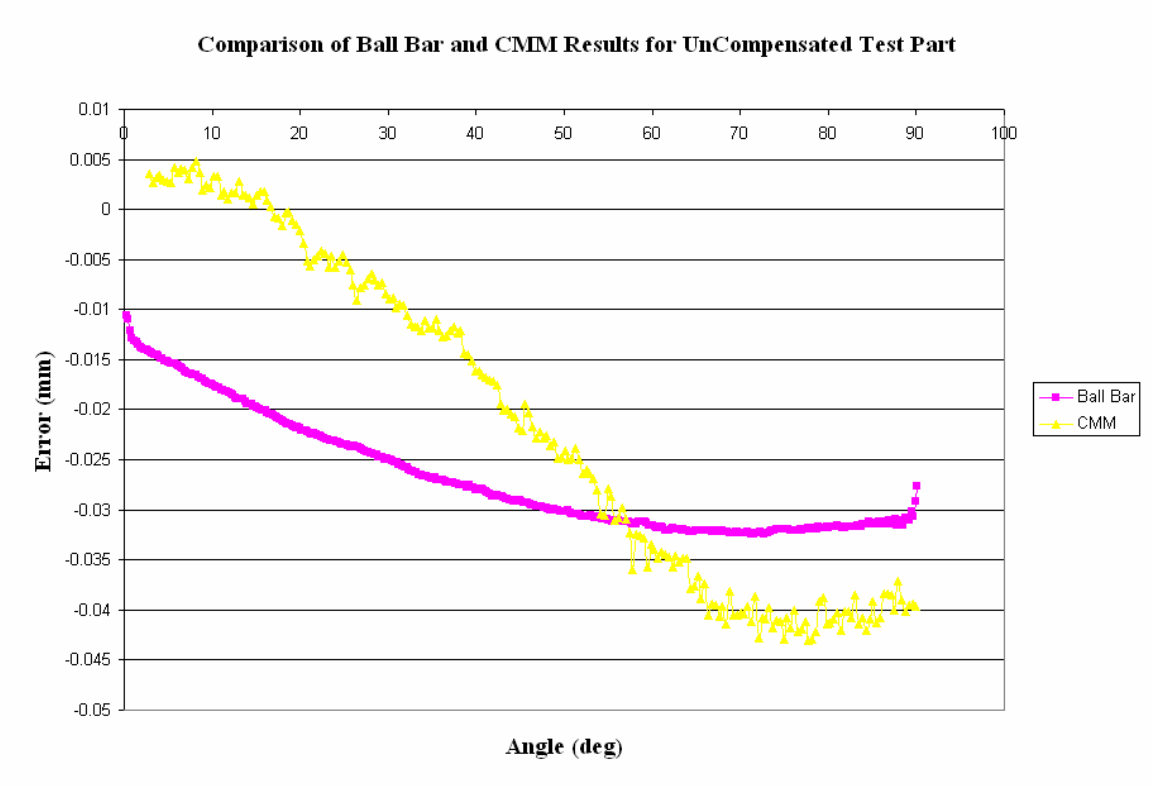

Figure 75- Comparison of errors found from ball bar test to CMM results for uncompensated part

The ball bar and CMM results differ due to several factors. The main factor is that the ball bar measured a trajectory of the tool path for a radius of 100mm. The ball bar test rules out any tool offset error and only determined errors in the machine slides (thus

spindle errors or cutting errors are not taken into account). The results of this ball bar test were scaled down from 100mm to 31.75mm (the ratio was used) and compared to the CMM results. The CMM measures the actual cut part that can absorb tool offset error and spindle errors.

The tool offset error derives from the initial set up of the work piece in the machine tool. An estimate is used to tell the machine where the tool tip is in relation to the center of the spindle. The workpiece is rotated while the machine tool tip is brought into the workpiece in the x-direction. The material is removed until a proper surface is created along the z-axis with constant x distance. A Vernier caliper is then used to measure the diameter of the workpiece. The caliper measurement could cause deviations in the true x-offset. The reason is that the caliper may not find the correct "sweet" spot on the workpiece. This position is the maximum diameter of the workpiece and is then input into the machine tool. The measured workpiece diameter (twice Δx) in conjunction to the x position of the tool along the edge of the workpiece is the x-offset.

The following figure illustrated this process.

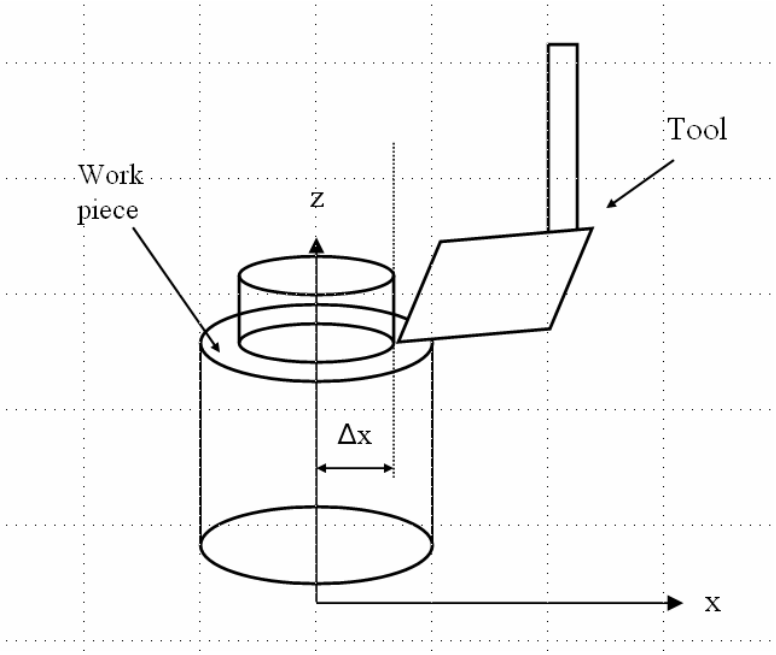

Figure 76- Illustration of x-offset

The CMM data is less stable then the ball bar data due to the nature of the different metrology measuring instruments. The ball bar uses an LVDT with a resolution of 0.1mm and accuracy of 0.5 μm, while the CMM has a resolution of 0.01mm and accuracy of 0.001 mm.

Like wise the machine tool errors found from the ball bar test was compared to the CMM results when the ball bar compensated part program was used.

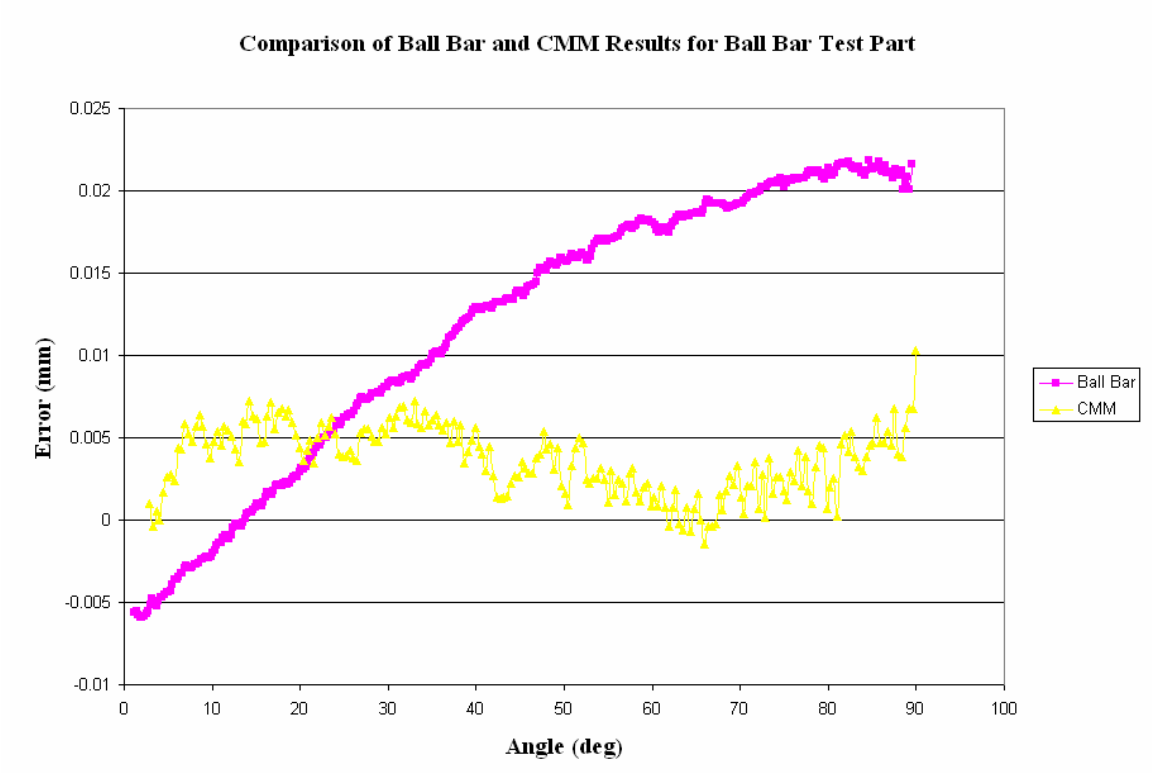

Figure 77- Comparison of errors found from ball bar test to CMM results for ball bar compensated part

Of course, ideally the CMM results and Ball Bar Results in Figure 77 should overlap; however, they are in close proximity to each other. The results differ for the same reasons explained in the uncompensated test part. Finally, the ball bar test results were compare to the HTM compensated part program. The result of this test was compared to the results of the CMM.

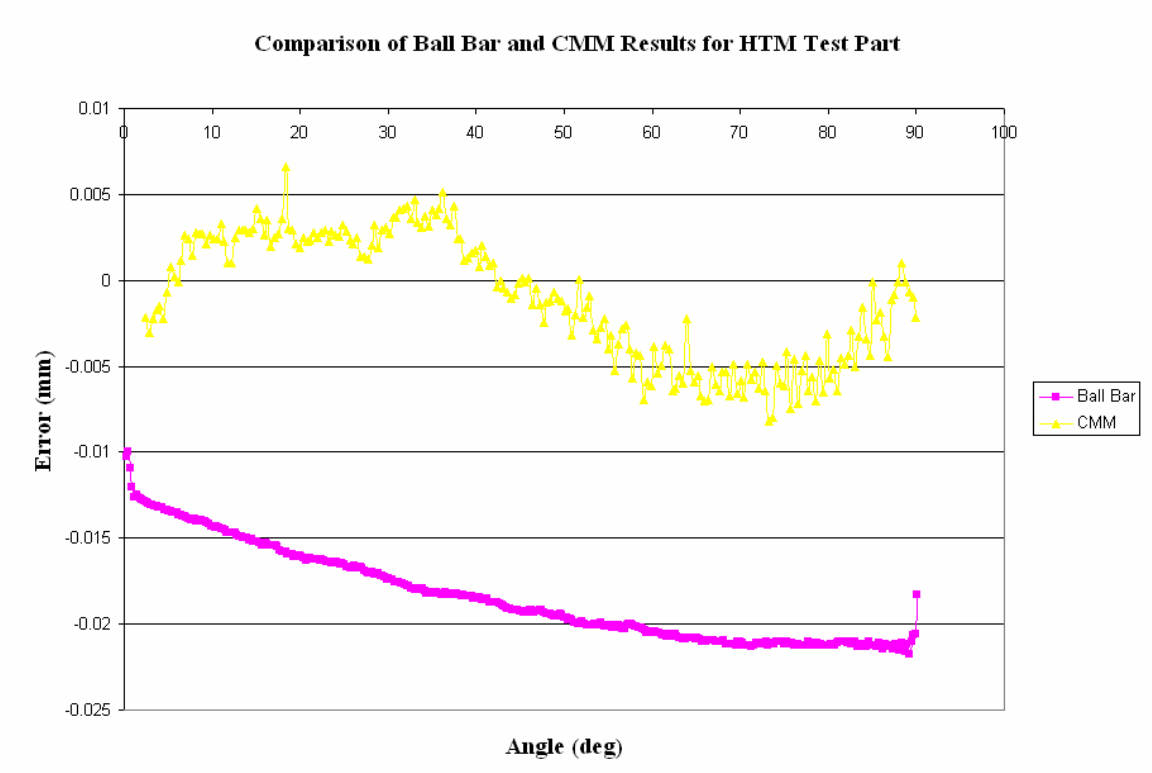

Figure 78- Comparison of errors found from ball bar test to CMM results for HTM compensated part

The offset between the ball bar test results and CMM results are due to machining errors. The part may have been inaccurately cut due to the x tool offset. The root of the sum of the squares of the errors were taken for each case and presented in Table 9.

Table 9- Root of sum of squares of the errors for each case

Type	Root of Sum of Squares of Errors (mm)	Percent Improvement
Uncompensated	0.3909	-
HTM Compensation	0.0554	85.82
Ball Bar Compensation	0.0617	84.20

The ball bar and HTM compensated tool paths improved the accuracy of the test part as expected from the results of the ball bar system. The HTM compensated tool path is

slightly different from the Ball bar compensated tool path. The HTM uses highly accurate laser interferometer measurements over a range that most closely resembled the workpiece volume. The ball bar measured the errors of the machine 100 mm away from the work volume. Therefore, errors that were present at 100 mm away were applied to the workpiece (even though these errors were scaled down by the ratio of radii). Furthermore, the ball bar compensated tool trajectory is more accurate then the HTM for a 100mm radius, however this may not be the case for the 31.75mm.

Figure 67 shows the tool path trajectory of the HTM compensated path using the ball bar system. This HTM compensate trajectory is less accurate then the ball bar compensated trajectory. Therefore it is intuitive to think that the ball bar compensated test part is more accurate then the HTM compensated test part. The trajectories are both scaled down (using the ratio of the radii) and compared to the CMM results in the previous figures. The ball bar system collected data farther away from the workpiece volume then the interferometer. Therefore the interferometer had more accurate work volume machine tool error assessment then the ball bar.

The CMM was also used to inspect the test parts for the turn and facing operation. The test part in Figure 79 shows a 25.4mm turn and a 25.4mm facing.

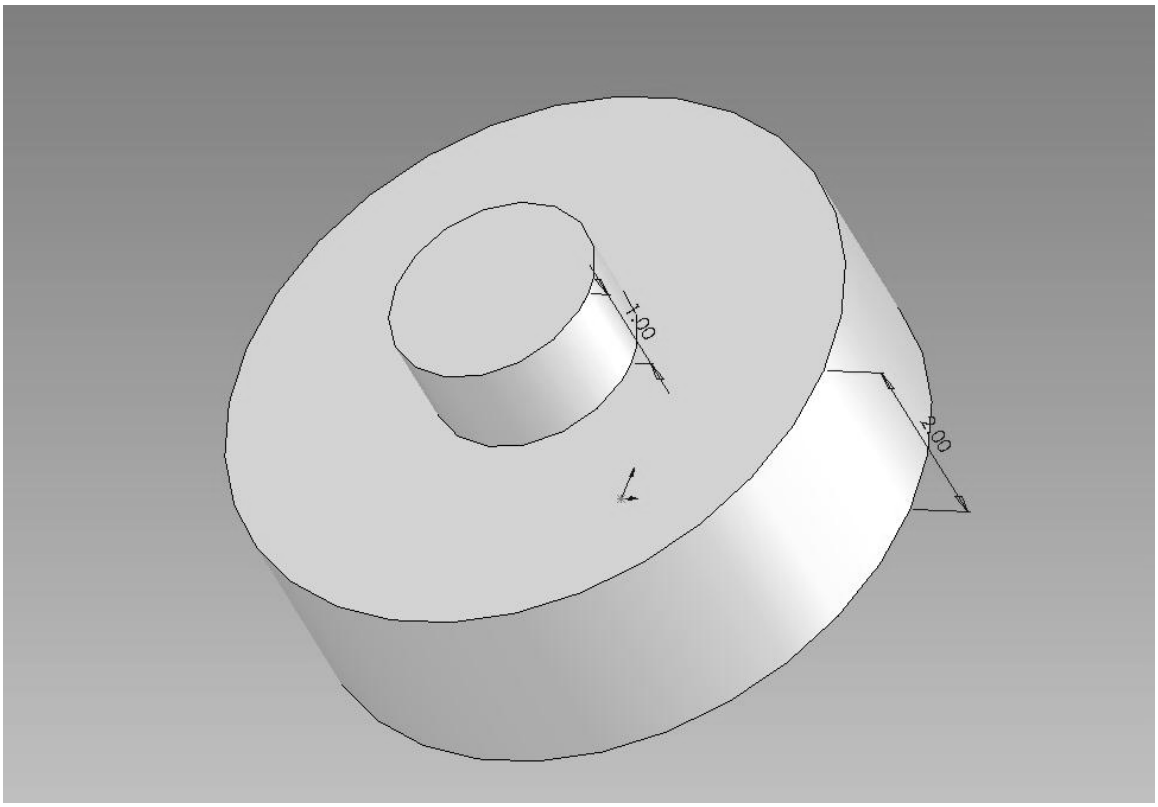

Figure 79- Test Part for facing and turning operation

The initial and final positions of the turning and facing operations that were determined by the HTM were implemented into the controller using G-code. An uncompensated test part was first created to verify machine tool errors. Data was collected over a 17.78 mm (0.7 inch) range to get rid of end effectors. The shortened range from 25.4 mm was also a result of the geometry of the probe. As the CMM path nears the center of the part, the probe is able to crash into the work piece. The CMM results of the uncompensated test part for facing are presented in Figure 80.

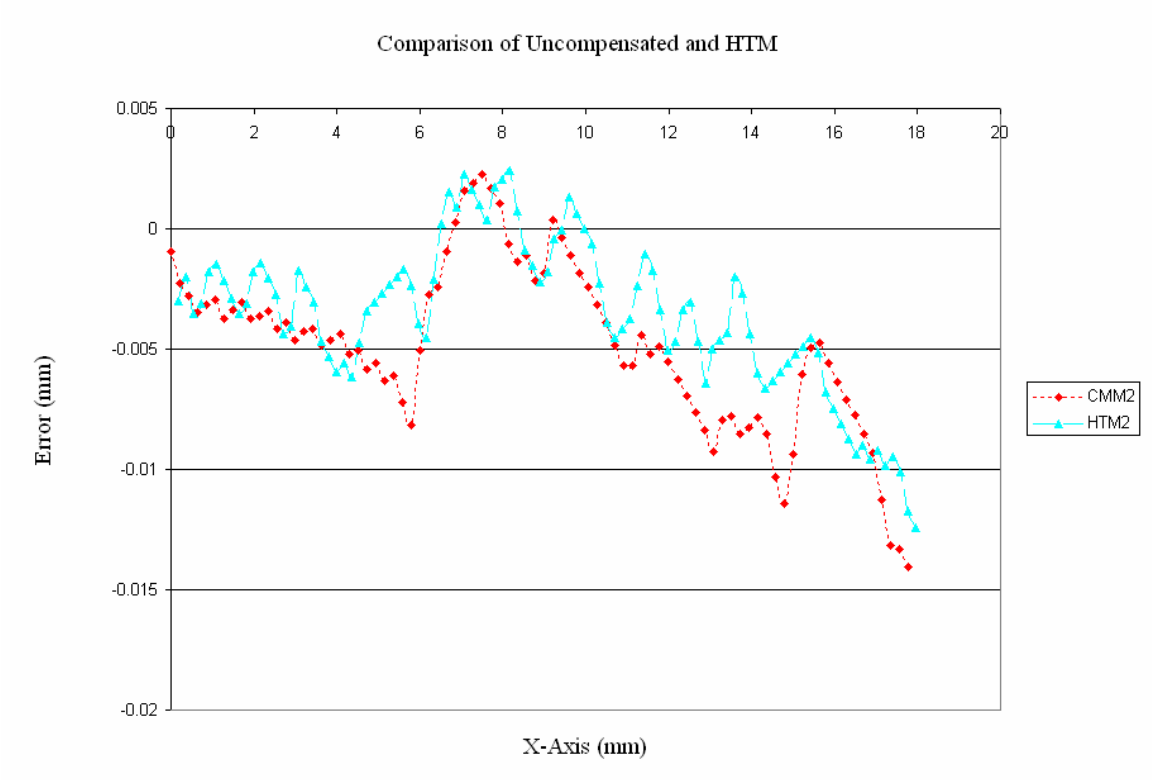

Figure 80- CMM results for uncompensated facing

This plot shows the errors for the uncompensated test part and the HTM compensated test part over a 17.78mm range. Once again, the spread in the data is from the resolution of the CMM. The HTM marginally shifts the errors in the correct direction. Essentially the HTM predicted that the machine tool would face a part off -0.008 mm from the nominal in the z direction as shown in Figure 81.

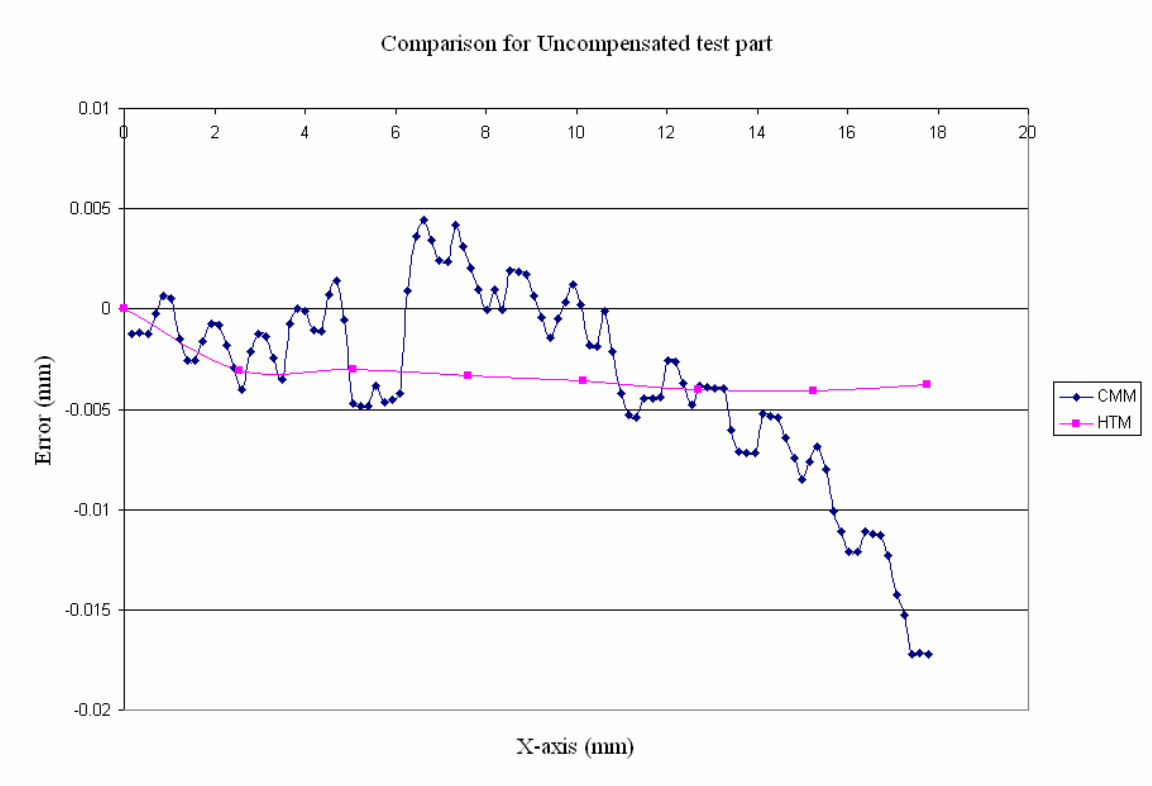

Figure 81- Comparison of CMM results for uncompensated test part and HTM prediction

Figure 81 shows that the HTM can estimate the actual tool path of the machine tool. This was expected because of the z-linear errors determined by the interferometer. The z linear position error of the machine tool causes the face to be below nominal. The root of the sum of the squares of the errors for the uncompensated and compensated test parts was conducted for a quantitative assessment.

Table 10- Results of Facing

	SSQ (mm)	Percent Improvement
Uncompensated	0.060	-
HTM Compensated	0.047	21.14

Thus the HTM improved the accuracy of the facing process by 21.14%. The facing process has the potential of error correction due to the magnitude of the z linear errors. The facing test part relies heavily on the accuracy of the z-axis positioning, which is 0.02286 mm according to the machine specifications. The z-linear errors are the largest genre in the work volume, therefore facing is susceptible to larger errors.

The last test part required the use of a 25.4mm turning process. The test part was turned on the machine tool and placed on a CMM for measurement over a 22.86 mm range. The range was limited from 25.4 mm to 22.86 mm due to the geometry of the probe. The HTM compensated tool path was implemented into the machine tool on a point to point basis. The coordinates of each 2.54 mm increment were added into the program (as shown in appendix A) with a G01 command. This command was used for linear motion. The CMM results of the HTM compensated test part was compared to the uncompensated test parts as shown in Figure 82.

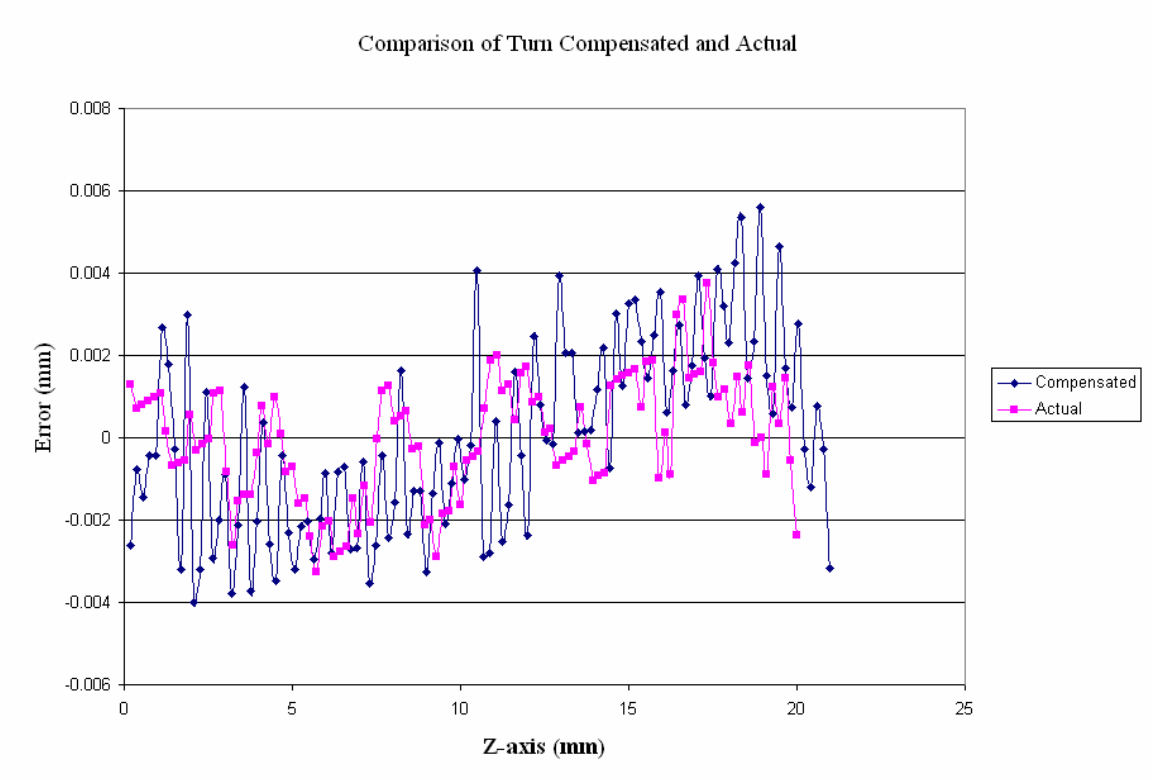

Figure 82- CMM results of uncompensated and HTM compensated turned parts

The HTM compensated program provided an improvement of 5.33%. This result was expected due to the magnitude of the x-axis errors. According to the specifications of the machine tool, the x-axis has a positioning error of 0.01524mm. The HTM predicted a maximum tool path error of 0.00254 mm. Therefore, the compensated path would only change the tool trajectory by at most 0.00254 mm. The CMM results of the uncompensated test parts were then compared to the actual HTM predicted tool path (as shown in Figure 83).

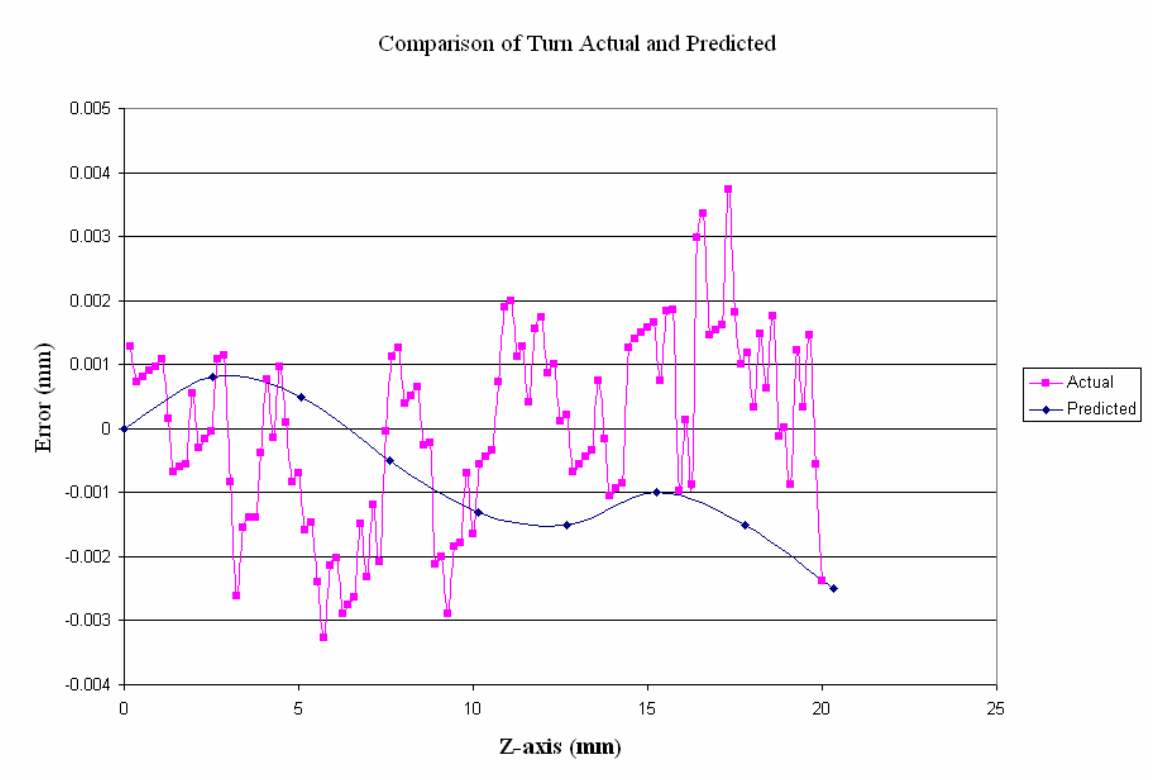

Figure 83- Comparison of HTM predicted tool path to CMM results of uncompensated test part

The HTM did not closely predict the actual machine tool path. In defense of the HTM compensated tool path, it did predict the direction of the offset. Essentially, the HTM predicted that the tool would travel too far towards the center of the spindle. Figure 84 shows the nominal turning occurs at x= 0.5 inches for the test part. A negative error means the tool did not move away from the origin far enough.

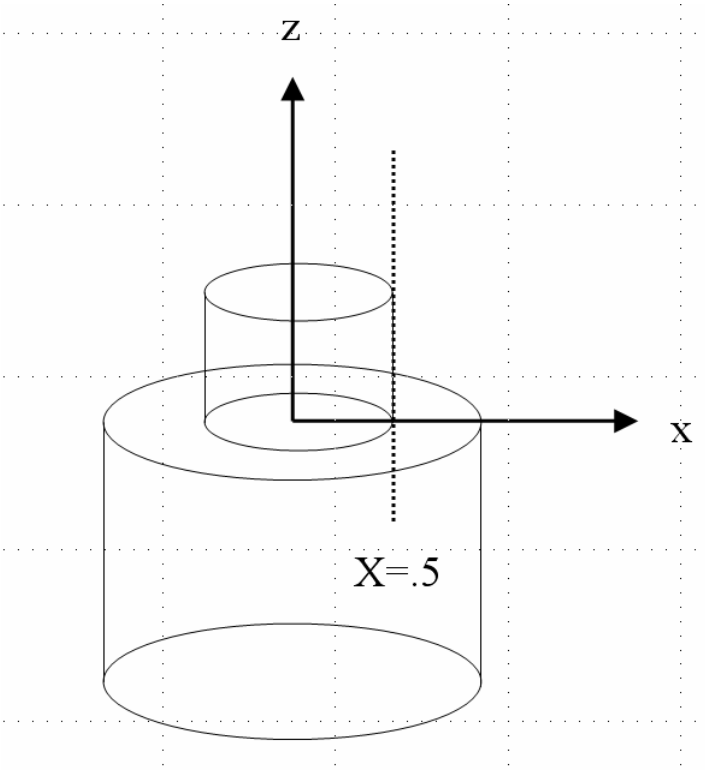

Figure 84- Schematic of turning

Unfortunately, the HTM did not closely predict the magnitude of this error. This could be attributed to inaccurate correlation of the interferometer data to the work volume. Recall the optical configuration made it impossible to measure displacement and angular errors in the work volume. This could also be due to a tool offset error.

Discussion of Sources of Error

This chapter consisted of cutting test parts to verify the improvement of the machine tool using a compensated tool path. These test parts were then measured on the CMM to quantify this improvement. There were several sources of error present in these steps. The machining process contains errors that are not accounted for in the

compensated tool paths. The compensated tool path is dependent upon the kinematic errors of the slide. As previously discussed the x-axis tool offset error was a major error source. A micrometer was used to estimate this offset. The measurement was made using two points along the circle, however three points are required to define a circle. Therefore the inaccurate measurement of the tool offset affected the machining process. The tool wear of the machine tool also contributed to the change in the x-axis tool offset. The functional point of the tool tip changes as the part is machined, thus changing this offset. There are also inherent cutting forces and vibrations that provoke error during the machining process. These errors were discussed in greater detailed in the literature survey. Previous sections of this text outlined the affect of thermal errors on machine tool accuracy, however thermal distortion of the workpiece itself is present. This thermal distortion is a result of the cutting fluid used during the machining process. Another source of error in the cutting process was chucking the workpiece. Precision practices were not used in fixturing the workpiece. More specifically, the jaws of the chuck were bored out using the machine tool. Variation in the roundness of the jaw translates to variation in radial compliance of the chuck and workpiece. This out of roundness of the workpiece contributes to inaccurate machining. Furthermore, a collet chuck was not used to correct for the out of roundness. In conclusion, the machining process of the test parts contained error that was no accounted for because this genre of errors was outside the scope of the research.

CHAPTER X

CONCLUSIONS AND RECOMMENDATIONS

Conclusions

The main scope of this research was to characterize a two axis vertical lathe in a manner that allowed for error correction. The manner of this characterization involved the following. The geometric errors of importance were determined and applied in a manner to compensate for variations in the ideal tool path. This compensation was implemented via two main vehicles. An HTM was developed and applied in conjunction with the laser interferometer measurements. The other vehicle involved the direct use of the ball bar measurements. The results were verified through the use of the CMM.

The thermal behavior of the machine was identified even though tool errors affected by thermal variance were not measured. The thermal time constant for the spindle and z axis were determined. This provided an indication of when the machine would reach thermal steady state. Thermal steady state of the machine tool implies invariable thermal errors. Thus, once the machine achieves this state, geometric error is the dominant factor in ideal tool path deviance. The thermal time constants for warming and cooling of the spindle are 54.50 and 81.97 minutes respectively. The thermal time constants of the z slide for cooling and warming are 92.59 and 95.42 minutes.

A case study was conducted involving the ball bar system. The ball bar was used to measure the geometric errors of the slides. A compensated tool path was constructed using these errors. The compensated tool path was then fit to a circle in order to

communicate this compensation to the machine tool. The uncompensated tool path contained a root of the sum of the squares of 2.7 mm, while the compensated ball bar had an SSQ of 0.284 mm. The improvement for a circular arc was 89.49 %. The compensation was also tested for robustness. The machine was manipulated to achieve thermal steady state and the compensated program was used again with the ball bar system. The improvement from uncompensated (SSQ of 1.998mm) to compensated (SSQ of .732 mm) was 63.63%.

The determination of geometric errors was the major effort in this research. A laser interferometer was used to measure respective deviations of the machine tool slides from the nominal, while a ball bar was used to determined tool path deviations from a 31.75 mm circular arc. A homogeneous transformation matrix was developed and implemented with the proper interferometer measurement results. This allowed for the determination of the actual tool path which in turn provided the compensated tool path. A compensated tool path for the circular arc was also directly determined using the ball bar. A linear interpolation scheme was used in order to correlate the linear interferometer results to the coordinates of the circular profile. An efficient method of implementing the circular compensated tool path into the machine tool was selected. The compensated tool path was fit to a circle, and then applied to the controller by altering the radius and shifting the center of the circle. A test part was used to allow for verification of the success of the compensation modes on a CMM. The root of the sum of the squares (SSQ) for the uncompensated circular profile was 0.3909 mm while the SSQ of the HTM and ball bar compensated part program was 0.0554 mm and 0.0617 mm respectively. The ball bar provided an 85.82% improvement on achieving the ideal radius, while the HTM

improved 84.20%. The HTM was slightly more accurate then the ball bar compensated tool path. Intuitively, one would think that the ball bar would be more effective because it measures the accuracy of the machines ability to travel in a circle. The ball bar collected measurements farther away from the work volume and thus could introduce errors that were found at 100 mm away from the center, but not 37.15 mm away from the center. The accuracy of the ball bar is 0.5 micrometers while the interferometer is 0.36 micrometers. Therefore the interferometer made more accurate measurements that were closer to the work volume and over a range closer to the range of the workpiece. Furthermore, the ball bar compensated program is more accurate the HTM compensated for a circular profile of 100mm, but may not be for a circular profile of 31.75mm.

The ball bar test results were compared to the CMM results of the test parts. The behaviors of the results coincide, but are not exact. The ball bar only predicts the measurement of the machine tool slides. The spindle and cutting forces are not included in the ball bar tests. The finished part experiences errors in the spindle, cutting forces, vibrations, improper tool offsets etc. For example, the workpiece was not perfectly round and flat when chucked in the machine tool. Therefore, these aforementioned variables are responsible for the difference in ball bar test results and CMM results of the test parts. This can also be said of the HTM compensated test parts.

A compensation method was also applied to a turning and facing process. Of course the ball bar tests could not be correlated to compensate for a facing or turning. The sole compensation vehicle used the HTM and a test piece consisting of a 25.4 mm facing. The uncompensated test part exhibited a SSQ of 0.060 mm, while the compensated program improved the SSQ to 0.047 mm. This was a 21.14% improvement. The facing

process had the potential for compensation because the z-axis linear errors were the greatest in magnitude. The facing process is most sensitive to the z-linear position errors (or z-axis errors in general). Equivocally, the same process was used for a 25.4 mm turning. The HTM compensated tool path for the turning process improved the part accuracy by 5.33 %. Such a small improvement was made because the x-axis errors were so small. Although the ball bar was a much faster and accurate compensation vehicle, it was inadequate for compensating a face or turn. A laser interferometer in conjunction with an HTM needed to be used to compensate for the face and turn.

This research provided a start to a complete methodology for producing a more accurate hemisphere. This methodology included a detailed explanation in determining the geometric errors of the machine tool via a ball bar system and interferometer. It is important to mention that only the geometric errors of the machine tool slides were determined (the spindle was not compensated for). A process involving the development of an HTM was then explained and implemented via test parts. These test parts were then inspected on a CMM. The HTM was much more time consuming but improved the circular profile more then the ball bar. The HTM compensation was the only means in improving the turning and facing accuracy of the test part.

Recommendations

The circular profile has the potential for further improvement. The errors of the circular profile were calculated using a ball bar in one case and an HTM with interferometer measurements in the other. The compensated tool path was constructed from this data. The potential for improvement of the accuracy of the circular profile is translating this compensated tool path to the machine tool. This researched used a circle

fit to describe the compensated tool path. This circle was then applied to the machine tool using G-code. Several arc segments could be constructed to more accurately describe the compensated tool path to the controller. Furthermore, the data points of the compensated tool path could be implemented causing the machine tool to move point to point along the corrected arc). This point to point construction was used for the turning and facing.

There were inherent errors in cutting the test parts. These errors included out of round workpieces and inaccurate estimates of the x axis tool offset. A tool set station could be used to accurately determine this x-offset and cut a more accurate part. The spindle is also a source of machine tool errors. The radial errors of the spindle could be determined and implemented into the HTM to create a more accurate part.

APPENDIX A-

PART PROGRAMS

The following part program was used to implement compensation of the circular profile in the machine tool:

```
O2005(Arc)
N1M26
M05
G0G28U0
G28W0
G00T0405
G96S750M03
G00X3.1Z.1/M08
G1Z0F.01
X-.025F.008
Z.1
Z0X3.0F.08
G71U.075R.010
G71P20Q40U.005W.005F.008
N20G0X0
G1Z0F.008
G3X2.5Z-1.25R1.2498F.008
G1X2.5Z-1.5
G1X3.0
N40G1X3.0
G70P20Q40
T0404
G00X3.5
Z.2
G42G01Z0X0F.015
G03X2.5Z-1.25R1.2498F.008
G1X2.5Z-1.5
G01X3.0
G40X3.2
G00G28U0
G28W0M9
M5
M27
M30
```

The following part program was used for implementing the turning and facing compensation:

```
O2012(Turn/Face)N1
M26
M05
G0G28U0
G28W0
G50S1800
G00T0404
G96S750M03
G00X3.1Z.1/M08
G1Z0F.01
X-.025F.008
G1X3.0Z0
G71U.075R.01
G71P20Q40U.005W.005F.008
N20G0X1.0
G01Z-1.0
X2.0
N40Z-1.0
G00X3.1Z1.0
M01
T0404
G00X3.5Z1.0
G42G01X1.0006 Z0F.015
G1 X1.0002 Z-.1 F.008
G1 X1.0002 Z-.2
G1 X1.0002 Z-.3
G1 X1.0004 Z-.4
G1 X1.0004 Z-.5
G1 X1.0004 Z-.6
G1 X1.0004 Z-.7
G1 X1.0006 Z-.8
G1 X1.0006 Z-.9
G1 X1.0004 Z-1.0
G1X2.0
G1X4.0
G0Z1.0
G40X3.0
G00G28U0
G28W0
M9
M5
M27
M30
```

REFERENCES

Anjanappa, M., D.K. Anand, J.A Kirk, S. Shyam, Error Correction Methodologies and Control Strategies for Numerical Control Machining, Control Methods for Manufacturing Processes. ASME. DSC 7 (1988) 41-49

Bryan, J.B., "SIMPLE METHOD FOR TESTING MEASURING MACHINES AND MACHINE TOOLS", Precision Engineering 4 (1982) 125-138

Choi, J.P, Lee S.J, Kwon, H.D, 2003, Roundness Error Prediction with a Volumetric Error Model Including Spindle Error Motions of a Machine Tool. Advanced Manufacturing Technology, 21, 923-928

Donmez, Alkan, A General Methodology for Machine Tool Accuracy Enhancement Theory, Application and Implementation. 1985

HP manual for HP5529A Laser Interferometer

Kiridena, V.S.B., P.M. Ferreira, Kinematic Modeling of Quasi-static Errors of Three Axis Machine Centers, International Journal of Machine Tools and Manufacture 34 (1994c) 127-145

Kurfess, T.R., Jenkins, H.E., Control Systems Applications, chapter on *Ultra-High Precision Control*, editor, William Levine, 2000, pp. 212-231, CRC Press, Inc., Boca Raton, FL.

Lee, Jin-Ho, Lee, Sun-Kyu, Chucking compliance compensation with a linear motor-driven tool system, International Journal of Manufacturing Technology 23 (2004) 102-109

Liang, Steven. Class notes from ME6224

Pahk, Heui, Kim, Young, A NEW TECHNIQUE FOR VOLUMETRIC ERROR ASSESSMENT OF CNC MACHINE TOOLS INCORPORATING BALL BAR MEASUREMENT AND 3D VOLUMETRIC ERROR MODEL, International Journal of Machine Tools & Manufacture 97 (1997) 1583-1596

Palm, William J. Modeling, Analysis, and Control of Dynamic Systems, John Wiley & Sons, New York 1999.

Slocum, Alexander, Precision Machine Design, pgs. 282-285; chapter 6. PRENTICE HALL, New Jersey, 1992.

Thomas, M., Y. Beachamp, "Statistical Investigation of modal parameters of cutting tools in dry turning", International Journal of Machine Tools and Manufacture 43 (2003) 1093-1106

Tseng, P.C., Ho, J.L., 2002, A study of high-precision CNC lathe thermal errors and compensation. International Journal of Advanced Manufacturing Technology, 19, 850-858.

Ulmer, Bernard, "Fabrication and Calibration of an Open Architecture Diamond Turning Machine" pg. 41. 1997

Wang, Shih-Ming, Yuan-Liang Liu, Yuan Kang, An efficient error compensation system for CNC multi-axis machines, International Journal of Machine Tools & Manufacture 42 (2002) 1235-1245

Yang, S, Kim, K., and Park, Y., 2004, Measurement of Spindle Thermal Errors in Machine Tool using Hemispherical ball bar test. International Journal of Machine Tool & Manufacture, 44, 333-340.

Yun, W., Kim, S. and Cho, D., 1999, Thermal Error Analysis for a CNC Lathe Feed Drive System. International Journal of Machine Tool & Manufacture, 39, 1087-1101.

Zhou, B.K. A Ngoi, "Effect of tool wear and tool setting on profile accuracy of diamond-turned nonferrous components", Materials and Manufacturing Processes, 16 (1), 79-89 (2001)

Ziegert, John, "MEASUREMENT OF MACHINE TOOL PARAMETRIC ERRORS USING THE LASER BALL BAR," ASPE 1994 Annual Meeting, pp. 76, October 1994.